BIOFILMS AND BEYOND:
CHARACTERIZING NOVEL CYCLIC DI-GMP CONTROLLED PHENOTYPES IN *VIBRIO CHOLERAE*

By

Nicolas Luis Fernandez

A DISSERTATION

Submitted to
Michigan State University
in partial fulfillment of the requirements
for the degree of

Microbiology and Molecular Genetics – Doctor of Philosophy

2019

ABSTRACT

BIOFILMS AND BEYOND:
CHARACTERIZING NOVEL CYCLIC DI-GMP CONTROLLED PHENOTYPES IN *VIBRIO CHOLERAE*

By

Nicolas Luis Fernandez

The second messenger cyclic dimeric guanosine monophosphate (c-di-GMP) is often utilized by bacteria to transduce external information inside the cell to allow the appropriate response. Soon after investigations began, the connection between c-di-GMP signaling and the transition between sessile and motile lifestyles became clear. Numerous reports demonstrate c-di-GMP promotes production of the biofilm matrix while simultaneously decreasing motility through diverse mechanisms. Researchers also identified c-di-GMP as a signal in other cellular processes in organisms with niche specific phenotypes such as promoting asymmetric cell division, differentiation, predation, and pathogenesis. However, with such vast signaling networks in some bacteria, whether c-di-GMP had a larger influence on controlling cell behavior was to be determined.

In this work, I provide examples of how the aquatic organism and human pathogen *Vibrio cholerae* utilizes c-di-GMP signaling to connect disparate cell behaviors with biofilm formation and explore how these behaviors could promote survival in its natural reservoir. This is exemplified in Chapters 2 and 3, where I demonstrate c-di-GMP increases tolerance to DNA damage and oxidative stress. Importantly, these responses were independent of biofilm matrix production, which can often provide protection from antimicrobials. My data indicate c-di-GMP specifically increases

expression of genes involved in DNA repair and antioxidant production, which is sufficient to provide a growth advantage under stressful conditions. Thus, these data support a model where, under high c-di-GMP conditions, matrix production is co-regulated with DNA repair and antioxidant production, suggesting biofilm formation in *V. cholerae* involves a pre-emptive induction of stress responses, which could promote persistence in the environment.

In chapter 4, I uncover an important, previously unrecognized, role for c-di-GMP signaling: control of cell shape to promote biofilm formation. *V. cholerae* adopts a vibrioid, or curve-rod, appearance which was first observed by early microbiology pioneers in the 1800's. Further examination by Arthur Henrici in 1928 found that *V. cholerae* shape is heterogenous and was influenced by growth phase. However, how *V. cholerae* regulated its shape change and the ecological benefits of such changes remained a mystery. In this work, I found that high c-di-GMP concentrations caused the straightening of the vibrioid shape. Disrupting this process by forcing cells to remain curved during surface colonization caused defects in biofilm formation. By using single-cell analysis, my work suggests curvature causes irregularities in cell-to-cell contact during the early stages of biofilm formation. In summation, by orchestrating matrix production, stress responses, and cell shape changes, my results indicate c-di-GMP plays a global role in *V. cholerae* by preparing cells as they transition to the biofilm lifestyle.

To my village:

My mother Lori,
my father John,
my sisters Lucy and Delia,
my brother Juan,
and my loving wife and partner Amy.

We did it.

ACKNOWLEDGEMENTS

I would first like to thank Christopher Waters, Ph.D for granting me the opportunity to conduct research in his lab. He provided encouragement during the difficult times and pushed me to keep developing and to become a better scientist. I would also like to thank my guidance committee, Victor DiRita, Ph.D, Robert Hausinger, Ph.D, and Lee Kroos, Ph.D. Together, this panel of experts challenged me scientifically and, ultimately, influenced how I think about science and biology.

Dolli Lutes and the 2013 cohort of Ronald E. McNair Postbaccalaureate Scholars at Grand Valley State University – Thank you for providing a sense of community and introducing me to the possibilities of postbaccalaureate education.

To all of the members, past and present, of the Waters lab and members of the Department of Microbiology and Molecular Genetics – Thank you! In particular Eric Bruger, Ph.D for guidance during the early years of my Ph.D. Geoffrey Severin, for cultivating and maintaining a welcoming environment for everyone who walked through the lab, including me. Charnay Gloss and Christopher Rhoades for our banter on Kendrick Lamar's best album and the opportunity to learn from you. Neehal Tumma, for his work presented in Appendix 1 of this thesis and our many games of lab Nerf basketball. Megan Seyerle, for being an excellent mentee and her work on the project presented in Appendix 1. Brian Hsueh, for being a great lab mate and for constantly pulling plates out of the incubator for me. Benjamin Pursely, Ph.D for construction of vectors pBRP1, pBRP2, and pBRP333 as well as technical advice. Rudy Sloup, Ph.D for introducing me to pivot tables. Disha Srivastava, Ph.D for her work that started the

project of Chapter 2. Yann Dufour, Ph.D and Josh Franklin for sharing their expertise and microscope for experiments in Chapter 4.

I would like to thank the people who supported me in every endeavor from tee-ball to bacteria: my family. My parents and role models, John and Lori Fernandez, emphasized education and worked hard to provide our family with opportunities to succeed. My siblings, Lucy Ledesma, DNP, Juan Fernandez, M.F.A, and Delia Fernandez-Jones, Ph.D, broke barriers and paved the way to higher education for our family. Thanks for sticking with it and showing me how it's done!

Lastly, I would like to thank my wife, Amy Fernandez, MD, who has been an unrelenting source of support throughout this whole journey from applying to graduate school to defending my Ph.D. Thanks for asking me on our first date when I was too scared to ask you!

¡Todo para la familia!

TABLE OF CONTENTS

LIST OF TABLES _____ x

LIST OF FIGURES _____ xi

KEY TO ABBREVIATIONS _____ xiii

Chapter 1 – Introduction _____ 1
1.1 – Bacterial Signal Transduction through c-di-GMP _____ 2
1.2 – c-di-GMP Regulated Phenotypes in Bacteria: From Swimming to Sticking and Everything in Between _____ 4
1.2.1 – Control of Motility and Biofilm Formation by c-di-GMP _____ 5
1.2.2 – Outside the Box: Roles of C-di-GMP in Diverse Phenotypes _____ 7
1.2.2.1 – Cell Cycle Regulation, Predation, Differentiation, and Virulence _____ 7
1.3 – *Vibrio cholerae:* Human Pathogen and Model System for Studying Bacterial Signal Transduction _____ 9
1.3.1 – C-di-GMP Signaling in V. cholerae _____ 10
1.3.1.1 - Beyond Biofilms and Motility: Evidence for Additional C-di-GMP Regulated Phenotypes in *V. cholerae* _____ 11

Chapter 2 – Cyclic di-GMP Controls DNA Repair in *Vibrio cholerae* _____ 14
2.1 – Preface _____ 15
2.2 – Abstract _____ 15
2.3 – Introduction _____ 16
2.4 – Materials and Methods _____ 19
2.4.1 – Growth Conditions and Strain Construction. _____ 19
2.4.2 – DNA Manipulations. _____ 20
2.4.3 – Reporter Gene Expression. _____ 20
2.4.4 – RNA Isolation, Quantitative Real-Time PCR, and 5'Rapid Amplification Of cDNA Ends (RACE). _____ 21
2.4.5 – Protein Expression and Purification. _____ 21
2.4.6 – Electrophoretic Mobility Shift Assay (EMSA). _____ 22
2.4.7 – Growth Assays. _____ 23
2.4.8 – Statistical Analysis. _____ 23
2.5 – Results _____ 24
2.5.1 – C-di-GMP Induces Expression of *tag* _____ 24
2.5.2 – VpsT and VpsR are Necessary for *tag* Expression _____ 27
2.5.3 – VpsT Activates *tag* Transcription in *E. coli* and Binds to the *tag* Promoter in vitro _____ 28
2.5.4 – C-di-GMP Increases Tolerance to the Alkylating Agent MMS _____ 32
2.6 – Discussion _____ 34

Chapter 3 – Cyclic di-GMP Controls Antioxidant Production and Hydrogen Peroxide Tolerance in *Vibrio cholerae* 39
3.1 – Preface 40
3.2 – Abstract 40
3.3 – Introduction 41
3.4.1 – DNA Manipulations and Growth Conditions. 44
3.4.2 – Catalase Assay. 45
3.4.3 – RNA Isolation and Quantitative Real-Time PCR (qPCR). 46
3.4.4 – Luciferase Reporter Assays. 47
3.4.4.1 – V. cholerae Reporter Assays. 47
3.4.4.2 – E. coli DH10b Luciferase Assays. 47
3.4.5 – Protein Purification and Electrophoretic Mobility Shift Assays (EMSA). 47
3.4.6 – Hydrogen Peroxide Survival Assay. 48
3.4.7 – Measurement of Intracellular c-di-GMP. 48
3.4.8 – Statistical Analysis. 50
3.5 – Results 50
3.5.1 – C-di-GMP Positively Regulates Catalase Activity 50
3.5.2 – Characterization of the *katB* Promoter and Regulation of *katB* Expression 53
3.5.3 – VpsT Induces *katB* Expression in a Heterologous Host and Binds to the *katB* Promoter In Vitro 57
3.5.4 – C-di-GMP mediated HOOH survival is Dependent on Catalase 59
3.6 – Discussion 61

Chapter 4 – Cyclic di-GMP Decreases Cell Curvature to Promote Biofilm Formation in *Vibrio cholerae* 67
4.1 – Abstract 68
4.2 – Introduction 69
4.3 – Methods and Materials 71
4.3.1 – DNA Manipulations and Growth Conditions. 71
4.3.2 – Phase Contrast Microscopy and Single-Cell Analysis. 73
4.3.3 – Luciferase Reporter Assay. 74
4.3.4 – RNA Isolation and qRT-PCR. 74
4.3.4 – Biofilm Formation and Fluorescence Microscopy. 75
4.3.4.1 – Analysis of Curvature of Attached Cells in Microcolonies. 75
4.3.4.2 – Determination of Curvature Cutoff Value. 76
4.3.4.3 – Microcolony Area Analysis 76
4.3.4.4 – Crystal Violet Biofilm Assay. 77
4.3.5 – Growth Curve Analysis and Calculation Of Growth Rates. 78
4.4 – Results 78
4.4.1 – High Intracellular C-di-GMP Decreases Cell Curvature 78
4.4.2 – The c-di-GMP Dependent Transcription Factors VpsT and VpsR Control c-di-GMP Mediated Changes to Cell Curvature 80
4.4.3 – c-di-GMP Decreases CrvA Production to Decrease Curvature 82
4.4.4 – *V. cholerae* Adopts a Straight Morphology During Early Stages of Biofilm Formation 85
4.4.5 – Cell Shape Influences Biofilm Production at the Single-Cell and Population Level. 86

4.5 – Discussion _____ 91

Chapter 5 – Concluding Remarks _____ 96
5.1 – Conclusions and Significance _____ 97
5.2 – Future Directions _____ 100
5.2.1 – Single Cell Analysis Of *tag* And *katB* Expression During Different Stages of Biofilm Formation _____ 100
5.2.2 – Mechanism of Curvature Mediated Decrease in Microcolony Formation 102

APPENDICES _____ 104
Appendix 1 - Using Vibrio cholerae as a Heterologous Host to Study c-di-GMP Signaling in Burkholderia cenocepacia _____ 105
Appendix 2 - Strains, Plasmids, and Oligonucleotides _____ 124

BIBLOGRAPHY _____ 131

LIST OF TABLES

Table 1: Plasmid Names and Descriptions 125

Table 2: Strains Names and Descriptions 126

Table 3: Oligonucleotides for Vector and Strain Construction 127

Table 4: Oligonucleotides for Experiments 130

LIST OF FIGURES

Figure 1.1: Synthesis and Degradation of C-di-GMP by Diguanylate Cyclase (DGC) and Phosphodiesterase (PDE) Enzymes. 2

Figure 1.2: Model for c-di-GMP Signaling in *V. cholerae* 11

Figure 2.1: Promoter Characterization of *tag* 25

Figure 2.2: VpsT and VpsR Are Necessary For c-di-GMP Mediated *tag* Expression 27

Figure 2.3: VpsT and c-di-GMP are Needed for *tag* Expression in *E. coli* 29

Figure 2.4: C-di-GMP Enhances VpsT Affinity at the *tag* Promoter in vitro 30

Figure 2.5: High c-di-GMP Increases Tolerance to the Methylating Agent MMS 32

Figure 2.6: Tag and MMS do not Contribute to Biofilm Formation in *V. cholerae*. 34

Figure 2.7: Model of c-di-GMP Regulatory Network in *V. cholerae*. 38

Figure 3.1: C-di-GMP Increases Catalase Activity 51

Figure 3.2: Characterization of the *katB* Promoter and Transcriptional Activity 54

Figure 3.3: *vpsT* and *vpsR* are Necessary for c-di-GMP Mediated Expression of *katB* but Dispensable for H_2O_2 Induction 55

Figure 3.4: VpsT and c-di-GMP Induce *katB* Expression in a Heterologous Host. 57

Figure 3.5: C-di-GMP Enhances VpsT Interaction with the *katB* Promoter in vitro. 58

Figure 3.6: C-di-GMP Enhances Survival After H_2O_2 Treatment 60

Figure 3.7: Model for the cyclic di-GMP Regulatory Network Controlling Biofilm Formation and H_2O_2 Tolerance 63

Figure 3.8: Over Production of KatG and KatB Complements Catalase Activity in Δ*katG* and Δ*katB* Backgrounds, Respectfully. 65

Figure 3.9: H_2O_2 Does Not Modulate Intracellular c-di-GMP 65

Figure 4.1: C-di-GMP Decreases Cell Curvature in a Dose-Dependent Manner 79

Figure 4.2: C-di-GMP Decrease Cell Length in a dose-dependent manner 80

Figure 4.3: The Transcription Factors VpsR and VpsT are Necessary for C-di-GMP Dependent Loss of Curvature. 81

Figure 4.4: Complementation of Δ*crvA* Restores Curvature and Response to c-di-GMP. 82

Figure 4.5: Regulation of *crvA* Expression Occurs at the Post-Transcriptional Level. ... 84

Figure 4.6: *V. cholerae* Has a Straight Cell Morphology in Microcolonies. 85

Figure 4.7: Complementation of the Δ*crvA* Background with pCrvA. 87

Figure 4.8: Curvature Influences Microcolony Development and Population Level Biofilm Formation. 88

Figure 4.9: Curvature Does Not Alter Surface Coverage 89

Figure 4.10: WT and Complemented Δ*crvA* Have Similar Growth Curves and Growth Rates. 90

Figure 4.11: Model for c-di-GMP Regulated Transition from Curved to Straight Cells... 91

Figure 5.1: Diagram of RpfR 107

Figure 5.2: Evolved RpfR Alleles Have Higher Intracellular c-di-GMP Pools Compared to the Ancestor 108

Figure 5.3: Ancestor RpfR Influences Biofilm Formation in *Vibrio cholerae* 114

Figure 5.4: RpfR Produces c-di-GMP in *Vibrio cholerae* 115

Figure 5.5: Biofilm and Intracellular c-di-GMP for Evolved Alleles in the Presence and Absence of BDSF 118

Figure 5.6: Hyperbiofilm Mutants of *Burkholderia cenocepacia* are Attenuated for Acute Virulence in *Galleria mellonella* Model of Infection 119

KEY TO ABBREVIATIONS

ATP ..... Adenosine Triphosphate
BDSF ..... *Burkholderia* Diffusible Signaling Factor
BER ..... Base excision repair
BME ..... Beta mercaptoethanol
c-di-GMP ..... Cyclic dimeric guanosine monophosphate
CFU ..... Colony forming units
CHIP ..... Chromatin Immunoprecipitation
CLSM ..... Confocal Laser Scanning Microscopy
CT ..... Cholera toxin
CV ..... Crystal violet
DGC ..... Diguanylate cyclase
DMSO ..... Dimethyl sulfoxide
DNA ..... Deoxyribonucleic acid
EDTA ..... Ethylenediaminetetraacetic acid
EMSA ..... Electromobility shift assay
EPS ..... Exopolymeric substances
EV ..... Empty vector
FAD ..... Flavin adenine dinucleotide
FAM ..... Carboxyfluorescein
FI ..... RpfF-Interaction Domain
GMP ..... Guanosine monophosphate
GTP ..... Guanosine triphosphate
HIS ..... Six Histidine tag
HNS ..... Histone-like nucleoid structuring protein
HPLC ..... High performance liquid chromatography
IF ..... Intermediate filament
IPTG ..... Isopropyl _-D-1-thiogalactopyranoside
IQR ..... Interquartile range
LB ..... Lysogeny broth

MMS ..... Methyl methanesulfonate
NTA ..... Nitrilotriacetic acid
NTP ..... Nucleotide triphosphate
OD ..... Optical density
ORF ..... Open reading frame
ORN ..... Oligoribonuclease
PAS ..... Per-Arnt-Sim domain
PBS ..... Phosphate buffered saline
PCR ..... Polymerase chain reaction
PDE ..... Phosphodiesterase
PG ..... Peptidoglycan
QS ..... Quorum sensing
5'-RACE ..... 5' Rapid amplification of cDNA ends
RBS ..... Ribosome binding site
REC ..... Receiver domain
RFP ..... Red fluorescent protein
RLU ..... Relative light units
RNA ..... Ribonucleic acid
RND ..... Resistance-nodulation-division
ROS ..... Reactive oxygen species
RPM ..... Revolutions per minute
RT ..... Reverse transcription
SD ..... Standard deviation
SDS ..... Sodium dodecyl sulfate
T4P ..... Type four Pili
TBE ..... Tris borate EDTA
TCS ..... Two component system
TELCA ..... The ex vivo c-di-GMP assay
TM ..... Melting temperature
UTR ..... Untranslated region
VPS ..... Vibrio polysaccharide

WGS ..... Whole genome sequencing
WT ..... Wild type

Chapter 1 – Introduction

1.1 – Bacterial Signal Transduction through c-di-GMP

Through billioins of years of evolution, bacteria have developed systems with the primary function to identify a signal, transduce that information inside the cell, and to respond in a beneficial manner. While all systems have similar mechanisms to recognize signals, they differ in the transduction of the signal into the cell. For instance, bacterial two-component systems (TCS) utilize phosphate transfer to produce responses to stimuli while second messenger systems produce small molecules (reviewed in (1)). One group of widely utilized bacterial second messenger system are

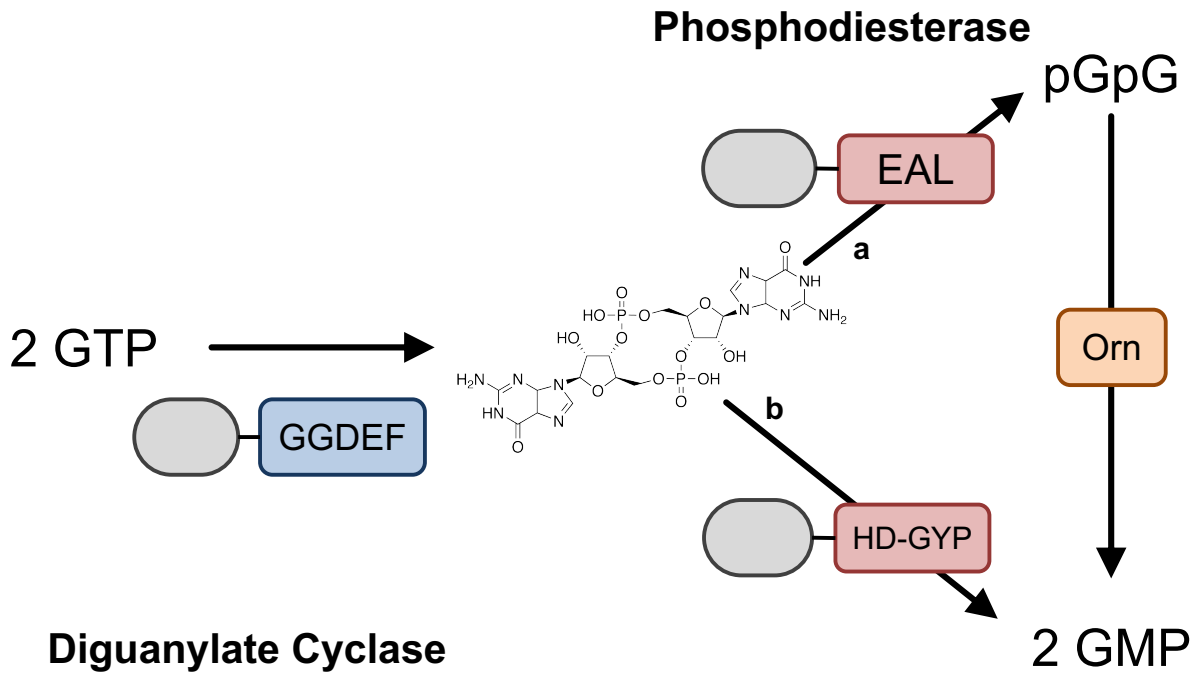

Figure 1.1: Synthesis and Degradation of C-di-GMP by Diguanylate Cyclase (DGC) and Phosphodiesterase (PDE) Enzymes.
C-di-GMP is synthesized by two molecules of GTP by enzymes called diguanylate cyclases which harbor a GGDEF active site motif. The signal is then sensed by molecular effectors in the cell (not shown), causing a change in cellular behavior. C-di-GMP is degraded to two molecules of GMP by two independent mechanisms: indirect (a) or direct(b). Indirect degradation (a) occurs through linearization of c-di-GMP into pGpG by EAL-type PDEs and further degradation by oligoribonuclease (Orn). Direct degradation (b) is carried out by HD-GYP-type PDEs. Figure adapted from (1).

cyclic dinucleotides, in particular the dinucleotide 3'-5' cyclic dimeric guanosine monophosphate (c-di-GMP).

c-di-GMP is synthesized by diguanylate cyclase enzymes (DGC), which catalyze the cyclization of two GTP molecules at the 5' and 3' position (Figure 1, adapted from (2)). DGC enzymes harbor a GG(D/E)EF active site motif which is important for GTP binding (GG), catalysis, and metal coordination (D/E, E), although some variation in this active site motif has been described (3, 4). c-di-GMP is degraded by phosphodiesterase (PDE) enzymes which can have active site motifs of EAL or HD-GYP. EAL-type PDE enzymes degrade c-di-GMP into linear pGpG while HD-GYP-type PDE enzymes are capable of degrading c-di-GMP completely into 2 GMP (Figure 1, reviewed in (5)). The degradation product pGpG is specifically turned over by enzymes called oligoribonuclease (ORN) (6, 7).

c-di-GMP metabolizing enzymes are commonly found in modular associations with other protein domains, such as signal integration domains (e.g. PAS domain) or transduction domains (e.g. REC domain). For example, the PAS domain of the enzyme AxDGC2 from *Acetobacter xylinium* noncovalently binds to oxidized flavin adenine dinucleotide (FAD) which increases c-di-GMP production in vitro (8). WspR, a response regulator with an N-terminal REC domain and C-terminal GGDEF domain from *Pseudomonas aeruginosa,* becomes activated by phosphorylation by its cognate histidine kinase (9). Ultimately, enzyme activity can increase or decrease according to certain environmental conditions or ligand availability, leading to changes in intracellular c-di-GMP.

Reception of c-di-GMP occurs with a wide range of biomolecules and mechanisms. Numerous protein domains and motifs bind c-di-GMP such as PilZ domains, non-functional domains in c-di-GMP metabolizing enzymes, and transcription factors (5). Despite the wide range of receptors, a universal binding site for c-di-GMP has not been identified, indicating wide-range diversity in signal reception. Rather, c-di-GMP binding proteins have appeared to evolve multiple distinct mechanisms for binding to this signal. RNA molecules can also be c-di-GMP receptors in the form of c-di-GMP sensing riboswitches (10). First identified bioinformatically and characterized in a few bacterial species, c-di-GMP sensing RNA riboswitches are found in many bacteria that utilize c-di-GMP signaling (10–12). Thus, similar to other signal transduction pathways, cells utilizing c-di-GMP can integrate the widespread first-messenger signals into second messengers that are recognized by receptors, causing alterations to various phenotypic outputs.

1.2 – c-di-GMP Regulated Phenotypes in Bacteria: From Swimming to Sticking and Everything in Between

C-di-GMP was discovered as the signal that stimulated cellulose production in *Acetobacter xylinum* in 1987 (13, 14). Since then, the field of c-di-GMP signaling has exploded and the nearly ubiquitous relationship between c-di-GMP, motility, and biofilm formation emerged: increased pools of c-di-GMP lead to production of biofilms while inhibiting motility. However, c-di-GMP control of cell behavior is not strictly limited to motility and biofilm formation. There are numerous examples of bacteria utilizing c-di-GMP to regulate disparate phenotypes such as cell cycle control, cellular differentiation, predation, and pathogenesis (15–19, 12). These phenotypes highlight the ability of

signaling networks to repurpose already established networks to respond to changes in intracellular c-di-GMP.

1.2.1 – Control of Motility and Biofilm Formation by c-di-GMP

Motility occurs through various mechanisms such as flagellar based swimming, swarming over a surface, or Type IV pili (T4P) mediated twitching (reviewed in (20)). In bacteria that utilize c-di-GMP, the motile lifestyle typically occurs under low intracellular c-di-GMP conditions. As c-di-GMP concentrations increase, cells become less motile through two general mechanisms: 1) differential regulation of genes involved in motility and 2) physical interruption of motility by disrupting protein activity.

C-di-GMP can inhibit motility through transcriptional regulation of genes necessary for motility. This can occur by c-di-GMP binding to and allosterically inhibiting transcription factors that regulate motility genes (5). For example, FleQ from the human pathogen *Pseudomonas aeruginosa* positively regulates expression of genes at the top of the flagellar biosynthesis hierarchy under low c-di-GMP conditions (21). As c-di-GMP concentrations increase in the cell, c-di-GMP binds to FleQ and inhibits flagella biosynthesis gene expression by decreasing the affinity of FleQ for its target promoters (21). There may be cases, however, where immediate inhibition of motility is required First identified and characterized in *Escherichia coli,* the protein YcgR acts as a c-di-GMP dependent effector that locks the flagellar into counter-clockwise rotation, causing an increase in tumbling and a decrease in chemotaxis (22). Twitching motility allows for directional movement through a process of surface adhesion and T4P retraction (20, 23). Similar to flagella biosynthesis and activity, c-di-GMP regulates T4P at both the transcriptional and post-translational levels. In the soil microbe *Myxococcus xanthus,* c-

di-GMP represses expression of genes involved in T4P biogenesis (24). c-di-GMP can also regulate T4P mediated motility and adhesion through direct protein interactions. For example, in *P. aeruginosa*, lower concentrations of c-di-GMP promote polar T4P assembly and motility by positively affecting ATPase-containing motor proteins while higher c-di-GMP concentrations promote delocalized T4P better suited for surface adhesion (25, 26).

After cells encounter a suitable surface, motility is downregulated, and production of a biofilm matrix initiates. Biofilm matrices are composed of exopolymeric substances (EPS) such as polysaccharides and extracellular DNA, but protein and lipids are also found in varying ratios depending on the organism and conditions (27, 28). In many organisms, expression of genes involved in EPS production increase under high intracellular c-di-GMP conditions (29–32). Regulation of EPS production additionally occurs at the post-transcriptional level in *E. coli* and *A. xylinum* where c-di-GMP facilitates intermolecular interactions between membrane bound glycosyltransferases, increasing activity and production of EPS (33, 34).

1.2.2 – Outside the Box: Roles of C-di-GMP in Diverse Phenotypes

In a database of 500 bacterial and archaeal genomes, 80% encode at least one pair of c-di-GMP metabolizing enzymes, which invites the idea that c-di-GMP may have other functions that are more species specific (35). Indeed, through targeted and untargeted approaches, a role for c-di-GMP in cell cycle regulation, predation, differentiation, and virulence has been discovered.

1.2.2.1 – Cell Cycle Regulation, Predation, Differentiation, and Virulence

Caulobacter crescentus is a free-living freshwater bacterium that undergoes asymmetric cell division to produce two distinct cell types: the free-swimming, non-replicative swarmer cells or surface adhered, replicative stalk cells (36). During early studies screening for genes important for development of stalked cells, mutations in the response regulator PleD inhibited development (37). PleD harbors a C-terminal GGDEF domain that is necessary for development (37). Further studies found that a key point in the transition from a swarmer cell to a replicative stalked cell is the phosphorylation, activation, and localization of the PleD to the stalked pole of the cell (15). c-di-GMP produced by PleD stimulates a signaling cascade that ultimately decreases the concentration of a replication inhibitor, promoting replication and asymmetric cell division (17). After replication and division, the PDE PdeA is activated by phosphorylation and depletes intracellular c-di-GMP resulting in oscillations of c-di-GMP in synchronized populations of *C. crescentus*, corresponding to replication and division (38).

Bdellovibrio bacteriovorus is an obligate predatory bacterium that invades the periplasm of Gram-negative bacteria periplasm, utilizes host nutrients to replicate, and

disseminates from the exhausted host to repeat the cycle (39). After identifying 5 genes encoding GGDEF containing proteins, Hobley *et al.* discovered 3 out of 5 had roles in prey recognition, invasion, and dissemination after host killing. (19). Recently, a studying looking to identify novel c-di-GMP effector proteins in this organism found 84 potential c-di-GMP effector proteins with some having functions in metabolism and signal transduction, suggesting c-di-GMP may have functions throughout a wider range of the predation process than appreciated (40).

Streptomyces species undergo three stages of development: a vegetative growth state, an aerial hyphae state, and sporulation (41). Studies in in *S. venezuelae* found that production of a DGC delayed differentiation while expressing a PDE accelerated differentiation, solidifying the notion that c-di-GMP was an important signal controlling cellular differentiation (18). Using a CHIP-chip approach, researchers found the transcription factor necessary for differentiation (BldD) was enriched upstream of genes with predicted c-di-GMP metabolizing functions (41), and BldD was subsequently demonstrated to be a c-di-GMP responsive transcription factor that controlled expression of genes involved in the metabolism of c-di-GMP in addition to differentiation (42).

Many bacterial pathogens have c-di-GMP signaling pathways, such as *P. aeruginosa, S.* Typhimurium, and *V. cholerae* (16). Due to its pleiotropic effects of promoting biofilm formation and inhibiting motility, which need to be tightly controlled during host infection, there is a general negative relationship between c-di-GMP and virulence in many organisms (16). One specific case highlighting a connection between c-di-GMP signaling and virulence regulation is the role of the two-component system

VieSA and a major regulator of cholera toxin production, ToxT in *V. cholerae* (43). VieS is a membrane-bound histidine kinase that responds to some signal within the host during infection and VieA response regulator with a PDE domain (43). Mutants lacking *vieA,* or ectopically expressing a DGC, result in decreased CT production and a decrease in animal models of cholerae infection, but how c-di-GMP controls these phenotypes is uncharacterized (43).

These examples demonstrate the wide range of c-di-GMP regulated phenotypes that are conserved among many bacterial species (e.g. virulence) or are specific to smaller groups (e.g. predation)

1.3 – *Vibrio cholerae:* Human Pathogen and Model System for Studying Bacterial Signal Transduction

V. cholerae is a Gram-negative human pathogen that causes the diarrheal disease cholera. In parts of the developing world where water infrastructure is lacking, cholera cases can be endemic, but there are also cases where outbreaks occur, such as the current outbreak in Yemen (44). The main route of infection occurs through ingestion of contaminated food or water. After passing through the stomach, *V. cholerae* traverses to the small intestine and colonizes the intestinal lumen. It then produces cholera toxin which causes diarrhea by dysregulating ion channels resulting in influx of water into the small intestinal lumen. Cholera disease is distinct from other gastrointestinal diseases in that patients lose liters of stool, leading to dehydration and death if left untreated (reviewed in (45)).

1.3.1 – C-di-GMP Signaling in *V. cholerae*

V. cholerae has 62 genes that encode proteins with c-di-GMP metabolizing functions, which accounts for 1.6% of its predicted proteome (35). Comparatively, other biofilm forming human pathogens, such as *E. coli* O157:H7 and *P. aeruginosa,* only have 0.53% and 0.70%, respectively, of their proteome dedicated toward c-di-GMP signaling (35). Most of these enzymes have N-terminal or C-terminal signal reception functions, thus the large number of c-di-GMP metabolizing enzymes are likely responsible for integrating multiple signals from the environment and transducing them into intracellular pools of c-di-GMP (46, 47).

Similar to other organisms, high intracellular c-di-GMP promotes biofilm formation while simultaneously inhibiting motility in *V. cholerae* (Figure 1.2). At the start of my thesis research, numerous c-di-GMP receptors had been identified in *V. cholerae,* including transcription factors and c-di-GMP responsive riboswitches, with either characterized or predicted roles in biofilm formation or motility (48, 30, 49–51, 10). The transcription factors VpsR and VpsT, for example, bind c-di-GMP and promote expression of genes involved in the production of *Vibrio* polysaccharide (VPS) to produce mature biofilms (30, 48, 49) (Figure 1.2). The master regulator of flagella biosynthesis, FlrA, also binds to c-di-GMP, which causes anti-activation, resulting in down-regulation of flagellar motility (Figure 1.2) (52, 50). Additionally, *V. cholerae* encodes two c-di-GMP responsive riboswitches: Vc1 upstream of the uncharacterized gene *tfoY* and Vc2 upstream of *gbpA,* a gene involved in colonization of N-acetylglucosamine (GlcNAc) coated surfaces (51, 53). Recent studies elucidated that c-

di-GMP positively regulated expression of *gbpA* through Vc2 while c-di-GMP inhibited expression of *tfoY,* which decreased dispersive motility (54, 55).

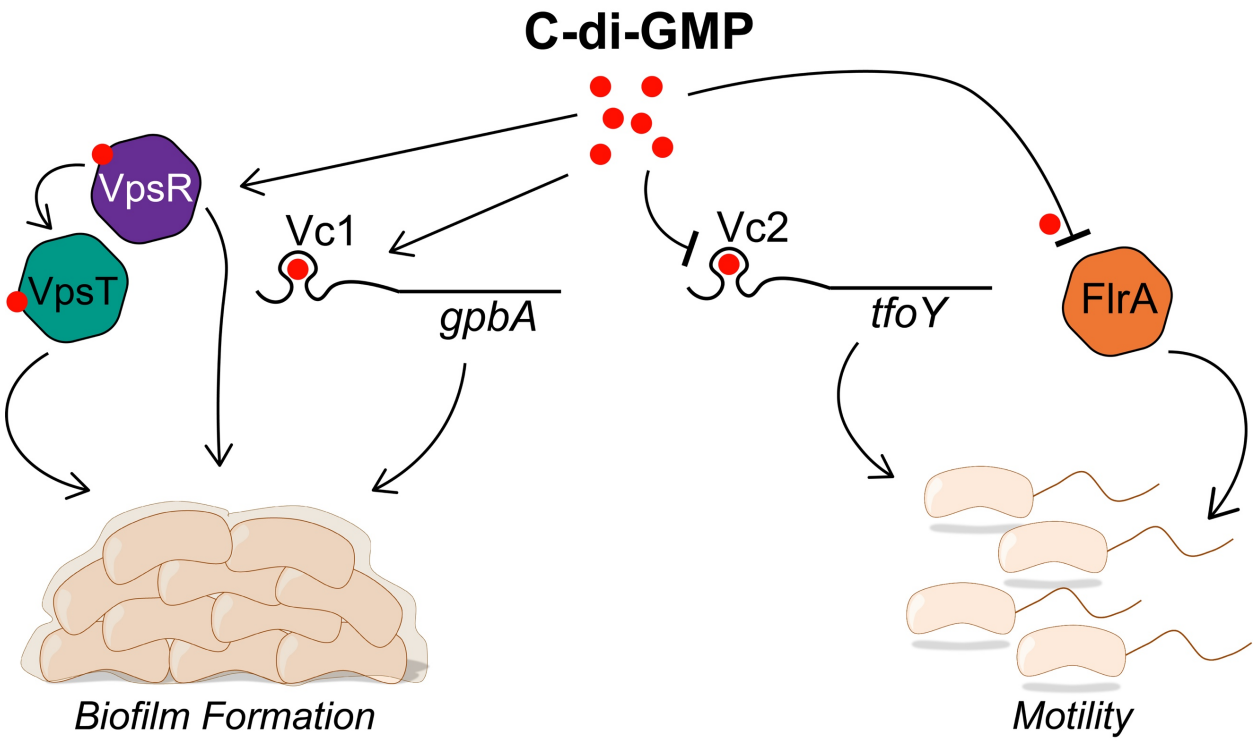

Figure 1.2: Model for c-di-GMP Signaling in *V. cholerae*
Under high c-di-GMP conditions, c-di-GMP binds to the transcription factor VpsR and increases transcriptional activity. Activated VpsR induces the expression of VpsT and both transcription factors promote biofilm formation by upregulating genes involved in biofilm matrix production (16, 17, 47, 15). At the same time, c-di-GMP binds to the master regulator of flagella biosynthesis FlrA to inhibit its ability to positively regulate genes involved in flagella biosynthesis. There are two c-di-GMP riboswitches in *V. cholerae* (Vc1 and Vc2). Vc1 is upstream of *gpbA*, a gene involved GlcNAc colonization and biofilm formation while Vc2 is an off-switch for *tfoY* expression, a gene involved in promoting dispersive motility (50, 52).

1.3.1.1 - Beyond Biofilms and Motility: Evidence for Additional C-di-GMP Regulated Phenotypes in *V. cholerae*

Several studies support the hypothesis that c-di-GMP controls a wide range of cellular behaviors in *V. cholerae.* A microarray analysis of El Tor and Classical *V. cholerae* expressing a DGC from a plasmid unveiled hundreds of genes in both biotypes

that were differentially regulated 15 and 30 minutes after DGC induction (56). Another study expressed the c-di-GMP responsive transcription factor VpsT and identified hundreds of genes with differential expression patterns, including genes involved in stress responses and hypothetical functions (30). Lastly, analysis of transcripts from *V. cholerae* grown in biofilm inducing conditions also identified many differentially regulated genes with functions other than biofilm formation and/or motility (57). Despite the changes in the patterns of gene expression, functions for c-di-GMP in phenotypes other than biofilm formation and motility in *V. cholerae* are not well characterized. A better understanding of the c-di-GMP regulon in this model organism could help inform strategies to modulate signaling in this or other disease-causing organisms.

The central hypothesis of my thesis was that c-di-GMP regulated additional phenotypes in *V. cholerae* other than biofilm formation and motility. In this work, I expand the functions regulated by c-di-GMP in *V. cholerae*. I found that populations with elevated c-di-GMP are more tolerant to DNA damage by methylation at the 3 position of adenine (Chapter 2). My research is the first to connect c-di-GMP levels to the regulation of DNA repair pathways. I also found that c-di-GMP increased tolerance to oxidative stress from hydrogen peroxide by upregulation of a catalase gene (Chapter 3). Bacterial biofilms are known to increase bacterial survival to stress, but I demonstrated that c-di-GMP induction of these stress responses was independent of production of a biofilm matrix, indicating c-di-GMP also functions through a complex transcriptional network to increase bacterial survival to stress. In Chapter 4, I explore the relationship between c-di-GMP and cell shape and found that c-di-GMP decreases cellular curvature to produce straight rod-shaped cells rather than the canonical comma-

shaped cells. I also provide evidence supporting the hypothesis that cell straightening could be an ecologically adaptive feature of biofilm formation in *V. cholerae.* In all cases, these c-di-GMP phenotypes were dependent on the c-di-GMP transcription factors and biofilm matrix regulation VpsR and VpsT, suggesting alternative c-di-GMP phenotypes are coregulated with biofilm formation itself and that these phenotypes increase fitness during a biofilm growth state. In summation, these findings expand our knowledge of c-di-GMP signaling and provide insight into the global reach of c-di-GMP in *V. cholerae.*

Chapter 2 – Cyclic di-GMP Controls DNA Repair in *Vibrio cholerae*

2.1 – Preface

Contents of this chapter were published in the Journal of Bacteriology in 2018 (Citation: Fernandez NL, Srivastava D, Ngouajio AL, Waters CM. 2018. Cyclic di-GMP Positively Regulates DNA Repair in Vibrio cholerae. Journal of Bacteriology 200:1–13). Srivastava D and Ngouajio AL carried out the initial c-di-GMP responsive promote screen and characterized the promoter region. Per American Society for Microbiology guidelines "Authors in ASM journals retain the right to republish discrete portions of his/her article in any other publication (including print, CD-ROM, and other electronic formats) of which he or she is author or editor, provided that proper credit is given to the original ASM publication. ASM authors also retain the right to reuse the full article in his/her dissertation or thesis".

2.2 – Abstract

In *Vibrio cholerae*, high intracellular cyclic di-GMP (c-di-GMP) is associated with a biofilm lifestyle while low intracellular c-di-GMP is associated with a motile lifestyle. C-di-GMP also regulates other behaviors such as acetoin production and type II secretion; however, the extent of phenotypes regulated by c-di-GMP is not fully understood. We recently determined that the sequence upstream of the DNA repair gene three methyladenine glycosylase (*tag*) was positively induced by c-di-GMP, suggesting this signaling system might impact DNA repair pathways. We identified a DNA region upstream of *tag* that is required for transcriptional induction by c-di-GMP. We further showed that c-di-GMP induction of *tag* expression was dependent on the c-di-GMP-dependent biofilm regulators VpsT and VpsR. *In vitro* binding assays and heterologous host expression studies show that VpsT acts directly at the *tag* promoter in response to

c-di-GMP to induce *tag* expression. Lastly, we determined that strains with high c-di-GMP are more tolerant to the DNA damaging agent methyl methanesulfonate. Our results indicate that the regulatory network of c-di-GMP in *V. cholerae* extends beyond biofilm formation and motility to regulate DNA repair through the VpsR/VpsT c-di-GMP-dependent cascade.

2.3 – Introduction

Many bacterial species use the second messenger signaling molecule cyclic dimeric guanosine monophosphate (c-di-GMP) to control cellular behavior. Since its discovery in 1987, research in c-di-GMP signaling has uncovered a largely invariable paradigm: high intracellular c-di-GMP stimulates an adherent, static lifestyle known as a biofilm while decreasing c-di-GMP results in a motile lifestyle (58). Two classes of enzymes are responsible for changes in intracellular c-di-GMP. Diguanylate cyclase enzymes (DGCs), containing GGDEF active site motifs, catalyze the cyclization of two GTP molecules to form c-di-GMP. c-di-GMP is degraded into pGpG or 2 GMP molecules by phosphodiesterase enzymes (PDEs), containing EAL or HD-GYP active site motifs, respectively (58, 59). pGpG is further degraded to GMP by the Orn nuclease (60, 61). Furthermore, enzymatic activity of DGCs and PDEs are thought to be controlled by environmental cues (5). Thus, c-di-GMP functions as one of the major global regulatory pathways that allows bacteria to respond and adapt to their environment.

C-di-GMP additionally regulates bacterial behaviors beyond biofilm formation and motility. For example, *Streptomyces* species undergo a morphological transition between vegetative and aerial mycelial growth that is dependent on the c-di-GMP

dependent transcription factor BldD (62). In *Caulobacter crescentus,* certain DGC and PDE enzymes localize to different cellular regions to control the transition from a swarmer to stalked cell phenotype (63, 64). C-di-GMP also regulates virulence and the type II secretion apparatus in *V. cholerae* (65, 66). However, this list of bacterial phenotypes controlled by c-di-GMP has not been fully elucidated. Further, whether these phenotypes act in a coordinated manner to promote adaption to a sessile or motile lifestyle is not clear. Here, we report that DNA repair is a new phenotype controlled by c-di-GMP in *V. cholerae*.

The human pathogen *V. cholerae* causes the diarrheal disease cholera, ultimately resulting in death by dehydration if left untreated. Currently, the 7th *V. cholerae* pandemic caused by the El Tor biotype is responsible for numerous infections worldwide including recent outbreaks in Haiti, Ethiopia, and Yemen (67–69). While infamously known for its epidemics throughout human history, *V. cholerae* resides harmlessly in between disease outbreaks in marine environments where it is thought to associate with chitinous surfaces as biofilms (70–72). Biofilm formation and motility also contribute during *V. cholerae* infections. Growth in biofilms induce a hyperinfectious state while motility is necessary for colonization of the proximal small intestine (73–75). Thus, the transition between biofilm formation and motility is considered a key aspect of the pathogenesis of this bacterium.

The mechanism for c-di-GMP-dependent biofilm formation in *V. cholerae* has been well studied. In response to specific environmental cues, such as bile acids (76), intracellular c-di-GMP increases. C-di-GMP binds to and activates the c-di-GMP-dependent transcription factor VpsR. Activated VpsR then induces the expression of

another c-di-GMP-dependent transcription factor, VpsT, which is also directly activated by c-di-GMP binding (30, 77). In high c-di-GMP concentrations, these two transcription factors induce the expression of genes needed for biofilm formation, in particular the *Vibrio* polysaccharide (VPS) operons and the gene cluster *rbmBCDEF* encoding biofilm matrix proteins (78, 79). Concurrently, high c-di-GMP directly decreases expression of the flagellar biosynthesis gene cluster through inhibition of the transcription factor FlrA (50). Thus, high c-di-GMP increases expression of genes involved in biofilm formation while simultaneously decreasing expression of genes involved in flagellar motility. Moreover, production of VPS itself inhibits motility (50).

In response to c-di-GMP, VpsT and VpsR regulate gene expression of other processes in addition to biofilm formation. *aphA,* a gene involved in virulence regulation and acetoin biosynthesis, is induced by VpsR and c-di-GMP, but only acetoin utilization is significantly impacted (80, 81). VpsR activated by c-di-GMP induces transcription of the *eps* operon encoding genes necessary for production of the type II secretion system. While not impacting protein secretion, induction of *eps* leads to production of a surface pseudopilus (66). VpsR and c-di-GMP induce transcription of the transcription factor *tfoY,* which impacts motility and type VI secretion (56, 66, 82, 83). In addition, transcriptomic analyses indicate c-di-GMP signaling and VpsT regulate expression of various genes; however, the physiological effect of these global gene responses is not well characterized (30, 56).

In the marine environment and human host, *V. cholerae* likely incurs DNA damage that must be repaired to maintain genome integrity and fitness. Indeed, mutations in key genes of the base excision repair (BER) pathway decreases infant

mouse colonization and increases sensitivity to DNA damaging chemicals (84). DNA glycosylases stimulate repair of DNA damage through the BER pathway by specifically recognizing and removing lesioned bases (85). While the mechanistic details of the BER pathway have been well studied, only a handful of regulatory pathways controlling BER gene expression in bacteria have been identified (85–87). Here, we report our findings that increased c-di-GMP induces transcription of the DNA glycosylase Tag (three methyladenine glycosylase) in *V. cholerae*. We demonstrate c-di-GMP positively regulates *tag* expression through the c-di-GMP-dependent transcription factors VpsT and VpsR, but not FlrA, indicating this gene likely plays a role in homeostasis within a biofilm or during biofilm formation. We further demonstrate VpsT directly regulates the expression of *tag* in a c-di-GMP-dependent manner. Lastly, we show that cells with high intracellular c-di-GMP have increased tolerance to the DNA methylating agent methyl methanesulfonate (MMS).

2.4 – Materials and Methods

2.4.1 – Growth Conditions and Strain Construction.

All strains, primers, and plasmid used in this study are listed in Appendix 2 (Tables 1-4). The *V. cholerae* strains used in this study were derived from the El Tor biotype strain C6706str2 and contain a deletion in *vpsL* (88). This mutation disrupts biofilm formation and allows for accurate measurement of optical density and *lux* reporter gene expression. Δ*vpsT,* Δ*vpsR,* Δ*vpsT*Δ*vpsR,* and Δ*tag* unmarked mutant strains were constructed in the Δ*vpsL* parent strain using the pKAS32 suicide vector as described previously (89). All *V. cholerae* strains were grown overnight in Lysogeny broth (LB) broth at 35 °C with shaking at 220 revolutions per minute (RPM) unless stated

otherwise. 100 μg/mL ampicillin, 100 μg/mL kanamycin, 10 μg/mL chloramphenicol and 100 μM isopropyl β-D-1-thiogalactopyranoside (IPTG) were added when needed. *Escherichia coli* S17-λ*pir* was used as the donor in biparental conjugation to mobilize plasmids into *V. cholerae* with selection against the donor using Polymixin B (10 U/mL).

2.4.2 – DNA Manipulations.

Standard procedures were used for DNA manipulations (90). PCR was carried out with Phusion polymerase (NEB). Restriction enzymes were purchased from NEB. The primers used are listed in Table 3. Reporter plasmids were constructed by Gibson Assembly (NEB) using PCR generated inserts and pBBRlux linearized by BamHI and SpeI restriction digest. Expression vectors were constructed by Gibson Assembly using PCR amplified insert (vpsT, vpsR, and tag) and pEVS143 linearized by EcoRI and BamHI restriction digestion. Vectors used for gene deletion were generated by Gibson Assembly using three fragments: 1 kb of sequence upstream of the gene of interest, 1 kb of sequence downstream of the gene of interest, and MfeI and BglII linearized pKAS32. pET28B (Novagen) was used for protein purification. PCR amplified vpsT (vca0952) was cloned into linearized pET28b XhoI and NcoI using Gibson Assembly.

2.4.3 – Reporter Gene Expression.

Overnight cultures of *V. cholerae* or *E. coli* harboring reporter plasmids (pBBRlux derivatives) were diluted to a starting OD_{600} of 0.04 in 1 mL LB supplemented with appropriate concentrations of antibiotics and IPTG. 200 μL of dilutions were added to black 96-well plates (Cellstar) in triplicate and grown at 35 °C while shaking at 220 RPM. Luminescence readings were taken at mid-exponential phase using an EnVision Multilabel Plate Reader (PerkinElmer) and were normalized for relative light units (RLU)

by dividing the luminescence reading by the OD_{600}.

2.4.4 – RNA Isolation, Quantitative Real-Time PCR, and 5'Rapid Amplification Of cDNA Ends (RACE).

Overnight cultures of *V. cholerae* harboring QrgB or QrgB* were diluted 1:1000 in 10 mL LB in triplicate supplemented with appropriate concentrations of antibiotics and IPTG. Cultures were grown for three hours at 35°C with shaking at 220 RPM. Cells were pelleted and RNA was isolated using TRIzol® Reagent (Thermo Fischer Scientific) following the manufacturer's instructions. 5 µg of total RNA was treated with Turbo DNAse (Thermo Fisher Scientific) following the instructions in the manual. DNA free RNA was converted into cDNA using the GoScript™ Reverse Transcriptase and the instructions in the manual. qRT-PCR reactions were carried out using SYBR Green PCR Master Mix (Thermo Fisher Scientific) and the StepONE Plus Real Time PCR system (Thermo Fisher Scientific) with final primer concentrations of 250 nM. Data were analyzed via the ΔΔCt method using *gyrA* as a reference gene and cDNA from QrgB* overproducing strains as the calibrator.

5' RACE was carried out using the 5' RACE kit from Invitrogen following the manufacturer's instructions using RNA extracted from *V. cholerae* cells harboring the *tag1* pBBRlux reporter plasmid. Primers for nested PCR amplification can be found in Appendix 2.

2.4.5 – Protein Expression and Purification.

The VpsT-pET28b expression vector was transformed into *E. coli* BL21λ(DE3). Sequence verified clones were cultured into 250 mL LB supplemented with kanamycin and grown at 35 °C shaking at 220 RPM to an OD_{600} of 0.7. Protein expression was

induced by adding 1 mM final concentration of IPTG. Growth temperature was switched to 16°C, shaking speed was lowered to 160 RPM, and cells were incubated overnight (approximately 16 hours). Cells were pelleted and resuspended in Buffer A (25 mM Tris-HCL, pH 7.5, 550 mM NaCl, 20 mM imidazole, cOmplete™ mini EDTA-free protease inhibitor tablets (Roche®) (2 per 50 mL), 5 mM β-mercaptoethanol) and lysed by homogenization.

Nickel nitrilotriacetic acid (Ni-NTA) resin (Qiagen) was incubated in Buffer A for 20 minutes at 4 °C. Cell lysates were centrifuged for 25 minutes at 10,000 x *g* at 4 °C to pellet insoluble material. The soluble lysate was incubated with the Ni-NTA resin for 30 minutes at 4 °C. The column was washed with 20 column volumes of Buffer A and eluted by step elution with Buffer A supplemented with 75, 125, 250, and 500 mM imidazole. Elution fractions were analyzed by sodium dodecyl sulfate polyacrylamide gel electrophoresis (SDS-PAGE) and those containing protein were pooled and dialyzed against Dialysis Buffer (25 mM Tris-HCL, pH 7.5, 150 mM NaCl, 5 mM BME, 10% glycerol) overnight at 16 °C. Protein concentrations were estimated using Bradford reagent (BioRad) with purified bovine serum albumin (Sigma) to generate a standard curve.

2.4.6 – Electrophoretic Mobility Shift Assay (EMSA).

EMSA reactions were carried out by incubating purified HIS tagged VpsT with 5' FAM labeled probes (FAM-*tag3*). 20 µL reactions consisted of 25 mM Tris-HCL, pH 7.5, 150 mM NaCl, 5 mM BME, and 10% glycerol. Poly dI-dC (Sigma) was added to all reactions at a concentration of 1 µg/µL. When indicated, c-di-GMP was added at a final concentration of 50 µM, otherwise, an equal volume water was added. 22 bp wild-type

or 20 bp mutant VpsT binding site single stranded oligomers were annealed to generate double stranded oligomers by incubating equal molar ratios of complementary oligonucleotides (Table 3) at 94 °C for 2 minutes and were cooled at room temperature overnight. 100X molar excess competitor was added when indicated. All components, except the labeled probe, were mixed at room temperature and incubated for 10 minutes. FAM-*tag3* probe was then added at a final concentration of 2.5 nM and reactions were incubated for 30 minutes at 30 °C. 10µL of reactions were loaded onto a pre-run 5% polyacrylamide Tris-Borate-EDTA (TBE) gel and electrophoresis was carried out for 90 minutes at 90 volts at 4 °C. Fluorescent band migration was visualized on Typhoon FLA 9000 Imager (GE Healthcare Life Sciences).

2.4.7 – Growth Assays.

Overnight cultures were diluted to a starting OD_{600} of 0.004 in 1 mL LB supplemented with ampicillin and IPTG. 200 µL of the culture was moved into wells of a 96-well plate (Cellstar) in triplicate and incubated at 35 °C with shaking at 220 RPM. After 2 hours of growth, PBS or MMS (Santa Cruz Biotechnology) at the indicated concentrations was added and growth was monitored by measuring OD_{600} every hour for 10 hours using an EnVision Multilabel Plate Reader (PerkinElmer). For calculating percent survival, the quotient of the OD_{600} of MMS treated wells divided by the OD_{600} of untreated wells was multiplied by 100 at a given time point.

2.4.8 – Statistical Analysis.

Data are represented as the mean ± SD. Statistical analyses (details in figure legends) were calculated with GraphPad Prism Ver. 6 (GraphPad, San Diego, CA). A p-value of < 0.05 was considered significant.

2.5 – Results

2.5.1 – C-di-GMP Induces Expression of *tag*

Bacteria use c-di-GMP to modulate disparate aspects of cell physiology ranging from biofilm formation to cell-cycle progression. While some of these phenotypes have been characterized in *V. cholerae,* we hypothesized there were uncharacterized c-di-GMP-regulated phenotypes (91). Thus, we screened a library of transcriptional fusion reporters for promoters regulated by c-di-GMP as previously reported (81). Of the seven promoters identified, one mapped upstream of the gene VC1672 (referred to as 6:C9 in our previous publication (74), encoding the DNA repair protein three methyladenine-glycosylase (Tag). DNA glycosylases initiate the BER pathway which recognizes and repairs non-bulky lesions in DNA. The original region of DNA isolated from the promoter screen, which we refer to as *tag1*, (Figure 2.1A) was ~1.4kb long and extended into the upstream gene VC1673 which encodes the AcrB-family transporter VexK. Based on the orientation of this DNA sequence, transcription could proceed into *tag.* To determine the region necessary for c-di-GMP mediated reporter activity, we modified the lengths of the 5' and 3' ends of *tag1* and measured promoter activity under different c-di-GMP levels (Figure 2.1B, C). To increase intracellular c-di-GMP levels, we overproduced the *Vibrio harveyi* DGC QrgB from a plasmid. We found this system generates c-di-GMP at concentrations that are similar to growth at low cell density, a growth phase of *V. cholerae* that naturally has high intracellular c-di-GMP due to quorum sensing regulation (55, 88). As a negative control, the active site mutant QrgB*, which does not change c-di-GMP levels, was similarly induced. Induction of QrgB significantly increased promoter activity of regions *tag1* through *tag3* relative to QrgB*

(Figure 2.1B). Moreover, the DNA sequence from -1067 to -566 in both *tag1* and *tag2* increase basal expression at low c-di-GMP concentrations relative to *tag3* (Figure 2.1C,

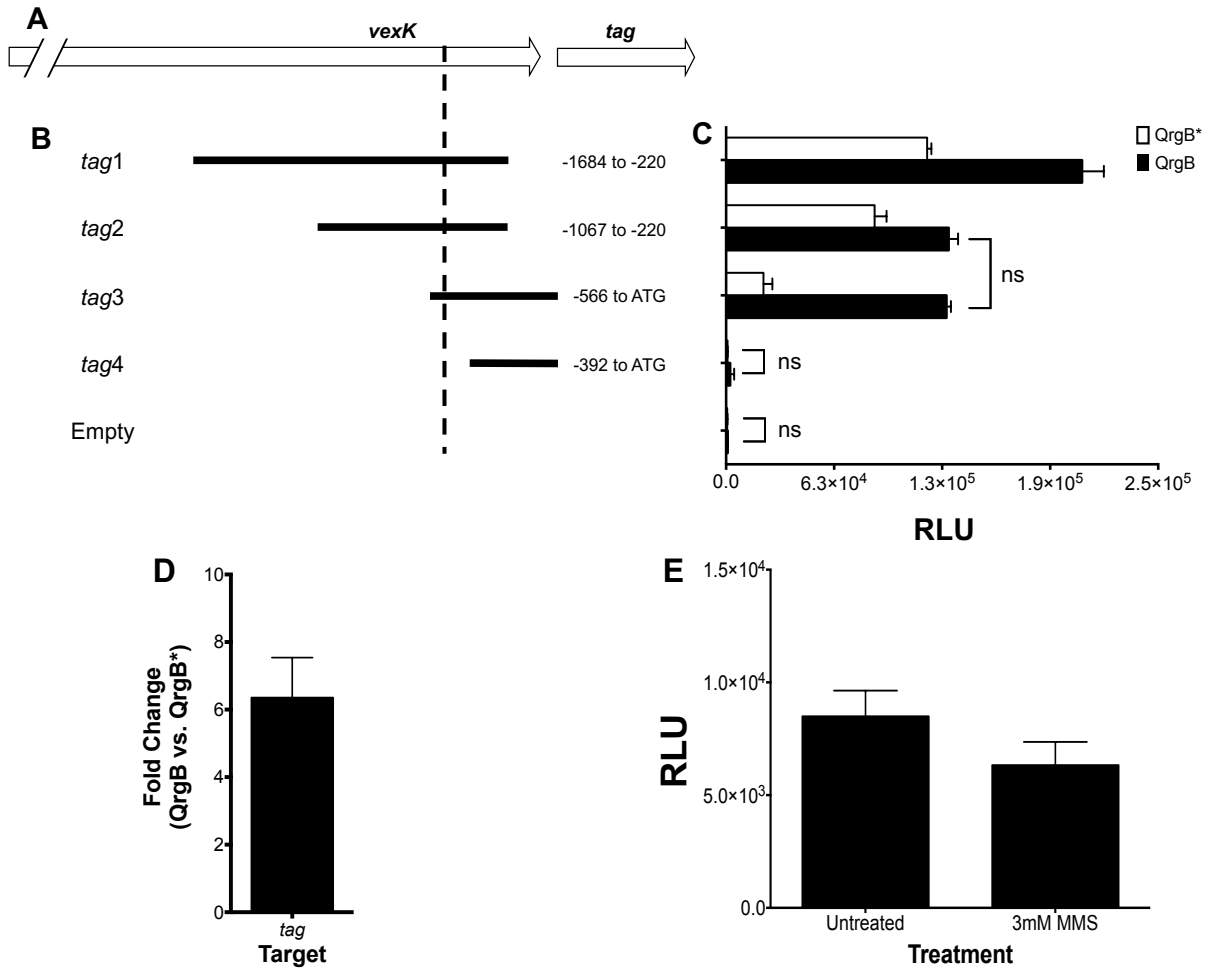

Figure 2.1: Promoter Characterization of *tag*

A and B) Diagrams depicting sizes and locations of promoter truncations relative to the ATG start codon of *tag* utilized for luciferase reporter assays. The vertical dashed line represents the +1 site determined by 5' RACE (see text). **C)** Luciferase reporter assay with promoter truncations in B. White bars are strains overproducing QrgB* while black bars are strains overproducing QrgB. Results are averages from three independent experiments with 3 technical replicates each. Error bars indicate standard deviation. All comparisons are considered significant except those with brackets and ns (non-significant) ($p > 0.05$) as determined by a Two-Way ANOVA followed by Tukey's Multiple Comparison Test. **D)** qRT-PCR analysis of *tag* mRNA expression levels. Data are average fold change between QrgB and QrgB* expressing strains from 3 biological replicates and error bars are standard deviation. **E)** The parent strain (Δ*vpsL)* harboring *tag3* (Luciferase reporter with *tag* promoter) was grown in the absence (left bar) or presence (right bar) of 3mM MMS. Data are the average from at least two experiments and error bars indicate standard deviation.

white bars). *tag3,* which encodes the sequence from -566 to the ATG start codon of *tag,* exhibited the greatest fold induction by c-di-GMP. Importantly, this reporter also demonstrates that transcription from these upstream regions proceeds into the *tag* open reading frame. Promoter activity of the DNA sequence immediately upstream of *tag* (*tag4*) was similar to activity of the promoter-less vector control indicating this region lacks an active promoter in our conditions (Figure 2.1C). To confirm that *tag* was induced by c-di-GMP, we quantified *tag* mRNA by quantitative real-time PCR and observed a ~6-fold increase in *tag* mRNA when QrgB is induced relative to QrgB* (Figure 2.1D).

In many instances, cellular stressors act as signals to induce gene expression of the pathways that respond to them, such as double-stranded breaks in DNA and the SOS response in *Escherichia coli* (92). We were interested in whether *tag* expression was also modulated by the addition of the methylating agent methyl methanesulfonate (MMS) as this chemical induces damage that would be repaired by Tag. Therefore, we constructed a transcriptional *lux* fusion to the *tag* promoter and measured *tag* expression in the presence and absence of 3 mM MMS. However, we observed no change in *tag* expression with the addition of MMS (Figure 2.1E).

Together these data indicate that c-di-GMP regulated expression of *tag* is driven by the sequence encoded from 566 to 392 base pairs upstream of the ATG start codon. Further, regions 5' to this promoter sequence increase basal expression. For the remainder of the experiments, the *tag3* reporter construct was used to assess *tag* transcription.

2.5.2 – VpsT and VpsR are Necessary for *tag* Expression

C-di-GMP stimulates biofilm production by activating the transcription factors VpsT and VpsR (30, 81). It also inhibits motility by anti-activation of the master regulator of flagella biosynthesis FlrA (50). Therefore, we reasoned c-di-GMP induction of *tag* could depend on either of these three c-di-GMP-dependent transcription factors. To test this hypothesis, we conjugated the *tag* reporter plasmid into *V. cholerae* strains

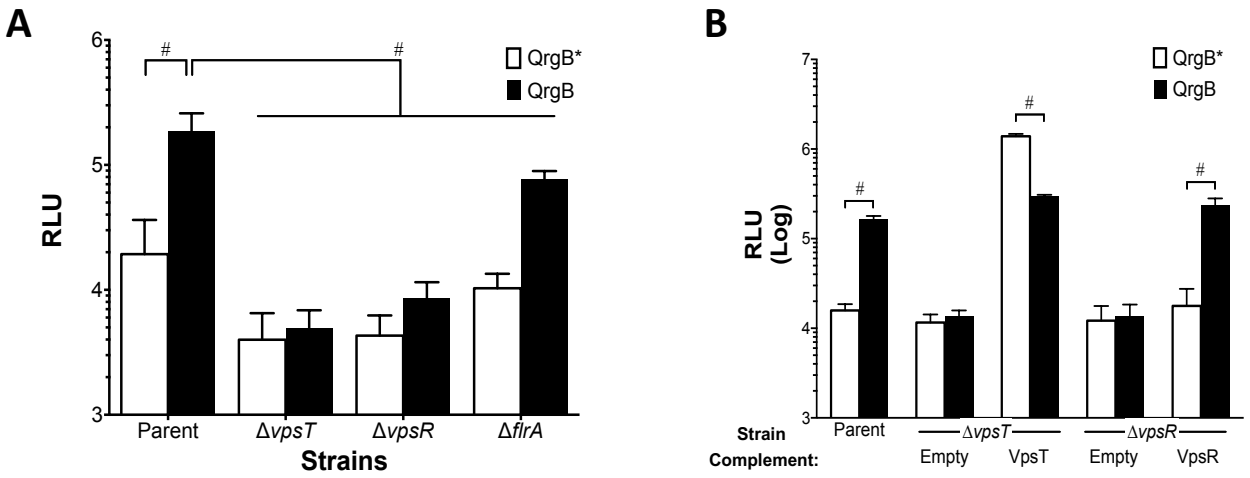

Figure 2.2: VpsT and VpsR Are Necessary For c-di-GMP Mediated *tag* Expression **A)** Parent strain (Δ*vpsL)* and isogenic knockouts (Δ*vpsT,* Δ*vpsR,* and Δ*flrA*) harboring either QrgB* or QrgB and the *tag3* luciferase reporter construct were grown in the presence of 100 μM IPTG to induce protein expression. Data are the average from at least three experiments and error bars indicate standard deviation. # indicate statistical significance ($p < 0.05$) between strains as determined by a Two-Way ANOVA followed by Tukey's Multiple Comparison Test. **B)** *tag* expression in the Δ*vpsT* and Δ*vpsR* mutant backgrounds with vectors harboring IPTG inducible VpsT or VpsR, respectively. All strains contain *tag3* as well as either QrgB* or QrgB. Expression in strains with an empty expression vector were included as controls. Data represent averages from at least three different experiments. Error bars indicate standard deviation. # indicate statistical significance ($p < 0.05$) comparing QrgB* and QrgB for that given strain/condition as determined by a two-tailed Students *t*-test.

lacking either *vpsT, vpsR,* or *flrA* and we assayed *tag* promoter activity at different intracellular c-di-GMP levels. In the parent and Δ*flrA* isogenic mutant, *tag* expression increased approximately 10-fold with QrgB overproduction compared to the QrgB*

control. Although *tag* expression with QrgB overproduction was 2.4-fold lower in the Δ*flrA* strain compared to the WT, this difference was not statistically significant (Figure 2.2A). However, in the Δ*vpsT* and Δ*vpsR* backgrounds, QrgB overproduction had no effect on *tag* expression compared to the QrgB* control, indicating VpsT and VpsR are necessary for *tag* expression (Figure 2.2A). We then complemented the Δ*vpsT* and Δ*vpsR* mutants by over-expressing VpsT or VpsR, respectively, from a plasmid. Complementing the Δ*vpsR* strain with VpsR restored c-di-GMP mediated *tag* expression similar to that of the parent strain (Figure 2.2B). Interestingly, complementation of the Δ*vpsT* mutant by over-expressing VpsT resulted in increased *tag* expression regardless of QrgB* or QrgB expression (Figure 2.2B). We did observe a 2-fold decrease in *tag* expression when VpsT and QrgB were over-expressed compared to VpsT and QrgB*, however, this difference was relatively small compared with the 100-fold induction caused by VpsT when comparing to the empty vector control and thus we do not consider it biologically meaningful (Figure 2.2B). This experiment suggests that high concentrations of VpsT do not require elevated c-di-GMP to activate *tag*. Either VpsT can function in a c-di-GMP-independent manner, or the basal concentration of c-di-GMP in *V. cholerae* at these conditions is high enough to activate the increased concentrations of VpsT. These results demonstrate that VpsT and VpsR are necessary for c-di-GMP mediated *tag* expression.

2.5.3 – VpsT Activates *tag* Transcription in *E. coli* and Binds to the *tag* Promoter in vitro

Since *vpsT* expression is activated by *vpsR* in a c-di-GMP-dependent manner (93), and *vpsT* was required for *tag* expression (Figure 2.2A and 2.2B), we

hypothesized VpsT was the primary c-di-GMP-dependent activator of *tag*. To test this hypothesis, we measured *tag* expression in a heterologous host, *Escherichia coli*. We reasoned this *in vivo* system would allow us to isolate the impact of VpsT and VpsR on *tag* expression without pleiotropic effects due to the complex regulatory relationship between VpsT and VpsR (94, 95). Thus, we measured *tag* expression in *E. coli*

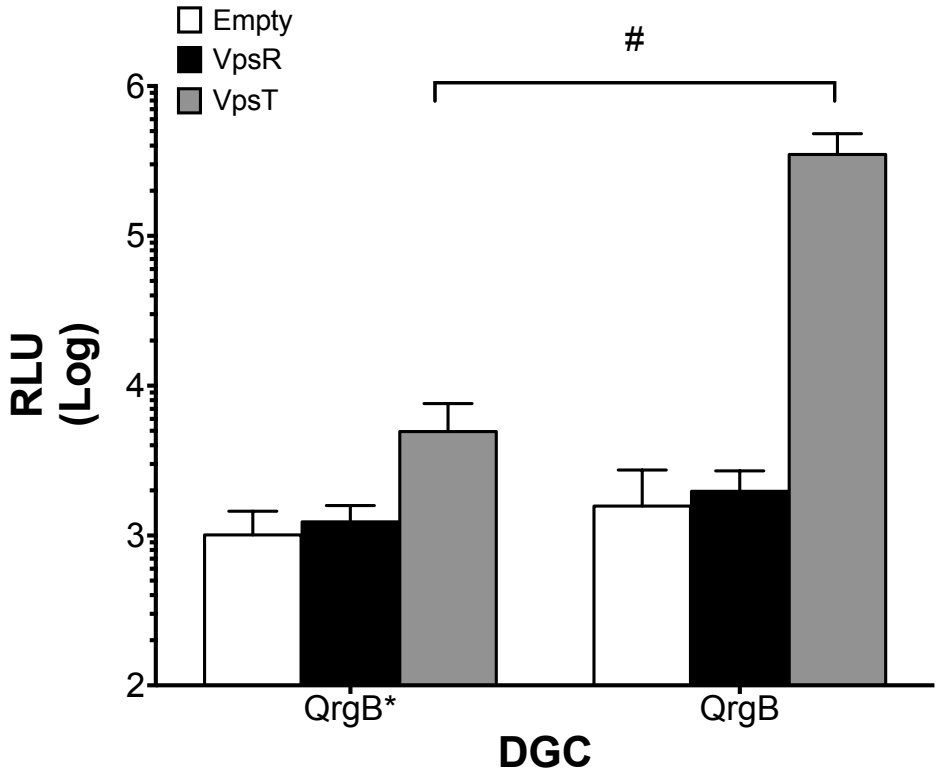

Figure 2.3: VpsT and c-di-GMP are Needed for *tag* Expression in *E. coli*
A three-plasmid system was established wherein the *tag* reporter, either QrgB* or QrgB, and either VpsT, VpsR, or empty vector were transformed into DH10b *E. coli*. IPTG (100 μM) was added at subculture and luciferase activity was measured at mid-exponential phase. Data are averages from three experiments. Error bars indicate standard deviation. # indicate statistical significance ($p < 0.05$) comparing QrgB* and QrgB for each condition as determined by a two-tailed Student's *t*-test.

expressing QrgB* and either an empty vector control, VpsR, or VpsT. In either condition, *tag* expression was not significantly induced. Next, we repeated the experiment co-expressing VpsR or VpsT with QrgB. High intracellular c-di-GMP with the vector control or with VpsR production did not alter *tag* expression in *E. coli.*

However, when VpsT and QrgB were over-expressed, *tag* expression increased approximately 200-fold relative to the empty vector control (Figure 2.3). These data indicate VpsT, but not VpsR, is sufficient to regulate *tag* expression in a c-di-GMP-dependent manner in *E. coli* and that no other *V. cholerae* specific proteins are required for this induction.

To determine if VpsT bound to the *tag* promoter *in vitro*, we carried out electrophoretic mobility shift assays (EMSA). We generated 5' FAM labeled probes containing the *tag3* region (Figure 2.1B, FAM-*tag3*) and incubated it with purified histidine tagged VpsT for *in vitro* binding. VpsT partially bound to FAM-*tag3* at a concentration of 300 nM and almost completely shifted the probe at 600 nM (Figure 2.4, lane 1-7). C-di-GMP enhances the *in vitro* DNA binding ability of VpsT at promoters of genes involved in biofilm formation (30). Thus, to determine if c-di-GMP enhanced DNA binding at the *tag* promoter, we included 50 μM c-di-GMP in the binding reaction (Figure

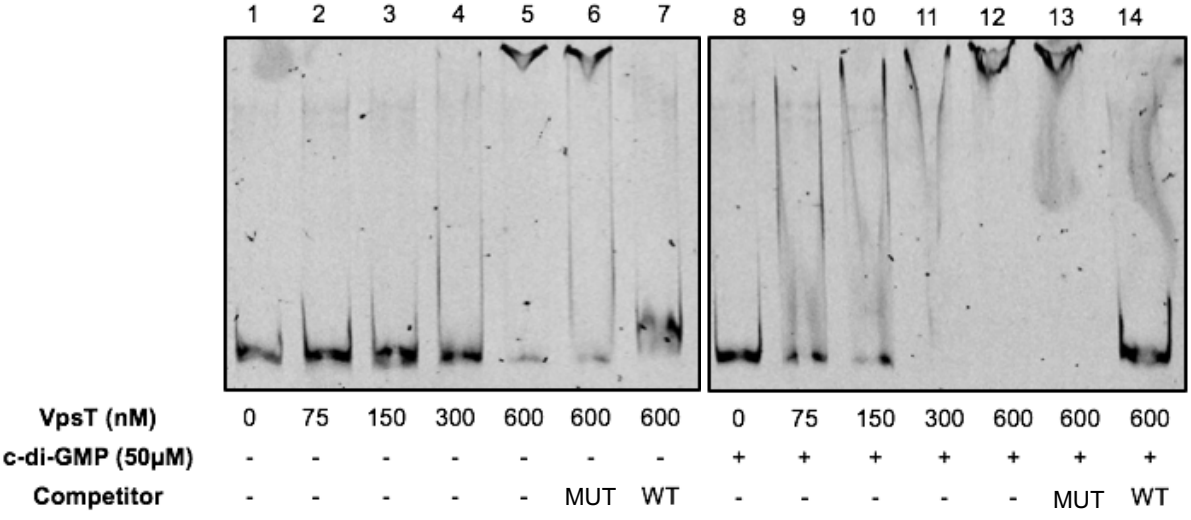

Figure 2.4: C-di-GMP Enhances VpsT Affinity at the *tag* Promoter in vitro
(Left, 1-7) Increasing concentrations of purified HIS tagged VpsT was incubated with the fluorescently labeled *tag* promoter (FAM-*tag3)*. When indicated, the mutant (MUT) or wild-type (WT) VpsT binding site competitor was added to the reaction at 100X excess relative to the probe concentration. (Right, 8-14) The same as part A except 50 μM c-di-GMP was added to the reactions.

2.4, lane 8-14). Partial binding occurred at 75 nM VpsT with near complete shifting observed at 300 nM VpsT, indicating c-di-GMP enhances VpsT DNA binding at the *tag* promoter *in vitro* in a similar manner to the *vpsL* promoter (31, 96). The U-shaped bands that we observed when c-di-GMP was added to the binding reaction (Figure 2.4, lane 9-11) are likely the result of the dissociation between c-di-GMP and VpsT during electrophoresis, which would result in VpsT dissociating from the labeled probe, as previously described by Ayala *et al.* (96).

Recently, a 20-22 bp VpsT binding consensus site containing a palindromic sequence was described (31). We reasoned if the interaction between VpsT and the *tag* promoter was specific, the addition of a 22 bp oligonucleotide containing the VpsT binding site to the binding reaction (WT competitor) would compete away interactions between VpsT and FAM-*tag3*. Conversely, adding an oligonucleotide with a disrupted palindromic region (MUT competitor) would have no effect on interactions between VpsT and FAM-*tag3.* Indeed, the addition of the WT competitor to the binding reaction without c-di-GMP resulted in a nearly complete reduction in the shifted probe while addition of the mutant competitor did not compete away VpsT binding from FAM-*tag3* (Figure 2.4, lanes 6 and 7). In the presence of 50 μM c-di-GMP, the WT competitor completely competed away binding of VpsT while the mutant competitor had no effect (Figure 2.4, lanes 13 and 14). These results indicate VpsT specifically binds to the *tag3* region and c-di-GMP increases the affinity of VpsT binding. Taken together, these data suggest VpsT directly regulates *tag* expression and that VpsR regulates *tag* expression indirectly through induction of VpsT (31).

2.5.4 – C-di-GMP Increases Tolerance to the Alkylating Agent MMS

Tag is an enzyme in the BER pathway that recognizes and removes methylated adenines (3meA) and guanines (3meG) at the N3 position. 3meA is a lethal, non-mutagenic lesion that blocks DNA replication whereas 3meG is innocuous (97). Since c-di-GMP induces *tag* expression, we hypothesized cells with high intracellular c-di-GMP concentrations would be more tolerant to MMS treatment, which generates 3meA,

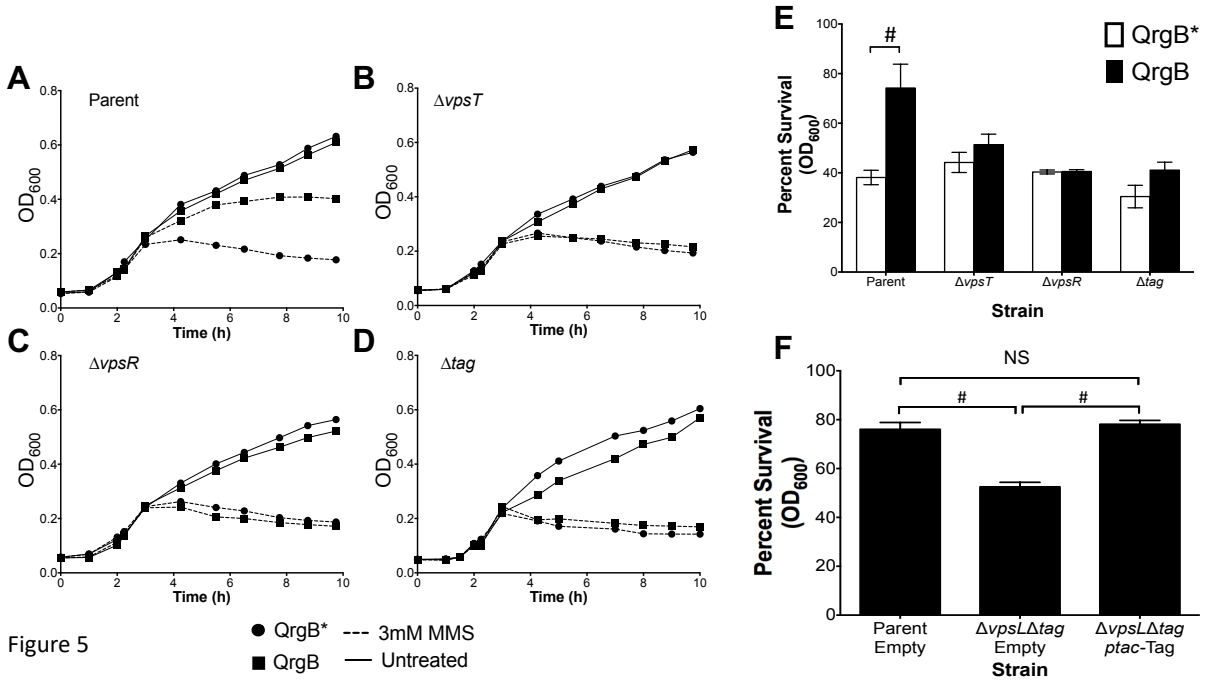

Figure 5

Figure 2.5: High c-di-GMP Increases Tolerance to the Methylating Agent MMS A-D) Strains were subcultured 1:1000 and grown in the presence of 100μM IPTG to overproduce QrgB* and QrgB. After two hours, cells were left untreated (solid lines) or treated with 3 mM MMS (dashed lines) and OD_{600} was measured every hour for 10 hours. Error bars, which are obscured by symbols, are standard deviation. **E)** Quantification of survival (percent of treated OD divided by untreated OD) for a given strain after 6hrs of treatment. **F)** Complementation of the Δ*vpsL*Δ*tag* strain by expressing Tag in trans. Error bars are standard deviation. # indicate a p-value < 0.05 determined by a two-tailed Student's *t*-test.

than cells with basal intracellular c-di-GMP concentrations. To test this, QrgB or QrgB* was induced for two hours in the parent background before treatment with 3 mM MMS and growth was quantified every hour for 10 hours by measuring OD_{600}. The parent

strain used in these experiments is a Δ*vpsL V. cholerae* mutant that is incapable of forming biofilms, thus biofilm formation itself induced by c-di-GMP is not responsible for the observed differences.

V. cholerae expressing QrgB* or QrgB displayed similar growth curves for all strains examined in the absence of MMS treatment (Figure 2.5A-D, solid lines), indicating c-di-GMP has no deleterious effects on growth under these conditions. In the parent strain, induction of c-di-GMP led to significantly more growth in the presence of MMS (Figure 2.5A, squares). Quantification of optical density after 6 hours of treatment revealed increased c-di-GMP led to an approximate 2-fold increase in survival compared to the QrgB* control (Figure 2.5E).

As VpsT and VpsR were necessary for *tag* expression, we repeated the experiment in Δ*vpsT* and Δ*vpsR* backgrounds and found these strains lacked a c-di-GMP mediated increase in MMS tolerance (Figure 2.5B, C, E). Similarly, high c-di-GMP did not significantly increase survival of a *V. cholerae* Δ*tag* mutant (Figure 2.5D, E). Interestingly, the Δ*tag* mutant was only slightly more sensitive to MMS compared with the parent strain (Figure 2.5E), indicating that in basal c-di-GMP conditions, Tag plays a small role in MMS resistance. Complementing the Δ*tag* strain by overproducing Tag from a plasmid restored parent survival (Figure 2.5F). Together, these data indicate high c-di-GMP conditions promote the growth in the presence of alkylation damage.

Induction of *tag* by c-di-GMP suggests that DNA repair might be important in *V. cholerae* biofilm formation. To test this, we measured biofilm formation of the WT and Δ*tag* mutant exposed to 0 and 6 mM MMS. Deletion of *tag* did not affect biofilm formation at either concentration, which we hypothesize is due to redundant

mechanisms for dealing with MMS damage in a biofilm. Further, there was no significant change in biofilm production in response to MMS addition (Figure 2.6).

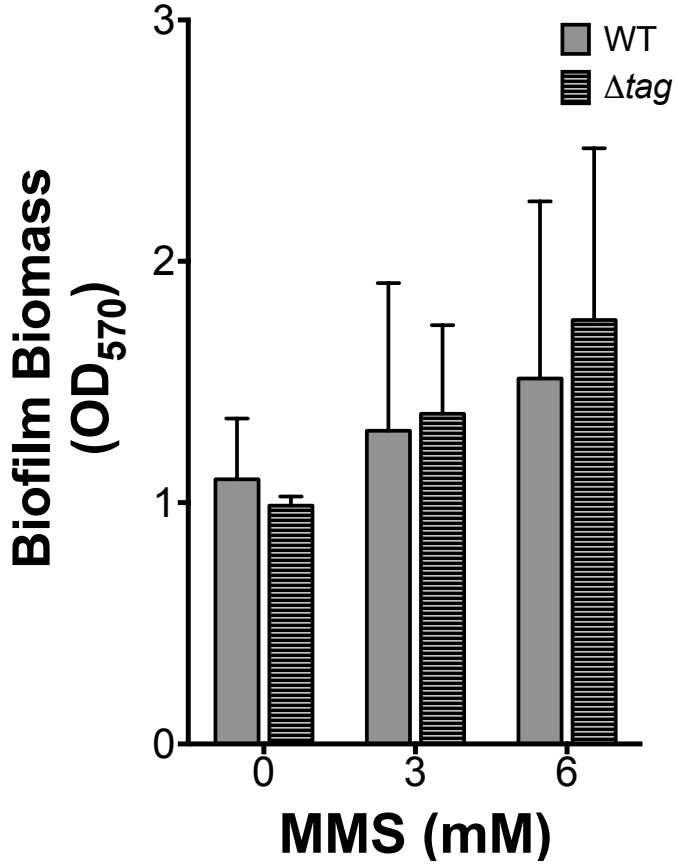

Figure 2.6: Tag and MMS do not Contribute to Biofilm Formation in *V. cholerae*. Strains were cultured 1:100 from overnight cultures into wells of a 96-well plate with either 0, 3, or 6 mM MMS added. Biofilms were grown at 35°C while shaking at 220 RPM for 24 hours. After 24 hours, cultures were removed and a crystal violet assay done using .4% crystal violet following the protocol from (56). Data are average biofilm biomass (absorbance at 570 nm) from three independent experiments and error bars are standard deviation.

2.6 – Discussion

The dinucleotide second messenger c-di-GMP is best known for its role in transition from a motile state to a biofilm in many Gram-negative bacteria including *V. cholerae* (98). In many cases, genes involved in biofilm formation are turned on through changes in the activity of transcription factors (99, 30, 81, 50). Past studies indicate

there are potentially multiple genes or pathways regulated by c-di-GMP besides genes directly related to motility or biofilm formation (66, 30, 81, 100). In this study, we demonstrate c-di-GMP regulates expression of the DNA repair gene *tag*. Strains lacking the biofilm regulators VpsT and VpsR were unable to induce *tag* expression with high c-di-GMP. Importantly, we demonstrate VpsT induction of *tag* leads to increased tolerance to MMS when cells have high intracellular c-di-GMP independent of biofilm formation.

We determined that the region necessary for *tag* expression by c-di-GMP is between 566 bp and 392 bp upstream of the ATG translational start codon. Additionally, this region is in the coding region of the upstream gene *vexK* encoding the Resistance-Nodulation-Division (RND) multidrug efflux pump VexK. Interestingly, VexK can efflux detergents and was upregulated in human volunteers of *V. cholerae* infection, while *tag* was not identified as an *in vivo* expressed gene, suggesting *tag* is not upregulated during human host infection and these genes are under independent regulatory control (101, 102).

The putative 5' untranslated region (UTR) for *tag* mRNA is approximately 400 bp. The most common 5' UTR lengths in the Gram-negative organisms *E. coli* and *Klebsiella pneumoniae* range from 25-35 bps, with the longest reaching 700 bps (103). Thus, the relatively long 5' UTR of the *tag* transcript suggests c-di-GMP may be only one of the signals regulating *tag* expression in *V. cholerae*. It is possible there may be additional transcriptional start sites closer to the translation start site of *tag* that were missed in our analyses; however, a luciferase fusion to this region (*tag4*) showed no activity above the vector control level and no such start sites were detected using a

systematic RNA-Seq approach by Papenfort *et al.* (Figure 2.1C, (155)). The function of this long 5'-UTR in DNA repair is an intriguing question that warrants further investigation. Interestingly, a systematic search for small RNAS (sRNAs) detected a putative sRNA in this 5'-UTR from bases -227 to -121 relative to the ATG start codon located on the coding strand of the *tag* gene (104). Due to the lack of additional transcription start sites in this region, we hypothesize this sRNA might be processed from the 5'-UTR of *tag.* Whether this sRNA has any biological function remains to be determined.

In *V. cholerae*, three transcription factors act to sense and respond to c-di-GMP by altering transcription at key promoters of genes necessary for VPS or flagella biosynthesis. VpsR and VpsT are c-di-GMP responsive transcription factors that induce expression of the VPS operon when intracellular c-di-GMP concentrations are high (16, 17, 74). We demonstrate both VpsR and VpsT are necessary for induction of *tag* by c-di-GMP, but VpsT appears to directly regulate this gene (Figure 2.6). Binding site sequences exist for VpsT in the promoters of *vpsL,* a component of the VPS operon, and the promoter for the stationary phase sigma factor *rpoS*; however, we could not identify a canonical VpsT binding site in the *tag* promoter (31, 106). We are currently working to determine the VpsT binding sequence in the *tag* promoter and speculate the divergence in sequence similarity between the VpsT binding sites represent a mechanism to fine-tune VpsT transcriptional activity in response to differing levels of c-di-GMP. FlrA, the c-di-GMP responsive transcription factor necessary for flagellar biosynthesis, was not needed for *tag* induction by c-di-GMP suggesting *tag* expression is not advantageous in a motile lifestyle. A previous microarray analysis suggests that

c-di-GMP can regulate other forms of DNA repair in addition to the BER pathway in *V. cholerae*. Overproduction of a DGC in the El Tor biotype A1552 resulted in upregulation of *mutL*, a gene involved in methyl-directed mismatch repair, while in the Classical biotype O395, DGC overproduction led to an increase in the gene encoding photolyase (*phrB*), which is involved in light-dependent DNA repair after ultraviolet radiation damage, although these regulatory pathways have not been studied (56). These multiple connections to DNA repair suggest that *tag* induction by c-di-GMP may just be one example of how *V. cholerae* uses c-di-GMP signaling to coordinate DNA repair.

Various stressors, including DNA damaging agents, increase biofilm formation in *E. coli* and *Pseudomonas aeruginosa* (107, 108). Additionally, the SOS response pathway regulates biofilm formation in *P. aeruginosa*, demonstrating a link between DNA damage and biofilm formation (109). In contrast, growth in a biofilm increases mutability in *P. aeruginosa* through production of endogenous reactive oxygen species (110). These findings demonstrate stress can induce biofilm formation, or, conversely, biofilms can induce stress. We hypothesized c-di-GMP induced *tag* expression likely accompanies environmental biofilm formation in *V. cholerae* from the following pieces of evidence: i) VpsT regulates *tag* expression in high c-di-GMP conditions (Figure 2.2), ii) *vpsT* expression is epistatic to *vpsR* (93), and iii)high levels of VpsR activated by c-di-GMP result in biofilm formation (48). However, biofilm formation was similar in the WT and Δ*tag* strains in untreated and MMS treated conditions. We hypothesize that the fitness advantage of *tag* induction by c-di-GMP may be relevant under other environmental conditions not tested here.

We demonstrate a novel example of dinucleotide second messenger signaling regulating a core cellular process, DNA repair. It is becoming clear that the roles of the VpsR and VpsT pathway expand beyond biofilm formation in *V. cholerae*. Indeed, this c-di-GMP regulatory node controls a variety of phenotypes in response to changing c-di-GMP including type II secretion, acetoin production, and *tfoY* transcription (Figure 2.7). Consequently, these two transcription factors should not be viewed solely as biofilm regulators, but rather as the central transcriptional regulators of c-di-GMP regulated phenotypes in *V. cholerae.*

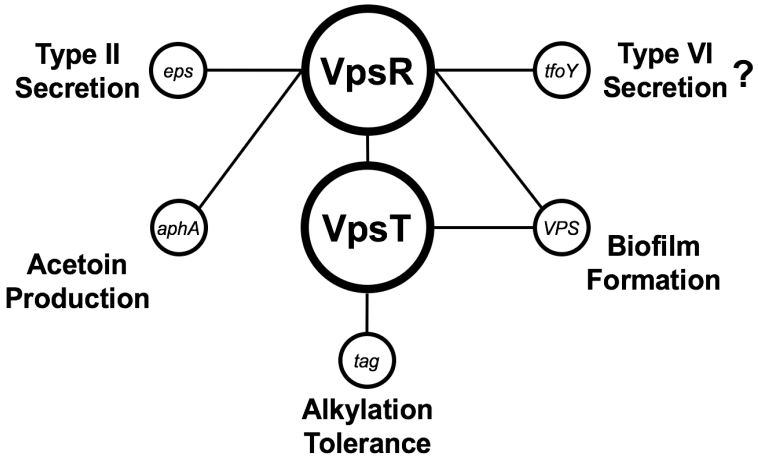

Figure 2.7: Model of c-di-GMP Regulatory Network in *V. cholerae*.
In response to high c-di-GMP, VpsR becomes an active transcription factor and induces the expression of *vpsT.* VpsT is also a c-di-GMP dependent transcription factor and, together, VpsT and VpsR induce expression of genes involved in biofilm formation. C-di-GMP activated VpsR has been shown to directly regulate promoters other than those that regulate biofilm production such as *tfoY,* which regulates motility and type VI secretion, the *eps* operon involved in type II secretion, and *aphA,* which regulates acetoin production. In this work, we uncovered another phenotype regulated by the central c-di-GMP dependent transcription factors: alkylation tolerance through induction of *tag* indirectly by VpsR and directly by VpsT.

Chapter 3 – Cyclic di-GMP Controls Antioxidant Production and Hydrogen Peroxide Tolerance in *Vibrio cholerae*

3.1 – Preface

Contents of this chapter were published in the journal Applied and Environmental Microbiology in 2019 (Citation: Fernandez NL, Waters CM. 2019. Cyclic di-GMP Increases Catalase Production and Hydrogen Peroxide Tolerance in *Vibrio cholerae*. Applied and Environmental Microbiology 85:e01043-19.). Per American Society for Microbiology guidelines "Authors in ASM journals retain the right to republish discrete portions of his/her article in any other publication (including print, CD-ROM, and other electronic formats) of which he or she is author or editor, provided that proper credit is given to the original ASM publication. ASM authors also retain the right to reuse the full article in his/her dissertation or thesis".

3.2 – Abstract

Vibrio cholerae is a Gram-negative bacterial pathogen that causes the disease cholera, which affects nearly 1 million people each year. In between outbreaks, *V. cholerae* resides in fresh and saltwater environments where it is able to persist through changes in temperature, oxygen, and salinity. One key characteristic that promotes environmental persistence of *V. cholerae* is the ability to form multicellular communities, called biofilms, that often adhere to biotic and abiotic sources. Biofilm formation in *V. cholerae* is positively regulated by the dinucleotide second messenger cyclic dimeric guanosine monophosphate (c-di-GMP). While most research on the c-di-GMP regulon has focused on biofilm formation or motility, we hypothesized the c-di-GMP signaling network encompassed a larger set of effector functions than reported. We found that high intracellular c-di-GMP increased catalase activity approximately 4-fold relative to strains with unaltered c-di-GMP. Genetic studies demonstrated that c-di-GMP mediated

catalase activity was due to increased expression of the catalase encoding gene *katB*. Moreover, c-di-GMP mediated regulation of catalase activity and *katB* expression required the c-di-GMP dependent transcription factors VpsT and VpsR. Lastly, we found that high c-di-GMP increased survival after H_2O_2 challenge in a *katB-, vpsR-,* and *vpsT*-dependent manner. Our results indicate antioxidant production is regulated by c-di-GMP uncovering a new node in the growing VpsT and VpsR c-di-GMP signaling network of *V. cholerae.*

3.3 – Introduction

The Gram-negative bacterium *Vibrio cholerae* is the human pathogen that causes the diarrheal disease cholera. The most common route to infection is consumption of contaminated food or water, after which *V. cholerae* traverses the stomach and colonizes the small intestines. Cholera patients lose liters of fluid and dissolved ions through toxin-mediated changes to the host intestinal tract, allowing *V. cholerae* to exit the host, re-enter a water source, and perpetuate its infectious cycle. In addition to the harsh conditions of the human gastrointestinal tract*, V. cholerae* must adapt to numerous stresses in the aquatic environment. These environmental stresses include temperature fluctuations, eukaryotic predation, and exposure to chemical insults like reactive oxygen species (ROS) (111).

As an aquatic organism, *V. cholerae* is exposed to varying concentrations of dissolved oxygen and ROS produced abiotically through photochemical reactions between sunlight and dissolved organic matter in the ocean (112, 113). ROS can also be produced biotically through metabolic processes in aerobic environments by phytoplankton, another potential reservoir of *V. cholerae* (114). In response to the

multiple routes of exposure to ROS, it is not surprising that *V. cholerae* has multiple ROS defense systems including two paralogues of the oxidative stress responsive transcription factor OxyR, two catalases, and multiple peroxidases (115–117). Another mechanism to increase tolerance to ROS is the production of surface adhered communities encased in an exopolysaccharide matrix also known as biofilms.

Many bacterial species, including *V. cholerae,* have increased tolerance to ROS such as hydrogen peroxide (H_2O_2) when grown in biofilms compared to planktonic counterparts (118–120). Biofilm formation in *V. cholerae* is regulated by the bacterial second messenger molecule cyclic dimeric guanosine monophosphate (c-di-GMP), which is produced by diguanylate cyclase (DGC) enzymes. C-di-GMP alters bacterial physiology by modulating transcription, translation, and/or protein function (5). In *V. cholerae,* a common mechanism of c-di-GMP signaling is modulation of gene expression by three c-di-GMP dependent transcription factors: VpsR, VpsT, and FlrA (48, 30, 50). c-di-GMP activates the transcription factors VpsR and VpsT, resulting in increased transcription of genes involved in synthesis of the biofilm matrix component *Vibrio* polysaccharide (VPS) (48, 30, 121). In contrast, c-di-GMP acts as an anti-activator of FlrA, which causes decreased expression of genes necessary for flagellar biosynthesis (50). C-di-GMP can also bind to two riboswitches, Vc1 and Vc2. Binding of c-di-GMP to Vc1 functions as an ON-switch to induce production of the adhesin GbpA, while binding of c-di-GMP to Vc2 functions as an OFF-switch to inhibit production of the transcription factor TfoY (12, 55). As cells receive signals to disperse from the biofilm, phosphodiesterase (PDE) enzymes, which degrade c-di-GMP, become activated.

These PDEs then deplete the intracellular concentration of c-di-GMP, promoting a switch from a sessile biofilm lifestyle to a motile one (reviewed in (5)).

While VpsR and VpsT were initially discovered as regulators of biofilm production, other c-di-GMP dependent functions have emerged. For example, c-di-GMP and VpsR transcriptionally regulate genes in the type II secretion operon as well as *tfoY,* a gene involved in driving dispersive motility and regulating type VI secretion (122, 66, 55). VpsT negatively regulates expression of genes involved in flagellar biosynthesis; however, the mechanism is not known (30). Additionally, Ayala *et al.* demonstrated VpsT negatively regulates the transcription of the stationary phase sigma factor RpoS (106). Recently, we found that c-di-GMP and VpsT induced expression of the DNA repair gene *tag* to promote survival after alkylation stress (123). These studies demonstrate c-di-GMP regulation extends beyond biofilm formation and motility in *V. cholerae*.

In this study, we uncovered an additional role for c-di-GMP: positively regulating catalase activity by increasing transcription of the catalase encoding gene *katB* via a VpsR- and VpsT-dependent mechanism. We further show that c-di-GMP dependent catalase activity was necessary for survival after exposure to the ROS H_2O_2. Our results expand the regulatory network of c-di-GMP to include antioxidant production, demonstrating that elevated c-di-GMP enhances the oxidative stress response in *V. cholerae.*

3.4 – Methods and Materials

3.4.1 – DNA Manipulations and Growth Conditions.

V. cholerae C6706 Str2 was used as the wild-type and the low biofilm forming derivative Δ*vpsL* was used as the Parent strain in the text (124, 88). All vectors were constructed by Gibson Assembly (NEB). Chromosomal deletion strains were constructed using the allele exchange vector pKAS32 digested with KpnI and SacI (NEB, High Fidelity). Luciferase reporters were constructed using the luciferase reporter vector pBBRlux digested with BamHI and SpeI (NEB). Expression vectors for VpsT and VpsR were constructed by removing the ribosome binding site (RBS), green fluorescent protein, and chloramphenicol acetyltransferase from pEVS143 with BamHI and EcoRI digests (NEB) (88). The VpsT purification vector was constructed elsewhere (123). Expression vectors for *katB* and *katG* were constructed as follows: pHERD20T was amplified with primers flanking the ampicillin resistance gene using inverse PCR resulting in a linear PCR fragment lacking the ampicillin resistance gene (125). The chloramphenicol resistance gene from pBBRlux was amplified by PCR and the two linear fragments were circularized by Gibson Assembly. Plasmids were introduced into *V. cholerae* through biparental conjugation using *Escherichia coli* S17 as the donor strain. *V. cholerae* harboring the plasmid of interest was selected for using Polymixin B (10 U/mL) with the relevant antibiotic. Antibiotics and reagents were used at the following concentrations unless stated otherwise: Ampicillin (100 μg/mL), Kanamycin (100 μg/mL), chloramphenicol (10 μg/mL), 100 μM isopropyl β-D-1-thiogalactopyranoside (IPTG). Cultures were grown in Lysogeny Broth (LB, Acumedia) at 35°C, 220 RPM unless otherwise stated.

3.4.2 – Catalase Assay.

Measurement of catalase activity was adapted from (126) with the following changes: Overnight cultures were diluted 1:100, the optical density at 600 nm (OD_{600}) was measured, and the resulting value was multiplied by the dilution factor (100) to obtain the actual optical density of the solution. The cell solutions were diluted to a starting OD_{600} of 0.040 in 5 mL LB in 18 x 150 mm borosilicate test tubes supplemented with necessary antibiotics and IPTG. Cultures were grown at 35°C with shaking at 220 RPM until the OD_{600} reached approximately 2.0, moved to 15 mL falcon tubes (Corning®), and were pelleted by centrifugation (4,000 x g for 3 minutes). Pellets were resuspended in 100 µL of sterile 1X PBS to create a viscous cell solution that were adjusted to an OD_{600} of 150 in 100 µL final volume in Pyrex test tubes (13 x 100 mm, borosilicate). 200 µL of catalase reaction buffer (1% Triton-X100, 15% hydrogen peroxide in 1X PBS) was added to the test tubes and the solution was mixed using disposable 10 µL loops (BD Difco). Tubes were incubated at room temperature until gas production subsided (approximately 5-10 minutes). A standard curve was generated by mixing purified bovine catalase (Sigma, 570 U/µL) diluted in 1X PBS with 200 µL of catalase reaction buffer. At 10 minutes of incubation, images of the tubes were taken with an iPad Air (iOS 12.1.4) and the height from the bottom of the tube to the top of the foam were measured in both the standards and samples using the software ImageJ and an internal 1-inch reference mark for each picture. GraphPad Prism was used to generate the standard curve and interpolate the sample catalase activity using linear regression. Data presented is catalase activity (Units) normalized to cell number (OD_{600}).

3.4.3 – RNA Isolation and Quantitative Real-Time PCR (qPCR).

Three biological replicate overnight cultures were diluted to a starting OD_{600} of 0.040 in 2 mL LB supplemented with ampicillin and IPTG and grown until an OD_{600} of approximately 1.0 at 35°C and 220 RPM. 1 mL of each replicate was pelleted and RNA was extracted using the TRIzol® reagent following the directions in the manual (Thermo Fischer Scientific). Purified DNA was quantified using a NanoDrop spectrophotometer (Thermo Fischer Scientific). 5 µg of purified RNA was treated with DNAse (Turbo DNAse, Thermo Fischer Scientific). cDNA synthesis was carried out using the GoScript™ Reverse Transcription kit (Promega). cDNA was diluted 1:30 into molecular biology grade water and used as template in qRT-PCR reactions using SYBR Green (Applied Biosystems™) as the method of detection. Reactions consisted of 5 µL 2.5 µM primer 1, 5 µL of 2.5 µM primer 2, 5 µL of diluted cDNA template, and 15 µL of 2X SYBR green consisting of dNTPs and AmpliTaq Gold® DNA polymerase (see Table 4 for primer sequences). Each plate had technical duplicates and biological triplicate samples as well as no reverse transcriptase controls to check for genomic DNA contamination. The StepOnePlus Real Time PCR system was used for qRT-PCR with the following thermocycling conditions: 95°C for 20 seconds then 40 cycles of 95°C for 2 seconds and 60°C for 30 seconds. Melting curves were included to ensure PCR products had single amplicons and primer dimers were absent. Data were analyzed by the ΔΔCt method using *gyrA* as a housekeeping or reference target.

3.4.4 – Luciferase Reporter Assays.

3.4.4.1 – V. cholerae Reporter Assays.

Overnight cultures of *V. cholerae* harboring *katB* transcriptional fusions to luciferase in pBBRlux were diluted 1:100 in 1 mL LB supplemented with ampicillin, chloramphenicol, and IPTG in 1.5 mL microcentrifuge tubes. 200 µL of cell solution was aliquoted into wells of a black 96-well plates (Costar). Plates were incubated at 35°C while shaking at 220 RPM until the OD_{600} reached approximately 0.250, and luciferase activity was measured using an Envision plate reader (Perkin Elmer). Luciferase activity (RLU) was normalized for cell number by dividing RLU by the OD_{600} at the time of the reading (Normalized Luminescence). For experiments where H_2O_2 were added to the cultures, overnight cultures of *V. cholerae* were diluted as described above except H_2O_2 was added to cultures at a final concentration of 50 µM when OD_{600} values reached approximately 0.225, followed by shaking at 35°C for an additional 30 minutes before measuring luciferase and OD_{600}.

3.4.4.2 – E. coli DH10b Luciferase Assays.

Overnight cultures of *E. coli* DH10b harboring vectors to modulate transcription factor, c-di-GMP production, and the luciferase reporter were diluted 1:100 as described above and grown at 35°C, 220 RPM until the OD_{600} reached 0.450. Luciferase activity was measured and normalized to the OD_{600} to yield normalized luminescence.

3.4.5 – Protein Purification and Electrophoretic Mobility Shift Assays (EMSA).

C-terminal HIS-tagged VpsT purification and EMSAs experiments using the FAM labeled *katB* promoter region from *katB2* were carried out as previously described (123). For purification, an overnight culture of *E. coli* BL21 harboring the pET28b-VpsT

expression construct was diluted 1:100 into 250 mL LB supplemented with kanamycin in a 1 L flask. The culture was grown until an OD_{600} of approximately 0.7 at which point 1 mM IPTG was added and the culture conditions were shifted to 16°C with shaking at 160 RPM for 16 hours to induce protein production. Protein purification was carried out by standard Ni-NTA resin purification protocols (19). For EMSA experiments, varying concentrations of purified HIS-tagged VpsT (0 – 600 nM) were incubated with 2.5 nM FAM-labeled *katB* probe along with the non-specific DNA competitor poly dI-dC (1 µg/µL) in VpsT buffer (25 mM Tris-Cl, 150 mM NaCl, 5 mM β-mercapthol, pH – 7.5) at 30°C for 30 minutes. The binding reaction was loaded into pre-run 5% non-denaturing TBE gels and gel electrophoresis was done by applying 90 volts for 90 minutes at 4°C. Fluorescent detection and images of the gels and were taken using a Typhoon FLA 9000 imager and the requisite software (GE Healthcare Life Sciences).

3.4.6 – Hydrogen Peroxide Survival Assay.

Overnight cultures were diluted to a starting OD_{600} of 0.040 in 1 mL LB supplemented with necessary antibiotics and IPTG in 1.5 mL microcentrifuge tubes. 140 µL aliquots were added to a 96-well plate (Costar) and grown until an OD_{600} of 0.300. H_2O_2 solutions were made from fresh H_2O_2 stocks in light-impermeable microcentrifuge tubes and sterile 1X PBS. At time 0, 10 µL of H_2O_2 was added to the cell solution and growth was monitored over time by measuring OD_{600}.

3.4.7 – Measurement of Intracellular c-di-GMP.

Overnight cultures of Δ*vpsL* harboring pBRP1 ($QrgB^{Mut}$) were diluted 1:100 in 2 mL LB ampicillin in 18 x 150 mm borosilicate test tubes and were grown to an OD_{600} of 1.0. The cultures were split into two 1 mL aliquots in microcentrifuge tubes, and H_2O_2 was

added to one aliquot at a final concentration of 500 μM. An equal volume of water was added to the other aliquot as the untreated control. Cultures were incubated statically at room temperature for 30 minutes and collected for total protein quantification and nucleotide extraction. Briefly, 100 μL of culture was removed from each tube to quantify total protein, pelleted by centrifugation at full speed (15,000 x g) for 1 minute, resuspended in 100 μL 1X PBS with 10% sodium dodecyl sulfate (SDS), and boiled at 95°C for 10 minutes. Lysed cell solutions were centrifuged at 15,000 x g for 1 minute and the supernatant was removed and placed in new tubes. Total protein was quantified using the DC Protein Assay (Bio-Rad) following the instructions in the manual. Protein standards consisting of bovine serum albumin (provided in DC Protein Assay) were used to generate a standard curve to interpolate unknown sample concentrations. Nucleotide extractions were carried out following the protocol here (127) with the following changes. 900 μL of the remaining culture were pelleted at 15,000 x g for 1 minute in a benchtop microcentrifuge. The supernatants were removed, and the remaining pellets were resuspended in 100 μL nucleotide extraction buffer (40:40:20 methanol/acetonitrile/water with 0.1 N formic acid). The extraction solution was incubated at 20°C for 20 minutes and pelleted for 10 minutes at 15,000 x g. The supernatants were placed into new microcentrifuge tubes, and the solutions were dried overnight using a heated, vacuum centrifuge (SpeedVac Concentrator, Savant). The resulting dried pellets were resuspended in 100 μL HPLC-grade water and subjected to mass spectrometry analysis for quantification of c-di-GMP (128). Data is represented as pmol of c-di-GMP normalized by total cellular protein (mg).

3.4.8 – Statistical Analysis.

Data are represented as the mean ± SD. Statistical analyses (details in figure legends) were calculated with GraphPad Prism Ver. 6 (GraphPad, San Diego, CA). A p-value of < 0.05 was considered statistically significant.

3.5 – Results

3.5.1 – C-di-GMP Positively Regulates Catalase Activity

We have shown that c-di-GMP regulates genes involved in DNA repair and that this regulation increased tolerance to the methylating agent methyl methanesulfonate (MMS) (123). Thus, we hypothesized c-di-GMP had a role in mitigating other forms of cellular stress besides DNA methylation damage. We chose to test if c-di-GMP increased H_2O_2 tolerance because it is a common ROS produced by aerobic microorganisms as a byproduct of cellular respiration, and H_2O_2 is found in high concentrations in aquatic environments (reviewed in (129)) . To test the effects of c-di-GMP on H_2O_2 tolerance in *V. cholerae*, we expressed the *Vibrio harveyi* DGC QrgB in a strain unable to form mature biofilms (Δ*vpsL,* designated as the parent strain for this text) which would introduce a confounding variable in our experiments (88). Additionally, we chose a heterologous DGC from *V. harveyi,* as opposed to *V. cholerae*, to minimize effects associated with potential protein-protein complexes within the *V. cholerae* c-di-GMP signaling network. As a control, we expressed an inactive allele of QrgB ($QrgB^{Mut}$) which is unable to synthesize c-di-GMP. Immediately after the addition of H_2O_2, both cultures began to produce gas bubbles, which is a phenomenon indicative of catalase activity as H_2O_2 is degraded into water and gaseous oxygen. Interestingly, the culture with higher intracellular c-di-GMP exhibited a higher amount of gas

production despite the cultures having similar numbers of bacteria, suggesting c-di-GMP increased catalase activity. Quantification of catalase activity revealed an approximate 5-fold increase when comparing strains expressing QrgB to QrgB^{Mut} (Figure 3.1), indicating c-di-GMP increased catalase activity. Importantly, we have previously demonstrated that the concentration of c-di-GMP generated by QrgB overexpression is similar to that seen naturally in the low-cell-density quorum sensing state, demonstrating that these results are physiologically relevant (55).

c-di-GMP can directly modulate protein activity or change gene expression through allosteric interactions with c-di-GMP-dependent transcription factors or riboswitches (30, 50, 121). The c-di-GMP dependent transcription factors VpsT and VpsR induce transcription of genes involved in biofilm formation, protein secretion, and

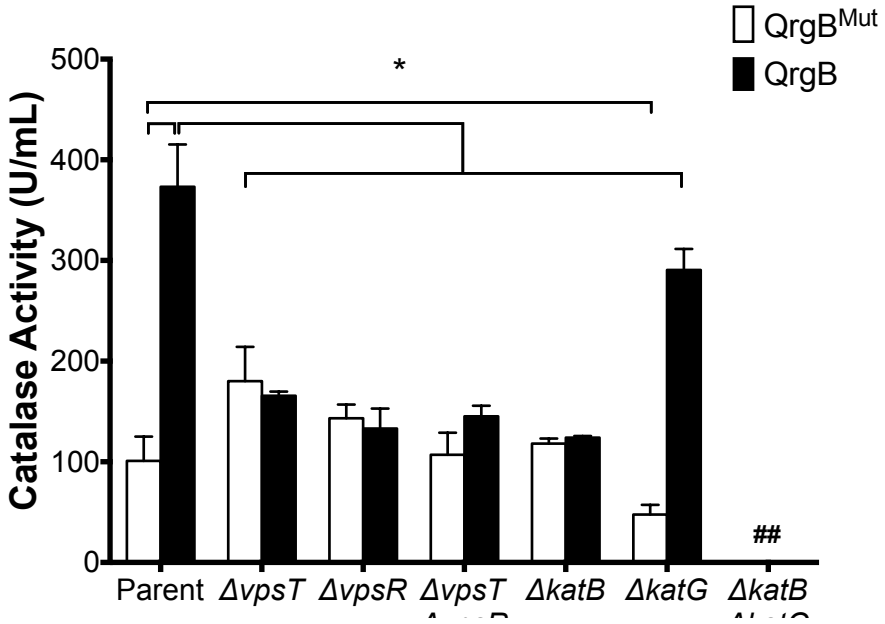

Figure 3.1: C-di-GMP Increases Catalase Activity
Catalase activity was measured in the parent and mutant strains overproducing QrgB^{Mut} (white bars) or QrgB (black bars). Brackets and * indicate differences with a $p < 0.05$ determined by Two-Way ANOVA followed by Tukey's multiple comparison test. Data are the average of three biological replicates with error bars indicating standard deviation. ## indicates activity was below the limit of detection.

DNA repair in high c-di-GMP conditions (48, 30, 66, 55, 123). Therefore, we hypothesized that these transcription factors control c-di-GMP regulated catalase activity. To test this hypothesis, we repeated the catalase assay using Δ*vpsT*, Δ*vpsR,* and the Δ*vpsT*Δ*vpsR V. cholerae* mutants and observed a loss of c-di-GMP mediated induction of catalase activity, suggesting the increased catalase activity was part of the VpsR/VpsT/c-di-GMP regulatory network (Figure 3.1).

V. cholerae encodes two catalases: *katG* (VC1560)*,* a bifunctional enzyme with both catalase and peroxidase functions, and *katB* (VC1585)*,* which only exhibits catalase activity (117, 130). Mutants of these enzymes render *V. cholerae* more susceptible to H_2O_2 treatment; however, regulation of either *katB* or *katG* by c-di-GMP has not been described (130). We therefore measured c-di-GMP induction of catalase activity in the mutants Δ*katB,* Δ*katG,* or Δ*katB*Δ*katG*. We observed that the Δ*katB* background did not display c-di-GMP regulated catalase activity but did possess basal level catalase activity similar to the parent strain expressing $QrgB^{Mut}$ (Figure 3.1). Expression of *katB* from an arabinose-inducible, multicopy plasmid in the Δ*katB* background complemented catalase activity regardless of the levels of c-di-GMP (Figure 3.8). Strains lacking *katG* were still able to induce catalase activity by c-di-GMP; however, the level of catalase activity induced by c-di-GMP was approximately 20% lower than that of the parent strain (Figure 3.1). Additionally, catalase activity in the Δ*katG* strain expressing $QrgB^{Mut}$ was approximately 2-fold lower than the parent strain in the same condition (Figure 3.1). Strains lacking both *katG* and *katB* did not have measurable catalase activity under these conditions, which is expected because

these are the only annotated genes encoding catalase activity in the El Tor *V. cholerae* reference genome N16961 (117) (Figure 3.1).

3.5.2 – Characterization of the *katB* Promoter and Regulation of *katB* Expression

Our results suggest *katB*, but not *katG*, is positively regulated by c-di-GMP at the transcriptional level. We addressed this hypothesis by measuring *katB* mRNA from cultures inducing QrgB and $QrgB^{Mut}$ using qRT-PCR. We found that *katB* expression increased approximately 12-fold in QrgB expressing strains relative to $QrgB^{Mut}$ expressing strains (Figure 3.2B).

We next were interested in the promoter architecture of the region upstream of *katB* driving expression and hypothesized specific regions in the *katB* promoter were necessary for c-di-GMP mediated transcriptional control. We tested this hypothesis by measuring luciferase activity from a series of *katB* transcriptional reporters that have been truncated at the 5' end in the presence of QrgB or $QrgB^{Mut}$ expression (Figure 3.2A). In the full-length promoter construct *katB1*, expression of QrgB induced *katB* expression 5-fold compared to strains over-producing $QrgB^{Mut}$ (Figure 3.2A). Inclusion of 212 bp upstream of *katB* was sufficient to maintain c-di-GMP induction (Figure 3.2A, *katB2* and *katB3*). However, if the promoter was truncated to include 172 bp upstream of *katB* (*katB4*), c-di-GMP dependent induction of *katB* was abrogated. This result suggested the necessary cis-acting sequences for c-di-GMP mediated activation of *katB* expression are found between -172 and -212 bp upstream of the *katB* relative to the ATG start codon (Figure 3.2A). Deleting 30 bps from *katB4* resulted in expression levels similar to that of the promoter-less vector control regardless of c-di-GMP concentrations, suggesting components necessary for the basal expression of *katB* are

between -172 and -142 relative to the ATG start codon (Figure 3.2A). We also measured the effect of c-di-GMP on a *katG*-luciferase transcriptional fusion and did not

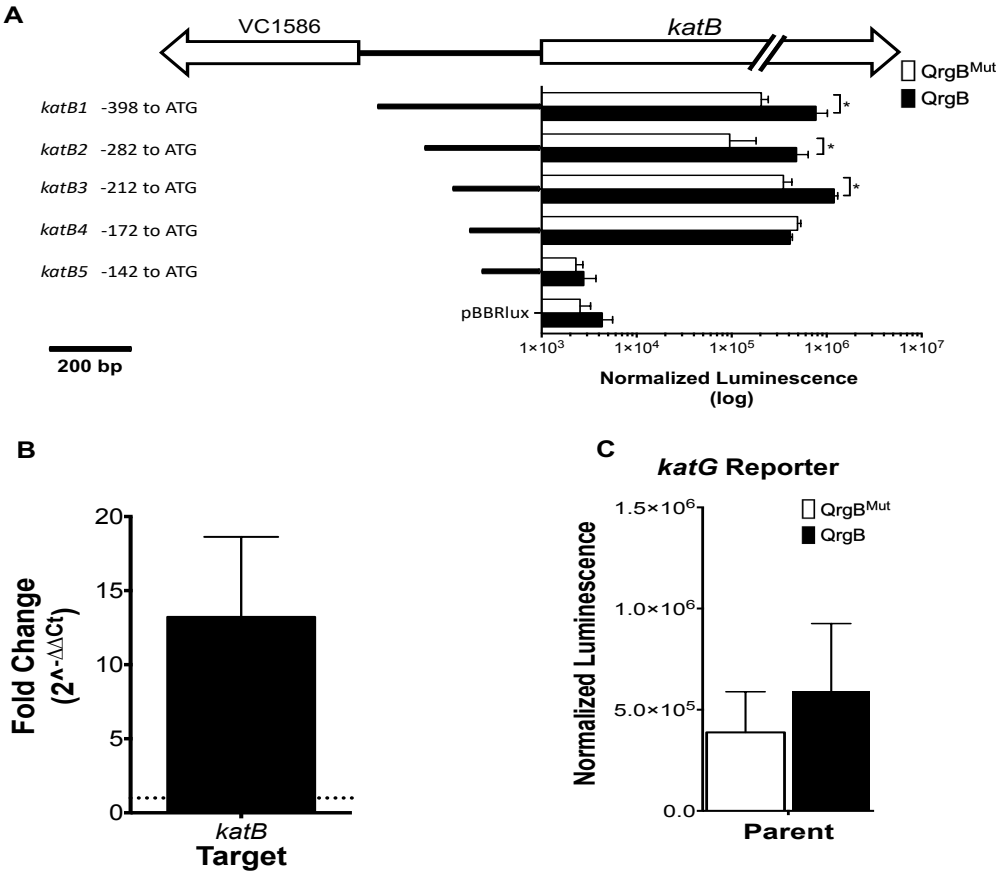

Figure 3.2: Characterization of the *katB* Promoter and Transcriptional Activity
A) katB genetic locus and promoter truncations and reporter activity. 5' promoter truncations were constructed and cloned upstream of the luciferase operon. Lines and numbers on the Y-axis indicate length of promoter relative to the ATG start codon for each promoter construct. Normalized luminescence is light production normalized to OD_{600} to control for cell number. For each promoter construct, luminescence was measured while overproducing $QrgB^{Mut}$ (white bars) or QrgB (black bars). An empty pBBRlux vector control was included in each experiment. Brackets and * indicate comparisons with a p-value < 0.05 determined by Two-Way ANOVA followed by Tukey's multiple comparisons testing. Data are the averages of three biological replicates and error bars indicate standard deviation. B) C-di-GMP Increases katB mRNA Abundance. qRT-PCR analysis comparing katB mRNA abundance between QrgB and QrgBMut conditions using the ΔΔCt method. Dashed horizontal line represents a fold change of 1. Bars represent the average of three biological replicates with error bars indicating standard deviation. C) katG expression is unresponsive to changes in c-di-GMP. katG expression was measured in the parent strain while overproducing $QrgB^{Mut}$ (white bars) or QrgB (black bars). Bars represent averages of three biological replicates with error bars indicating standard deviation.

observed significant c-di-GMP dependent changes in expression, in agreement with our initial hypothesis (Figure 3.2C).

VpsT and VpsR are necessary for the c-di-GMP-dependent induction of catalase activity, suggesting that these transcription factors activate transcription of *katB* at high intracellular concentrations of c-di-GMP (Figure 3.1). Thus, we hypothesized that c-di-GMP mediated induction of *katB* would be lost in strains lacking *vpsT, vpsR,* or both *vpsT* and *vpsR*. We tested this hypothesis by measuring *katB2* reporter activity under

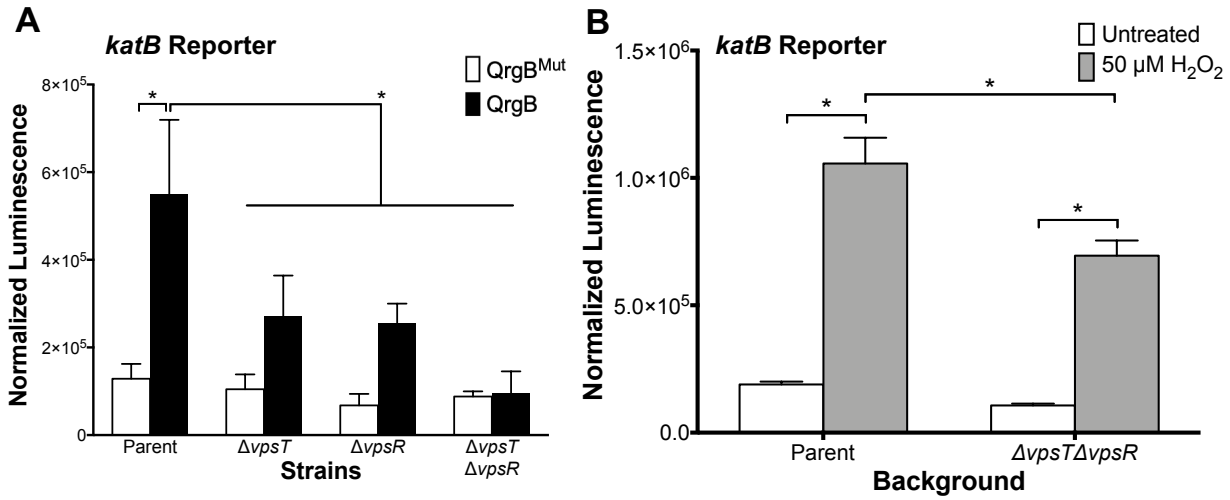

Figure 3.3: *vpsT* and *vpsR* are Necessary for c-di-GMP Mediated Expression of *katB* but Dispensable for H_2O_2 Induction
A) *katB* expression was measured in parent, Δ*vpsT,* Δ*vpsR,* and Δ*vpsT*Δ*vpsR* backgrounds while overproducing $QrgB^{Mut}$ (white bars) or QrgB (black bars). Brackets and * indicate differences with a p-value < 0.05 determined by Two-Way ANOVA followed by Tukey's multiple comparison test. Data are average of three biological replicates. Error bars indicate standard deviation.
B) *katB4* expression was measured in the parent and Δ*vpsT*Δ*vpsR* background 30 minutes after addition of 50 μM H_2O_2 or PBS control (untreated). Data are the average of three biological replicates and error bars indicate standard deviation.

different c-di-GMP conditions in the parent, single, and double knockout strains. We found that *katB2* expression increased 5-fold in the parent background. *katB* expression increased 2.5 to 3-fold in the Δ*vpsT* and Δ*vpsR* backgrounds, but the

differences in expression between QrgB^{mut} and QrgB were not statistically significant (Figure 3.3A). It was only in the double mutant Δ*vpsT*Δ*vpsR* background that c-di-GMP mediated *katB* expression was completely lost (Figure 3.3A). These data suggest that both VpsR and VpsT are needed for full induction by c-di-GMP and individually they may be able to change expression of the *katB* reporter. However, if induction of *katB* occurs in the single Δ*vpsT* and Δ*vpsR* mutants it is not sufficient to alter catalase activity (Figure 3.1).

katB expression is up-regulated in response to hydrogen peroxide in *V. cholerae* through the transcriptional activator OxyR (116, 130). To determine if the same region necessary for c-di-GMP mediated regulation of *katB* was necessary for H_2O_2 induction of *katB,* we measured the ability of H_2O_2 to induce *katB4,* the promoter region that no longer responded to c-di-GMP (Figure 3.2B). We found that 50 μM H_2O_2 induced *katB4* expression approximately 6-fold in the parent background (Figure 3.3B). Next, to determine if VpsT and VpsR contributed to the H_2O_2 inducible response of the *katB4* promoter, we repeated the assay in a Δ*vpsT*Δ*vpsR* background. In this background, H_2O_2 increased *katB4* expression to the same extent as the parent, however the basal and induced expression level was 1.5-fold lower compared to the parent (Figure 3.3B).

In *Mycobacterium smegmatis*, H_2O_2 can act as a first messenger to promote c-di-GMP synthesis (131). Whether H_2O_2 acts as a first messenger to modulate c-di-GMP in *V. cholerae* has not been demonstrated. To test the hypothesis that H_2O_2 acts as a first messenger, we measured intracellular c-di-GMP in control and H_2O_2 treated cultures and found no differences in intracellular c-di-GMP (Figure 3.9). Together, these results indicate that *katB* transcription is induced by c-di-GMP and the oxidative stress

response through distinct regulatory mechanisms and demonstrate that H_2O_2 does not alter global levels of intracellular c-di-GMP.

3.5.3 – VpsT Induces *katB* Expression in a Heterologous Host and Binds to the *katB* Promoter In Vitro

To test whether VpsT or VpsR directly regulates *katB*, we used *Escherichia coli* as a heterologous host to measure *katB* expression at high versus low concentrations of c-di-GMP in the presence of either VpsR or VpsT. We reasoned the genetic dissimilarity between *V. cholerae* and *E. coli* would allow us to isolate the effects of VpsR and VpsT directly on the *katB* promoter without the regulatory feedback for these transcription factors (17, 74, 33). Expression of QrgB with an empty vector increased *katB* expression in *E. coli* approximately 2.5-fold when compared to expression of $QrgB^{Mut}$ through an unknown mechanism (Figure 3.4). Similarly, co-expression of VpsR

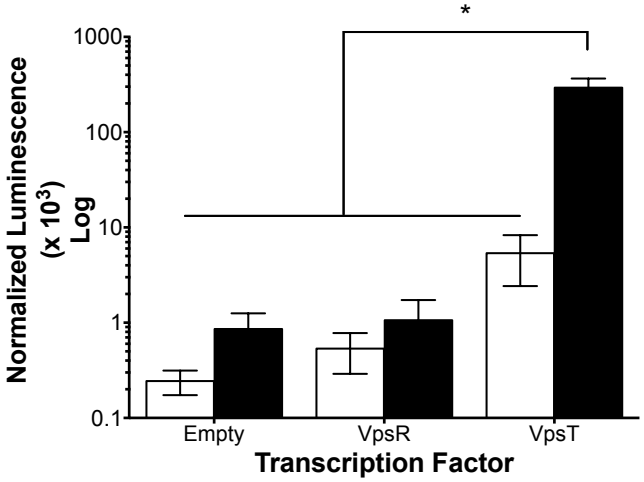

Figure 3.4: VpsT and c-di-GMP Induce *katB* Expression in a Heterologous Host. $QrgB^{Mut}$ or QrgB were overproduced along with either an empty vector, VpsR, or VpsT in DH10b *E. coli* harboring the *katB3* promoter fused upstream of the luciferase operon. Data is the average luminescence between strains overproducing QrgB and $QrgB^{Mut}$ from three biological replicates and error bars are standard deviation. Brackets and * indicate a statistically significant difference determined by Two-Way ANOVA followed by Tukey's multiple comparison testing.

along with QrgB resulted in approximately the same fold change (2-fold) as the empty vector, indicating VpsR is not sufficient to induce *katB* expression when expressed in *E. coli* along with increased c-di-GMP (Figure 3.4). Interestingly, expression of VpsT with $QrgB^{Mut}$ increased *katB3* expression 20-fold compared to the empty vector control. While this comparison had a p-value of 0.8, the large difference between averages suggests VpsT can contribute to modulating gene expression in low c-di-GMP conditions (Figure 3.4). The largest difference in *katB3* expression was observed when VpsT was expressed with QrgB, resulting in a 344-fold induction compared to the empty vector (Figure 3.4). Together, these data suggest VpsT is a key regulator of *katB* expression and that transcriptional activation is increased when c-di-GMP is present.

VpsT binds to DNA in the presence of c-di-GMP to modulated gene expression (30, 31, 106, 123). Since VpsT was necessary for c-di-GMP mediated *katB* expression

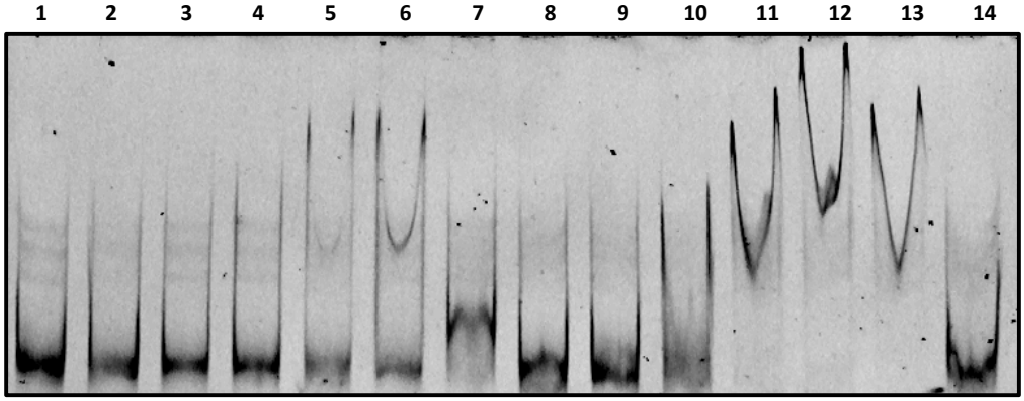

VpsT (nM)	0	75	150	300	600	600	600	0	75	150	300	600	600	600
c-di-GMP 50μM	-	-	-	-	-	-	-	+	+	+	+	+	+	+
Competitor	-	-	-	-	-	MT	WT	-	-	-	-	-	MT	WT

Figure 3.5: C-di-GMP Enhances VpsT Interaction with the *katB* Promoter in vitro. Increasing concentrations of HIS tagged VpsT were incubated with a FAM-labeled probe corresponding to the *katB4* promoter (Lanes 1-5). Unlabeled mutant (MT) or wild-type (WT) VpsT binding site competitor was added at 100X-molar excess relative to the labeled probe in reactions with 600 nM HIS tagged VpsT (Lanes 6,7). Lanes 8-14 are the same reaction conditions as Lanes 1-7 except 50 μM c-di-GMP was added to the binding reactions, as indicated by the + sign.

and was able to induce *katB* expression when expressed in a heterologous host, we hypothesized VpsT directly interacted with the *katB2* promoter in a c-di-GMP-dependent manner. Thus, we purified C-terminal HIS-tagged VpsT and measured its ability to bind to the *katB2* promoter in vitro. VpsT only partially shifted the *katB2* probe at the highest concentration tested (600 nM) in the absence of c-di-GMP (Figure 3.5, lane 5). However, with the addition of 50 μM c-di-GMP, VpsT was able to decrease the intensity of the unshifted band at 150 nM and completely shift the probe at 300 nM (Figure 3.5, lanes 10-12). Addition of an unlabeled, 20bp oligo composed of a VpsT binding site found in the *vpsL* promoter at 100-fold molar excess was able to outcompete VpsT binding to the labeled *katB2* probe in the presence or absence of c-di-GMP (Figure 3.5, lanes 7, 14) (31). When the unlabeled competitor had transversion mutations introduced into the palindromic region, it was no longer able to abrogate the VpsT-*katB2* band migration (Figure 3.5, lanes 6, 13) (31). Together, the in vivo and in vitro data suggest VpsT directly interacts with the *katB* promoter to induce expression under high c-di-GMP conditions.

3.5.4 – C-di-GMP mediated HOOH survival is Dependent on Catalase

Since c-di-GMP increased *katB* expression and catalase activity, we hypothesized that high intracellular c-di-GMP would provide a survival advantage during H_2O_2 stress. We tested this hypothesis by measuring survival after H_2O_2 treatment in *V. cholerae* backgrounds (Δ*vpsL)* unable to make mature biofilms to specifically test if the transcription regulation of *katB* by c-di-GMP was responsible for any observed protection as opposed to matrix production or formation of multicellular biofilms (118, 120, 132, 133). *V. cholerae* expressing $QrgB^{Mut}$ or QrgB were challenged with H_2O_2

and the gross culture viability (OD_{600}) was monitored for three hours. We found that in

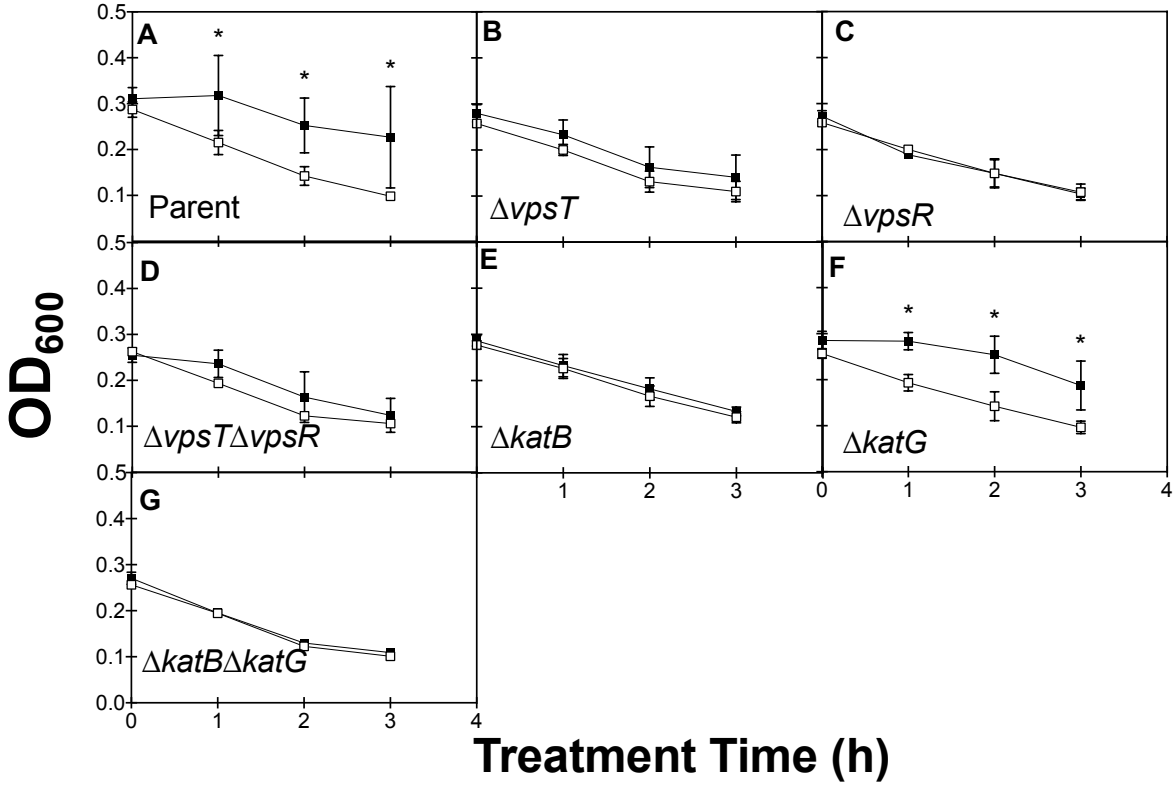

Figure 3.6: C-di-GMP Enhances Survival After H_2O_2 Treatment
$QrgB^{Mut}$ (open squares) or QrgB (squares) were induced with 100 μM IPTG in parent (a), Δ*vpsT* (b), Δ*vpsR* (c), Δ*vpsT*Δ*vpsR* (d), Δ*katB* (e), Δ*katG* (f), and Δ*katB*Δ*katG* strains until an OD_{600} of 0.3. H_2O_2 was added to cultures at a final concentration of 12.5 mM. Cell death was monitored by measuring OD_{600} every hour after H_2O_2 addition (Time 0). * Indicate a $p < 0.05$ when compared to the untreated control at that timepoint determined by Two-Way ANOVA followed by Tukey's multiple comparisons test. Bars are averages from three biological replicates and error bars indicate standard deviation.

the parent strain, expression of QrgB, but not $QrgB^{Mut}$, led to significant protection from H_2O_2 stress (Figure 3.6A). To test this if this production is dependent on c-di-GMP mediated catalase activity, we measured H_2O_2 survival in the Δ*katB,* Δ*katG,* and Δ*katB*Δ*katG* mutants. Consistent with our catalase activity results, deletion of *katB* in either the Δ*katB* and Δ*katB*Δ*katG* mutants displayed no c-di-GMP mediated H_2O_2

survival (Figure 3.6E and G) while survival of the Δ*katG* mutant during H_2O_2 treatment resembled the parent strain (Figure 3.6F).

Since *vpsT* and *vpsR* were necessary for c-di-GMP dependent induction of *katB* expression and catalase activity (Figure 3.1 and 3.4), we hypothesized deletion mutations of these transcription factors would decouple c-di-GMP signaling from survival during H_2O_2 treatment. Indeed, strains lacking *vpsT, vpsR,* or both *vpsT* and *vpsR* lost c-di-GMP-mediated survival during H_2O_2 treatment (Figure 3.6B-D). Taken together, these data suggest c-di-GMP increases *katB* expression and KatB catalase activity through the c-di-GMP dependent transcription factors *vpsT* and *vpsR* resulting in increased survival during H_2O_2 treatment (Figure 3.7).

3.6 – Discussion

In this work, we sought to determine if providing resistance to ROS is a c-di-GMP regulated phenotype in *V. cholerae*. Using a plasmid-based system to modulate intracellular c-di-GMP, we observed increased gas production after the addition of H_2O_2, suggesting c-di-GMP positively influenced catalase activity. We determined that *katB* was responsible for c-di-GMP regulated catalase activity and found that *katB* transcription was increased 5-fold in the parent background but was lost in strains deficient for the c-di-GMP dependent transcription factors VpsT and VpsR. Measuring *katB* transcription in a heterologous host revealed that VpsT was sufficient to induce *katB* expression under high c-di-GMP conditions and in vitro DNA binding assays demonstrated VpsT specifically bound to the *katB* promoter in a c-di-GMP dependent fashion. Lastly, we showed that c-di-GMP mediated survival after H_2O_2 treatment was dependent on *vpsT, vpsR,* and *katB.*

In agreement with our findings, other groups have observed an increase in *katB* expression under certain biofilm inducing conditions which modulate intracellular c-di-GMP, such as incubation with norspermidine (134) . Additionally, rugose variants of *V. cholerae* were shown to be resistant to H_2O_2 in a VPS independent manner and were later found to have increased expression of *katB* (135, 136). Transcriptomic data from experiments where c-di-GMP or VpsT was artificially induced in *V. cholerae* suggested *katB* expression was positively regulated by c-di-GMP (56, 30).

Interestingly, c-di-GMP and VpsT were shown to down-regulate production of the stationary phase sigma factor RpoS, in turn decreasing survival to various stressors including H_2O_2, which is in contrast to our results (Figure 3.5A) (106). These experiments were done with the El Tor biotype strain C7258, which is part of the serogroup Ogawa while the strain used in the current study (C6076 str2) is part of the serogroup Inaba. While there are no studies describing differences in transcriptional regulation between the two serogroups, we hypothesize there may be serogroup dependent differences in c-di-GMP signaling, which would explain the contrasting results.

Unlike the Δ*vpsT*Δ*vpsR* double mutant, c-di-GMP was able to induce the expression of the *katB* reporter in the single *vpsT* and *vpsR* deletion background, albeit the difference was not statistically significant. To further clarify which transcription factor was the direct effector, we reconstructed the system in *E. coli* and found that only production of VpsT and c-di-GMP, but not VpsR and c-di-GMP, increased expression of the *katB* promoter in *E. coli* (Figure 3.4). C-di-GMP mediated catalase activity and survival in H_2O_2 were also lost in both the Δ*vpsT and* Δ*vpsR* backgrounds. Thus, our

evidence suggests that phenotypes are primarily controlled by VpsT (Figure 3.7). VpsR is required for c-di-GMP mediated induction of *vpsT* in *V. cholerae,* therefore, we conclude it has an indirect effect on *katB* transcription (81) (Figure 3.7).

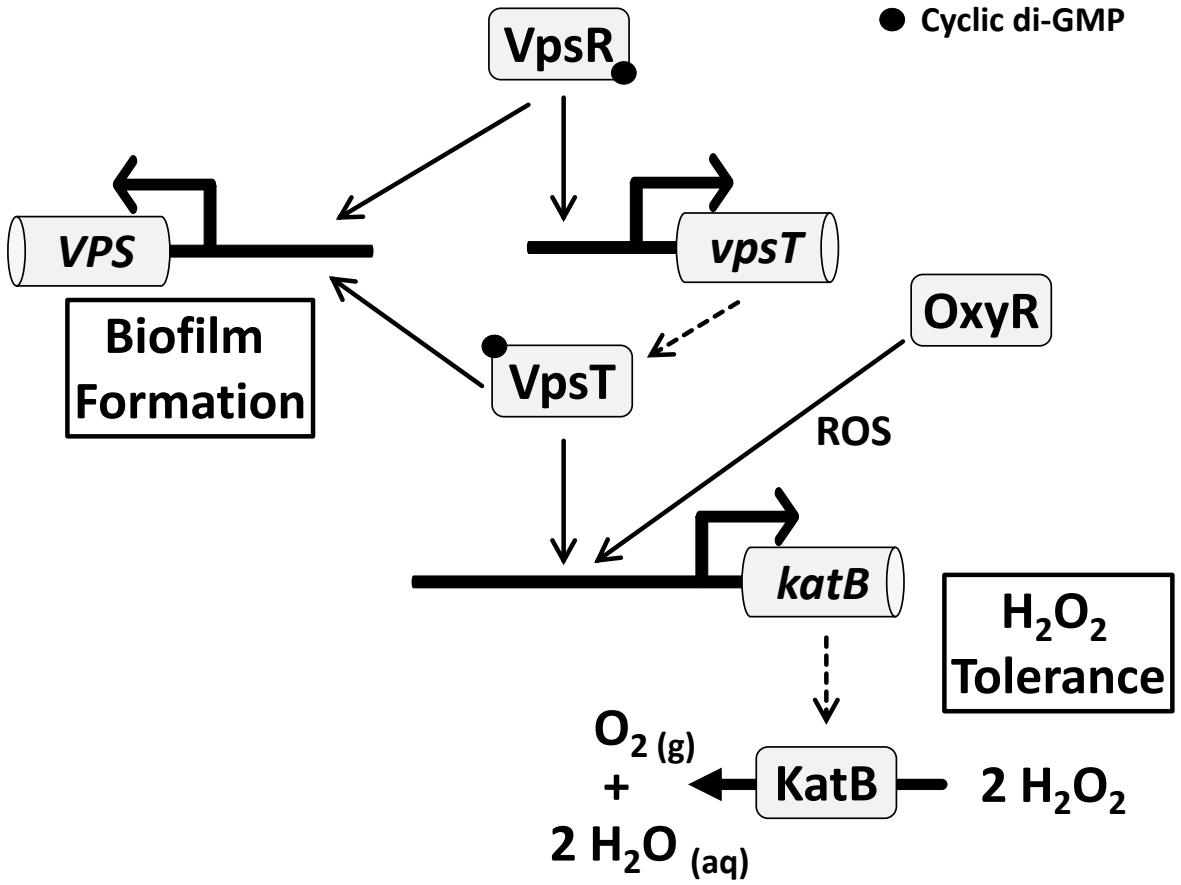

Figure 3.7: Model for the cyclic di-GMP Regulatory Network Controlling Biofilm Formation and H_2O_2 Tolerance
In response to high intracellular cyclic di-GMP, VpsR becomes activated and induces expression of *vpsT.* VpsT, in turn, is activated by cyclic di-GMP and both VpsR and VpsT activate genes in the *vps* operons to promote biofilm formation. Our data indicates cyclic di-GMP activated VpsT also induces expression of *katB* which increases catalase activity of the population which is able to turn over H_2O_2 and promote survival after H_2O_2 treatment. Our data also demonstrates induction of *katB* by H_2O_2 occurs independently of the cyclic di-GMP signaling network and is likely controlled by OxyR, a transcription factor involved in a broader antioxidant production program.

Interestingly, we observed that VpsT was able to induce *katB* expression 20-fold in unaltered c-di-GMP conditions in *E. coli* (Figure 3.4). Additionally, VpsT was also able

to bind to the *katB* promoter without exogenously added c-di-GMP, albeit at high protein concentrations (Figure 3.5). It is possible these results are a consequence of relatively high VpsT levels driven by the expression plasmid; however, it is also possible that VpsT may have some c-di-GMP independent effect on gene expression. Indeed, allele variants of VpsT that are unable to bind to c-di-GMP are still able to modulate gene expression (30). If and how VpsT functions in the absence of c-di-GMP is an area that requires more research.

A predicted VpsT binding site was found approximately 150 bps upstream of the ATG start codon was previously reported (96). Our results indicate that even when the VpsT binding site was present in the *katB4* transcriptional fusion, induction by c-di-GMP was lost. We note that the predicted VpsT sequence was found in the template strand while predicted and validated VpsT binding sites in the *vpsL* and *vpsA* promoters were found in the coding strand (31, 96). As a result of this difference, the binding site would position VpsT in different directionalities i.e, positioned toward or away from the open reading frame. Whether this difference in directionality alters VpsT transcriptional regulation warrants further investigation.

Although our work focuses on *V. cholerae,* the association between c-di-GMP and protection against ROS has been shown in other bacteria. In *Listeria monocytogenes,* deletion of genes encoding PDE domains have elevated biofilm production and H_2O_2 tolerance (119). However, it is not known whether H_2O_2 tolerance was caused by increased EPS production, antioxidant production, or both. In *Mycobacterium smegmatis*, a relative of the human pathogen *M. tuberculosis,* H_2O_2 stimulates

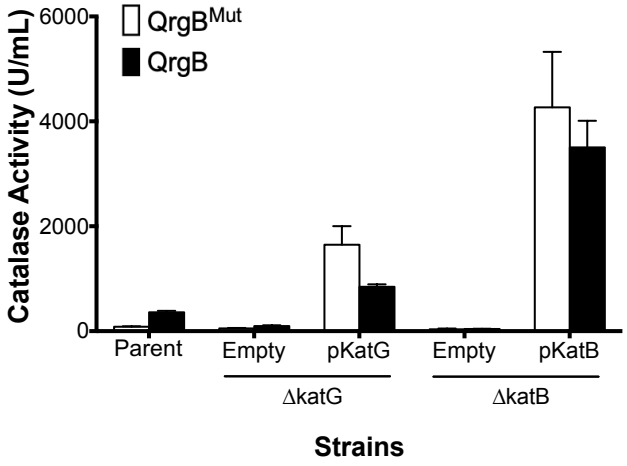

Figure 3.8: Over Production of KatG and KatB Complements Catalase Activity in Δ*katG* and Δ*katB* Backgrounds, Respectfully.
Catalase activity was measured in the parent, Δ*katG,* or Δ*katB* strains overproducing $QrgB^{Mut}$ (white bars) or QrgB (black bars) while overproducing KatG or KatB on a separate vector. Data are averages from three biological replicates and error bars are standard deviation.

production of intracellular c-di-GMP, which inactivates the transcriptional repressor HpoR. As a result, ROS defense genes are up-regulated and increase H_2O_2 tolerance (131). This differs from our work in two facets: first, H_2O_2 does not act as a first messenger that stimulates c-di-GMP activity in *V. cholerae* (Figure 3.9) and second,

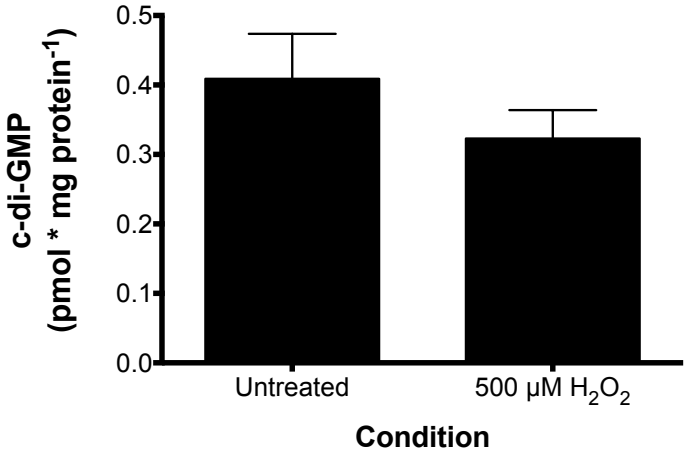

Figure 3.9: H_2O_2 Does Not Modulate Intracellular c-di-GMP.
Replicate cultures were grown to an OD_{600} of 1.0, split, and 500 μM H_2O_2 was added to one half, while PBS was added to the other. Cultures were incubated for 30 minutes at room temperature and then nucleotides were extracted. Data are averages from six biological replicates and error bars are standard deviation.

VpsT and c-di-GMP regulate a wide array of genes whereas HpoR-c-di-GMP has been shown to only regulate expression of the *hpoR* operon. Despite the differences in regulation, the connection between c-di-GMP and ROS tolerance is evident in bacteria from diverse phylogenetic backgrounds.

Chapter 4 – Cyclic di-GMP Decreases Cell Curvature to Promote Biofilm Formation in *Vibrio cholerae*

4.1 – Abstract

In rod-shaped bacteria, shape is imposed by the structure of peptidoglycan in the cell wall. The vibrioid shape of the human pathogen *Vibrio cholerae* is a derivative of the rod-shape and is generated by introduction of negative curvature during cell growth. While *V. cholerae* adopts a vibrioid shape under most conditions, there is evidence that cell shape is susceptible to regulation by growth conditions, with examples going back as far as the early 1900s. However, which signals regulate the change in cell shape and the potential consequences of cell shape change are not well characterized. In this work, we found that cell shape in *V. cholerae* is regulated by the bacterial second messenger cyclic dimeric guanosine monophosphate (c-di-GMP). We found that c-di-GMP downregulates *crvA*, a gene encoding an intermediate-filament like protein necessary for curvature formation in *V. cholerae.* Since c-di-GMP promotes the formation of surface adhered microbial communities known as biofilms in *V. cholerae* and other organisms, we explored the role of shape in biofilm formation. We discovered that wild-type cells adhered to a surface during biofilm formation are as straight as cells lacking *crvA*. Further, utilizing strains that maintain their curved shape under these conditions resulted in defects in biofilm formation. Single-cell analysis revealed curvature altered microcolony formation, with curved cells producing smaller and more scattered microcolonies compared to straight cells. Together, these data indicate shape change from curved to straight cells is a regulated process controlled by c-di-GMP and is necessary for mature biofilm formation.

4.2 – Introduction

Morphology is an important feature for nearly every form of life for it dictates how each organism interacts with its physical world. Various aspects of morphology, such as shape, length, and presence of appendages, are subject to selective pressures and contribute to adaptation of an organism to specific niches (137). As such, bacteria take on diverse shapes from simple rods and cocci to helices and curves, with each shape likely providing some adaptive benefit.

Shape in bacteria is determined by the structure of the peptidoglycan (PG) layer of the cell wall (138). During growth of a rod-shaped cell, new PG subunits are added to the growing PG layer by continuous rounds of cleavage and subunit insertion at the mid-cell (138). The vibrioid shape is a derivative of the rod-shape and is characterized by a curved-rod appearance and is common in many aquatic organisms, such as the fresh-water organism *Caulobacter crescentus* and the human pathogen *Vibrio cholerae*. These organisms have species specific genes that are responsible for inducing curvature during growth (139). In *C. crescentus,* CreS, an intermediate filament-like (IF-like) protein, forms intermediate filaments along the inner membrane and decreases the rate of PG synthesis along the longitudinal axis of one side of the cell (140, 141). As cells grow, they develop negative curvature and the canonical vibrioid morphology (141). Until recently, the mechanism controlling the vibrioid morphology in *V. cholerae* remained unknown. Bartlett *et al.* identified the IF-like protein they named CrvA that is responsible for curvature in *V. cholerae* through a similar mechanism as CreS (142). By forming filaments in the periplasm on one side of the cell, CrvA decreases rates of PG subunit insertion and introduces negative curvature (142). Mutants lacking *crvA* are

less motile in high percentage agar swim plates and less virulent in animal models of infection (142).

However, pathogenesis is just one facet of the *V. cholerae* lifestyle. As an aquatic organism, *V. cholerae* is more likely to interact with fresh and salt-water environments where it associates with chitin-coated organisms as surface adhered communities of bacteria encased in a matrix of exopolymeric substances (EPS) known as biofilms (143). *V. cholerae* biofilm formation is regulated by the bacterial second messenger signal cyclic dimeric guanosine monophosphate (c-di-GMP) (2). Upon synthesis by enzymes called diguanylate cyclases (DGCs), c-di-GMP binds to and activates the transcription factors VpsR and VpsT (30, 81). As a result, expression of the *Vibrio polysaccharide operons* (VPS), the EPS component of *V. cholerae* biofilms, is increased resulting in biofilm matrix production (135, 144). C-di-GMP also negatively regulates motility by inhibiting transcription of the flagellar biosynthesis genes and production of the transcription factor TfoY upon binding to a specific riboswitch (50, 55).

Early microscopic analysis of *V. cholerae* cells found the “comma shaped *Vibrio”* as the prominent shape, however there were also observations of *V. cholerae* existing as mostly “bacillary” or straight rod forms (145). Interestingly, Arthur Henrici measured cell shape during a batch culture growth curve and found that *V. cholerae* shape is rather heterogeneous, with bacillary cells more prevalent during the early stages of growth and comma shaped cells more prevalent during later stages of growth (145). This and other work on curvature in *V. cholerae* suggest cell shape is subject to environmental regulation (145).

Recently, our group and others have identified broader roles of c-di-GMP signaling in *V. cholerae* and other microorganisms, including the induction of genes involved in predation, cell division, DNA damage repair, and antioxidant production (17, 19, 146, 147). In this study, we report that c-di-GMP also controls *V.* cholerae cell shape. We found that high c-di-GMP concentrations decreased cell curvature by reducing *crvA* mRNA. The same transcription factors that directly bind to c-di-GMP to induce biofilm formation, VpsR and VpsT, were responsible for linking c-di-GMP and curvature inhibition, suggesting cell shape could impact biofilm formation. Indeed, analysis of the early stages of biofilm formation found that cells in surface associated microcolonies resemble straight-rods, similar to *crvA* mutant cells. Moreover, cells that maintain curvature under biofilm forming conditions exhibited deficiencies in microcolony formation and biofilm formation. Our results demonstrate how bacteria can modulate cell shape to influence interaction with surfaces and the development of multicellular communities such as biofilms.

4.3 – Methods and Materials

4.3.1 – DNA Manipulations and Growth Conditions.

WT *V. cholerae* C6706 Str2 and the biofilm mutant derivative (Δ*vpsL*) were used in these studies. In experiments that included modulating c-di-GMP in bacteria in solution, the biofilm mutant Δ*vpsL* was used. This was done so that individual bacteria could be imaged in solution rather than clumps that form when c-di-GMP is high (128). All other experiments were carried out in the WT background unless noted otherwise. Clean deletions of Δ*vpsT* and Δ*vpsR* as well as expression vectors for VpsT and VpsR were constructed elsewhere (81). For deletion and knock-in strains, the allelic replacement

vector pKAS32 was used (148). Unless otherwise stated, all cloning was done by Gibson Assembly (NEB). Briefly, for the deletion construct pKAS32_ΔcrvA, pKAS32 was digested with KpnI and SacI and cleaned by gel extraction (Promega). Primers (Integrated DNA Technologies) were designed with Nebuilder (www.nebuilder.com, NEB) to incorporate the appropriate 5' ends necessary for Gibson Assembly and 3' gene specific ends. Specifically, 700 bp upstream and downstream of *crvA* (VCA1075) were amplified by PCR (Q5 Polymerase, NEB) using *V. cholerae* gDNA as a template. For the knock-in construct pKAS32_pcrvA-CrvA, pKAS32 was similarly digested with KpnI and SacI. 700 bp upstream and downstream of the locus VC1807, which is an authentic frameshift used for insertion of antibiotic cassettes (149), were amplified by PCR. Additionally, the native promoter and ORF of *crvA* (-358 bp relative to the ATG start codon until the translational stop codon) were amplified using PCR. For pBBRLux_pcrvA, pBBRlux was digested with BamHI and SpeI and cleaned by gel extraction. Primers were designed to amplify -358 to -1 bp relative to the ATG start codon of VCA1075 (*crvA*) and PCRs were carried out as described above. For pHERD20C_CrvA, pHERD20C was digested with KpnI and SacI and cleaned by gel extraction. Primers were designed to amplify the ORF of *crvA* and PCRs were carried out as described above. In each case, assembly was carried out by following the instructions in the manual and transformed into S17 *Escherichia coli* by electroporation. Successful clones were screened by colony PCR using GoTaq polymerase (Promega) and sequenced by sanger sequencing (Genewiz Inc.) to ensure no mutations were incorporated during the cloning process. Construction of knock out and knock in strains were carried out by the protocol for Skorupski *et al*. (148). Plasmids were moved from

S17 *E.coli* into *V. cholerae* by conjugation using Polymixin B as to select against *E. coli* (10 U/mL). Unless otherwise stated, both *E. coli* and *V. cholerae* were propagated in LB with ampicillin (100 µg/mL), kanamycin (100 µg/mL), and/or chloramphenicol (10 µg/mL) when needed. The inducer isopropyl-β-D-thiogalactoside (IPTG) was routinely used at 100 µM unless stated otherwise. L-arabinose (Sigma) was used at the concentrations stated in the text when necessary.

4.3.2 – Phase Contrast Microscopy and Single-Cell Analysis.

Overnight cultures were subcultured into 2 mL LB supplemented with ampicillin and IPTG at appropriate concentrations. Cultures were grown until an OD_{600} of 1.3 to 1.5, at which point cells were diluted to an OD_{600} of .5 in microcentrifuge tubes. 1% agarose pads in deionized water were cut into squares of approximately 20 x 20 mm and placed on microscope slides (75 x 25 x 1.0 mm (LxHxW), Alkali Scientific Inc.). 2 µL of diluted cultures were spotted onto glass coverslips (22 x 22 mm, #1.0 thickness, Alkali Scientific) and the coverslip was gently placed onto the agarose pad. Phase-contrast microscopy was carried out with a Nikon Eclipse Ti-E inverted microscope equipped with a 100X phase contrast oil immersion objective (1.4 NA), a Nikon Perfect Focus System, a Prior H117 ProScan motorized stage, a Lumencor SOLA II SE 365 LED light source, and an Andor Zyla 4.2 sCMOS camera. The microscope and camera are controlled by a computer workstation with MATLAB (Mathworks Inc.) and Micromanager (micro-manager.org). Images with obstructions were removed with remaining images used for segmentation analysis using the Fiji plugin MicrobeJ with the following settings: area (0 – 4.5, μm^2), length (1.5 – max, µm) and width (0 – 3, µm) (150). Data from segmented images were analyzed using R to plot curvature (μm^{-1}), width (µm), and

length (μm). Representative images were cropped, and the scale bar was added using Fiji software (151).

4.3.3 – Luciferase Reporter Assay.

Overnight cultures of four biological replicates of *V. cholerae* harboring P_{crvA}-transcriptional fusions to luciferase in pBBRlux were diluted 1:100 in 1 mL LB supplemented with ampicillin, chloramphenicol, and IPTG in 1.5 mL microcentrifuge tubes. 150 μL of cell solution was aliquoted into wells of a black 96-well plates (Costar) in technical duplicates. Plates were incubated at 35°C while shaking at 220 RPM. Every hour, luciferase (Relative light units) and OD_{595} measurements were taken, and luciferase activity was measured using an Envision plate reader (Perkin Elmer). Estimated CFU/mL were calculated by fitting a linear regression between OD_{595} and CFU/mL by spot plating dilutions of culture onto LB and counting viable cells.

4.3.4 – RNA Isolation and qRT-PCR.

RNA isolation and qRT-PCR analysis were carried out following the protocols here (Fernandez 2018). In brief, overnight cultures were diluted to a starting OD_{600} of 0.040 in 2 mL LB supplemented with ampicillin and IPTG and grown until an OD_{600} of approximately 1.3 at 35°C and 220 RPM. 1 mL of each replicate was pelleted and RNA was extracted using the TRIzol® reagent following the directions in the manual (Thermo Fischer Scientific). Purified DNA was quantified using a NanoDrop spectrophotometer (Thermo Fischer Scientific). 5 μg of purified RNA was treated with DNAse (Turbo DNAse, Thermo Fischer Scientific). cDNA synthesis was carried out using the GoScript™ Reverse Transcription kit (Promega). cDNA was diluted 1:30 into molecular biology grade water and used as template in qRT-PCR reactions using SYBR Green

(Applied Biosystems™) as the method of detection. Reactions consisted of 5 µL 2.5 µM primer 1, 5 µL of 2.5 µM primer 2, 5 µL of diluted cDNA template, and 15 µL of 2X SYBR green consisting of dNTPs and AmpliTaq Gold® DNA polymerase. Each plate had technical duplicates and biological triplicate samples as well as no reverse transcriptase controls to check for genomic DNA contamination. The StepOnePlus Real Time PCR system was used for qRT-PCR with the following thermocycling conditions: 95°C for 20 seconds then 40 cycles of 95°C for 2 seconds and 60°C for 30 seconds. Melting curves were included to ensure PCR products had single amplicons and primer dimers were absent. Data were analyzed by the ΔΔCt method using *gyrA* as a housekeeping or reference target. The experiment was repeated with 10 biological replicates on separate days and the data from each experiment were pooled.

4.3.4 – Biofilm Formation and Fluorescence Microscopy.

4.3.4.1 – Analysis of Curvature of Attached Cells in Microcolonies.

Overnight cultures were diluted 1:1000 in 1 mL 1X phosphate buffered saline (PBS, Sigma) by 10-fold serial dilutions. Biofilms were grown on UV-sterilized #1 cover slips (22x22 cm) placed in 6-well plates (Costar®) submerged in 1 mL LB. Cultures, in six sets of biological replicates, were seeded in the wells with slides by further diluting 5-fold, resulting in a final dilution of 1:5000, and gentle swirling. Microcolonies were allowed to develop during static incubation at 21°C. At the given timepoint, the media for two biological replicates were removed by aspiration, the wells washed with 1 mL 1X PBS, and the resulting adhered bacteria on the cover slip were stained with 200 µL of the membrane stain N-(3-Triethylammoniumpropyl)-4-(6-(4-(Diethylamino) Phenyl) Hexatrienyl) Pyridinium Dibromide (FM4-64) (Sigma) at a final concentration of 20

μg/mL for 5 minutes. The stain was removed by an additional wash with 1 mL 1X PBS. Small sections of agarose pads (~5x5 mm) were arranged in a 20x20 cm square on glass microscope slides. The glass coverslip containing the stained microcolonies was then inverted and placed on top of the agarose pads. Biofilm imaging was carried out using a Leica DM5000b epifluorescence microscope with a 100X-brightfield objective (1.4 NA) equipped with a Spot Pursuit CCD camera and an X-cite 120 Illumination system. Images were acquired using the RFP fluorescence channel. Each slide was imaged with at least 20 fields of view for each biological replicate at each timepoint. Cells within microcolonies were manually outlined in MicrobeJ using the manual interface option with at least 500-1000 cells outlined per replicate. Data from MicrobeJ analysis were exported into R for analysis.

4.3.4.2 – Determination of Curvature Cutoff Value.

Δ*crvA V. cholerae* strains were grown in LB until OD_{600} of 1.3 in biological triplicate. Cultures were then diluted to an OD_{600} of 0.500, visualized by phase contrast microscopy, and the resulting images were analyzed using MicrobeJ as described above. The curvature cutoff value was calculated from n = 640 cells by finding the sum of the 75^{th} percentile and 1.5 multiplied by the interquartile range (IQR). To determine the percentage of straight cells within a population, the number of cells with curvatures below the curvature cutoff value were divided by the total number of cells and multiplied by 100.

4.3.4.3 – Microcolony Area Analysis

For single timepoint biofilm analysis, 8-well microchamber slides (μ-Slide, 8-well glass bottom, ibidi) were used. 1:1000 diluted overnight cultures were additionally diluted 1:5

in an individual well of the microchamber slide in 200 µL LB supplemented with chloramphenicol at the appropriate concentration. Each slide had three strains in biological duplicate. Microcolonies were developed by incubating the microchamber slide statically at 21°C for 8 hours, resulting in WT microcolony sizes between 10-20 μm^2. Media was removed from slides by aspiration, each well was washed with 200 µL 1X PBS, and the microcolonies were stained with FM4-64 (150 µL) at a final concentration of 20 µg/mL for 5 minutes. The remaining stain was washed with 200 µL 1X PBS and biofilms were imaged by inverting the microchamber (positioning the glass bottom upwards) by fluorescence microscopy using a Leica DM5000b epifluorescence microscope as described above. At least 20 fields of vision were captured per replicate per strain and the resulting images were processed using Fiji by enhancing contrast (Saturated Pixel % - 0.3). Processed images were then analyzed using MicrobeJ with the following settings: Background type (Dark), Mode of detection (Basic), Area (4.5 – 100, μm^2), and circularity (0-1). Data were exported into R for analysis. For all fluorescence microscopy, representative images were cropped, and the scale bar was added using Fiji software (151).

4.3.4.4 – Crystal Violet Biofilm Assay.

Overnight cultures were diluted 1:100 into 1 mL LB supplemented with chloramphenicol into new, unused 18 x 150 mm borosilicate test tubes and statically incubated at 21°C for 8 hours. After 8 hours, media and unattached bacteria were removed, and the biofilms were washed twice with 1 mL 1X PBS (PBS washes were removed by aspiration). 1 mL crystal violet (CV) (.4%) solution was added to each tube and the biofilm was stained for 10 minutes. After, the stain was removed by aspiration and the

stained biofilm was washed twice with 1 mL 1X PBS. CV was eluted with ethanol and the absorbance at 570 nm (OD_{570}) was measured.

4.3.5 – Growth Curve Analysis and Calculation Of Growth Rates.

Overnight cultures were diluted 1:100 into LB supplemented with appropriate antibiotics into clear 96-well plates (Costar®). Growth at 23°C was measured at 5-minute time intervals for 16 hours using a SpectraMax M5 plate reader (Molecular Devices) with agitation between measurements. Data were imported into R for analysis and generation of growth curves. Growth rates were calculated from the linear portions of the growth curve (black, horizontal lines in Figure 4.10) for each strain by calculating the slope and multiplying it by 60, resulting in growth rate (h^{-1}). Data shown are from four biological replicates.

4.4 – Results

4.4.1 – High Intracellular C-di-GMP Decreases Cell Curvature

During the course of our experiments where we modulate intracellular c-di-GMP, we observed that cells with high intracellular concentrations of c-di-GMP, induced by the DGC QrgB, were straighter than cells with unaltered c-di-GMP concentrations harboring an inactive DGC ($QrgB^{MUT}$). We have previously shown these conditions cause physiologically relevant changes in intracellular c-di-GMP concentration using liquid chromatography-tandem mass spectrometry (55). To explore this result further, we measured the dose-dependent effects of IPTG on cell curvature in strains harboring QrgB (Figure 4.1). Indeed, using single-cell image analysis, we observed that c-di-GMP decreased the average two-dimensional curvature in a dose-dependent manner and skewed the distribution of the population from mostly curved to mostly straight (Figure

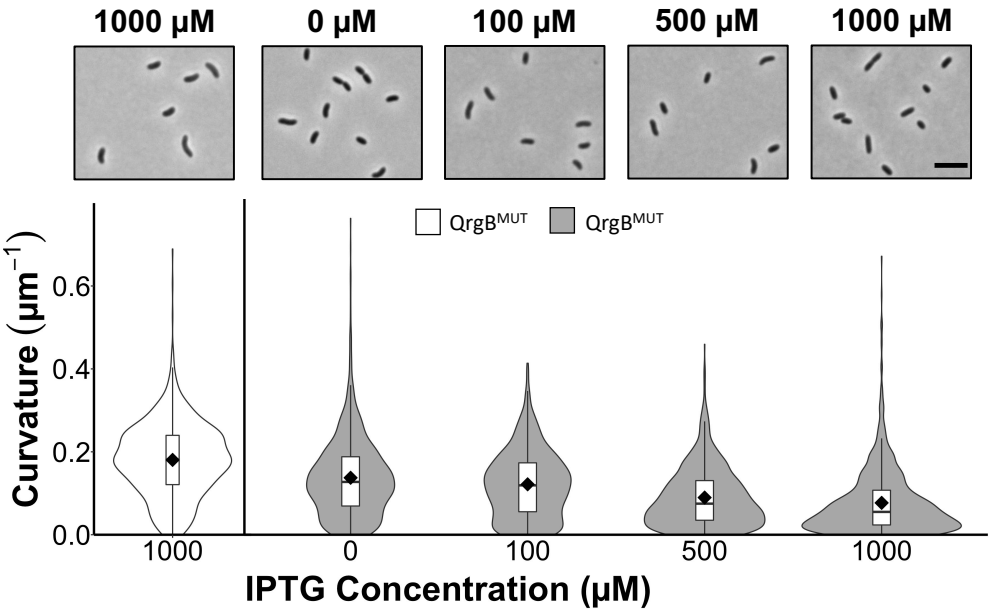

Figure 4.1: C-di-GMP Decreases Cell Curvature in a Dose-Dependent Manner Top) Representative phase-contrast micrographs of early stationary phase cells harboring a plasmid encoding an IPTG-inducible inactive DGC ($QrgB^{MUT}$) with 1000 µM IPTG and an IPTG-inducible active DGC (QrgB) with 0, 100, 500, and 1000 µM IPTG. The bar in each image represents 5 µm. **Bottom)** Quantification of curvature as a function of IPTG concentration in populations expressing the inactive control DGC ($QrgB^{MUT}$, White) or the active DGC (QrgB, Gray). Violin plots are rotated population density plots where the shape of the curve represents the distribution of curvatures within the population. Box and whisker plots internal to the violin plots represent summary statistics: mean (diamonds), median (horizontal black line), quartiles (box), and data 1.5 times below and above the interquartile range (vertical lines from box plots). Each plot represents between 1000 and 1200 cells analyzed and pooled from two to three separate experiments.

4.1). Further, this result was dependent on c-di-GMP, rather than the inducer IPTG, because incubation of the strain harboring the inactive DGC $QrgB^{MUT}$ with 1000 µM IPTG did not decrease curvature (Figure 4.1).

To determine if c-di-GMP altered other aspects of cell morphology, we also measured cell length and cell width under the same conditions. We found that cell width was similar regardless of intracellular c-di-GMP, but cell length decreased slightly as c-di-GMP increased with a fold-change less than one (Figure 4.2). Thus, our data

indicates that, high intracellular c-di-GMP causes cells to straighten and shorten but does not change cell width under the tested conditions.

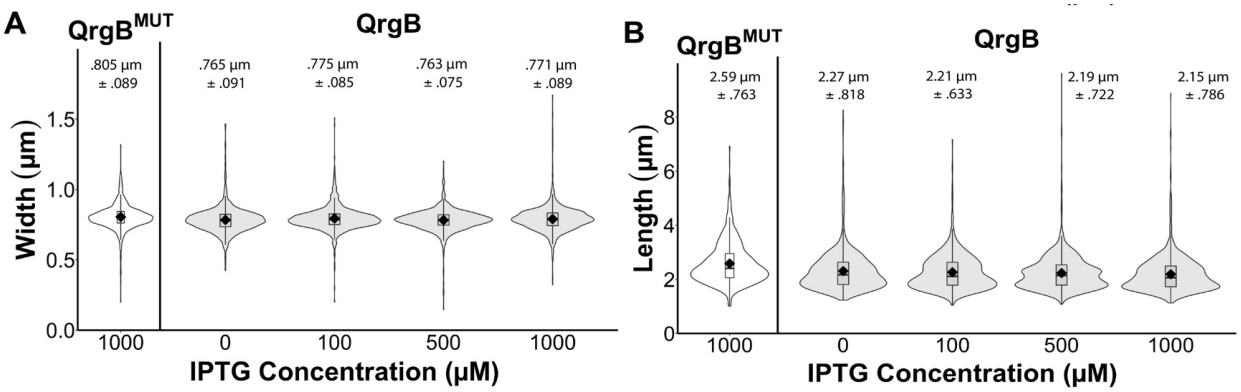

Figure 4.2: C-di-GMP Decrease Cell Length in a dose-dependent manner
(A) Quantification of the average width along the medial axis of cell particles from Figure 4.1. **(B)** Quantification of length of the curvilinear (medial) axis of cell particles from Figure 4.1. Inserts in graphs are mean +/- standard deviation width **(A)** and length **(B).**

4.4.2 – The c-di-GMP Dependent Transcription Factors VpsT and VpsR Control c-di-GMP Mediated Changes to Cell Curvature

In *V. cholerae*, three c-di-GMP dependent transcription factors (VpsR, VpsT, and FlrA) and two c-di-GMP-dependent riboswitches (Vc1 and Vc2), are known regulate genes that elicit diverse phenotypes such as biofilm formation, motility, DNA repair, and catalase production (49, 144, 94, 30, 50, 12, 147, 121, 146). Since VpsR and VpsT are necessary for c-di-GMP mediated regulation of phenotypes outside of their canonical roles in biofilm formation, we hypothesized these transcription factors are necessary for linking intracellular c-di-GMP to changes in cell curvature. To test this hypothesis, we measured curvature in the parent and Δ*vpsR* backgrounds at high (QrgB) and unaltered ($QrgB^{MUT}$) concentrations of c-di-GMP. Confirming our previous result, expression of QrgB decreased the average curvature by about two-fold compared to $QrgB^{MUT}$, and the distribution of curvatures within the population drastically decreased, indicating that

most cells lose curvature under these conditions (Figure 4.3A). However, in the Δ*vpsR* mutant, the c-di-GMP mediated decrease in curvature is essentially lost (Figure 4.3B). Complementation of VpsR from a multicopy plasmid in the Δ*vpsR* mutant restored c-di-GMP inhibition of cell curvature (Figure 4.3C). C-di-GMP inhibition of cell curvature was

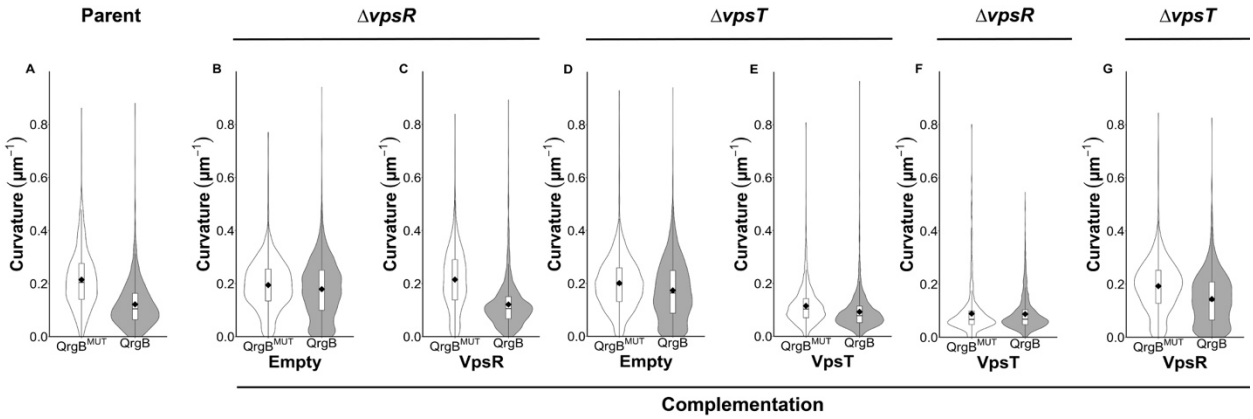

Figure 4.3: The Transcription Factors VpsR and VpsT are Necessary for C-di-GMP Dependent Loss of Curvature.
A) Curvature analysis from the parent background expressing the inactive DGC ($QrgB^{MUT}$, white) and the active DGC (QrgB, gray). **(B,C)** Δ*vpsR* background complemented with the empty vector or VpsR. **(D,E)** Δ*vpsT* background complemented with the empty vector or VpsT. **(F)** Δ*vpsR* complemented with VpsT and **(G)** Δ*vpsT* complemented with VpsR. Plots are the same as described in Figure 4.1.

similarly lost in the the Δ*vpsT* mutant (Figure 4.3D). In this case, complementation of VpsT using a multicopy plasmid resulted in decreased cell curvature, regardless of intracellular c-di-GMP concentration (Figure 4.3E). VpsT has been characterized as a c-di-GMP dependent transcription factor (30), and this result suggests that high levels of VpsT expression is sufficient to decrease curvature at the unaltered concentrations of c-di-GMP. Expression of VpsT in the Δ*vpsR* mutant decreased curvature at both unaltered and high concentrations of c-di-GMP while expression of VpsR in the Δ*vpsT* resulted in curved cells at both c-di-GMP concentrations (Figure 4.3F,G). Together, these data support a model where under high c-di-GMP conditions, VpsR inhibits

curvature indirectly by inducing transcription of *vpsT* while VpsT is sufficient for inhibiting curvature (Figure 4.11).

4.4.3 – c-di-GMP Decreases CrvA Production to Decrease Curvature

In *V. cholerae,* cell curvature is generated by the intermediate-filament like protein CrvA, which is the product of the gene *crvA*. CrvA generates cell curvature by decreasing net growth on the minor axis relative to the major axis by some uncharacterized mechanism. Deletions of *crvA* in *V. cholerae* are straight rods, similar to *E. coli* (142). Thus, we hypothesized c-di-GMP mediated inhibition of curvature was

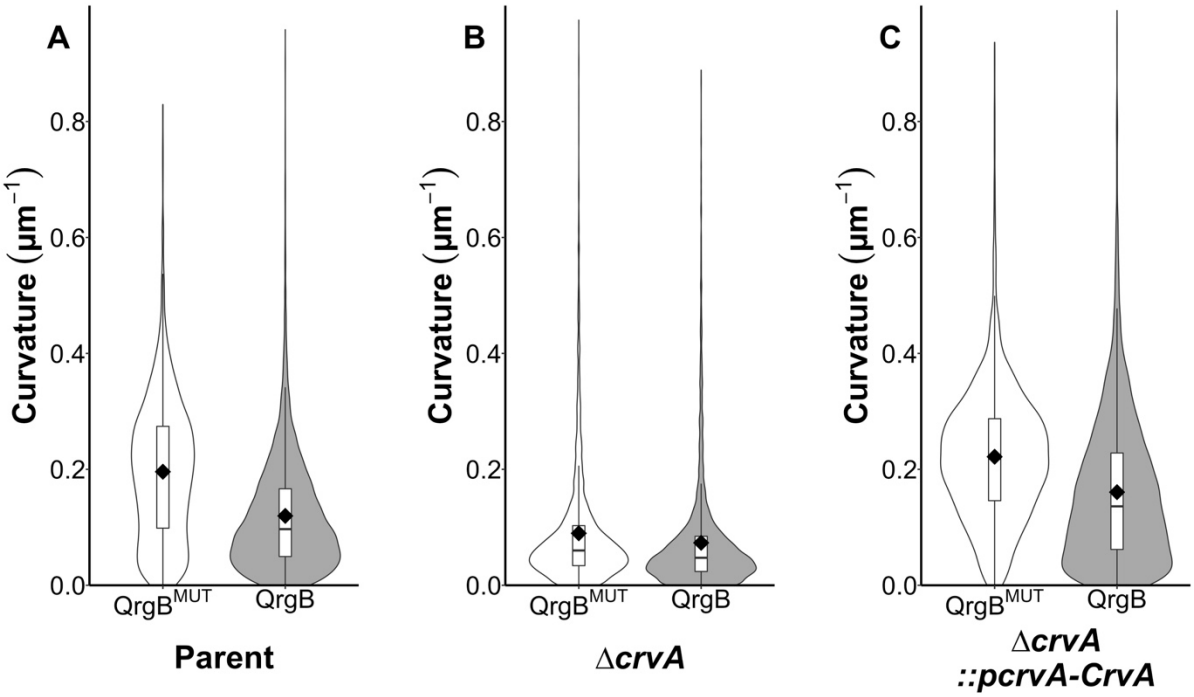

Figure 4.4: Complementation of Δ*crvA* Restores Curvature and Response to c-di-GMP.
Curvature in the **(A)** Parent, **(B)** Δ*crvA*, and **(C)** Δ*crvA* VC1807::P_{crvA}-*crvA* backgrounds under unaltered (QrgB^{MUT}, white) and high (QrgB, gray) c-di-GMP conditions. Plots are the same as described in Figure 4.1.

dependent on *crvA*. In a Δ*crvA* mutant, the cells remained straight regardless of c-di-GMP (Figure 4.4B), indicating CrvA is epistatic to changes in c-di-GMP.

Complementing the Δ*crvA* strain with the native promoter driving *crvA* expression at a

distal site on the chromosome restores the parent strain phenotype, with lower curvature at high c-di-GMP conditions (Figure 4.4A,C).

Since c-di-GMP mediated effects on curvature were dependent on the transcription factor VpsT, we hypothesized c-di-GMP negatively regulated *crvA* expression by inhibiting transcriptional activity of the *crvA* promoter (P_{crvA}). To test this, we generated a transcriptional reporter by fusing the *crvA* promoter to luciferase. This fusion contained 358 bp upstream of the *crvA* translational start site, which was sufficient to restore c-di-GMP inhibition of curvature in the *crvA* complemented strain (Figure 4.4C). However, P_{crvA} transcriptional activity was similar under normal ($QrgB^{MUT}$)

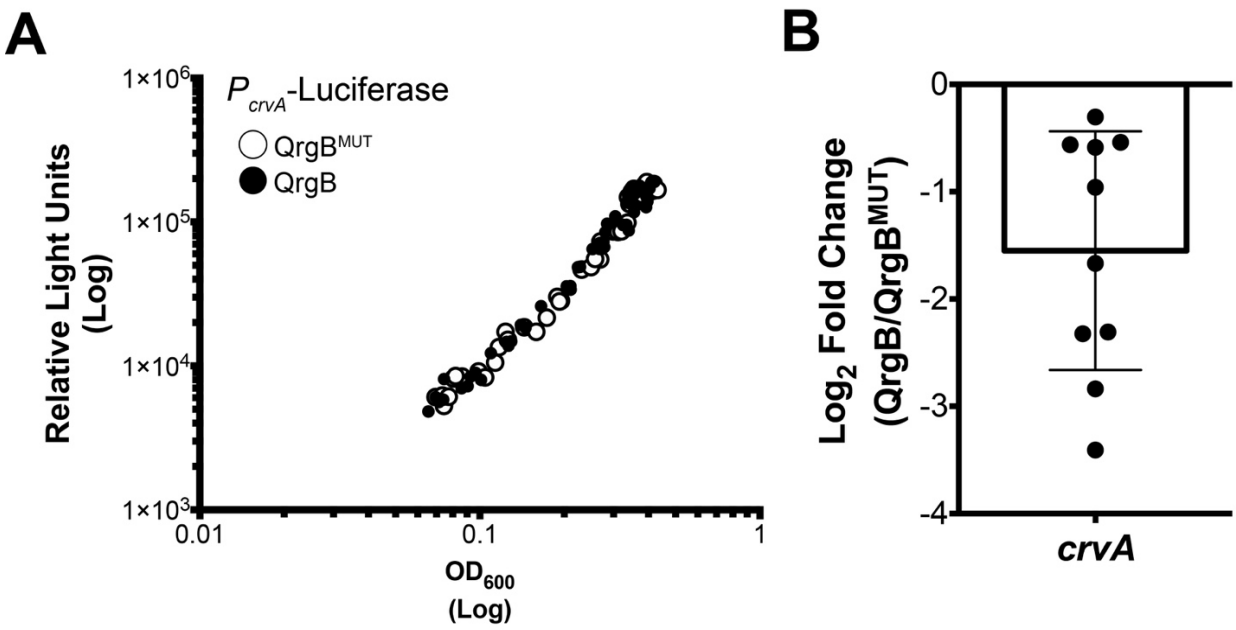

Figure 4.5: Regulation of *crvA* Expression Occurs at the Post-Transcriptional Level.
A) Luciferase reporter activity (relative light units, $\log_{10}$ transformed) of P_{crvA} – luciferase transcriptional fusion as a function of estimated cell concentration (CFU/mL, $\log_{10}$ transformed) under unaltered ($QrgB^{MUT}$, white) and high (QrgB, black) c-di-GMP conditions. Dots represent data for 4 biological replicates at different cell densities. **B)** qRT-PCR analysis of relative *crvA* transcript levels between high (QrgB) and unaltered ($QrgB^{MUT}$) c-di-GMP conditions. Each dot represents 1 biological replicate, the bar represents the mean fold change, and error bars indicate standard deviation.

or high (QrgB) c-di-GMP concentrations at all culture densities examined (Figure 4.5A).

P_{crvA} transcriptional activity increased with cell density, in agreement with earlier studies that observed increased curvature in high cell density conditions (Figure 4.5A) (142, 145).

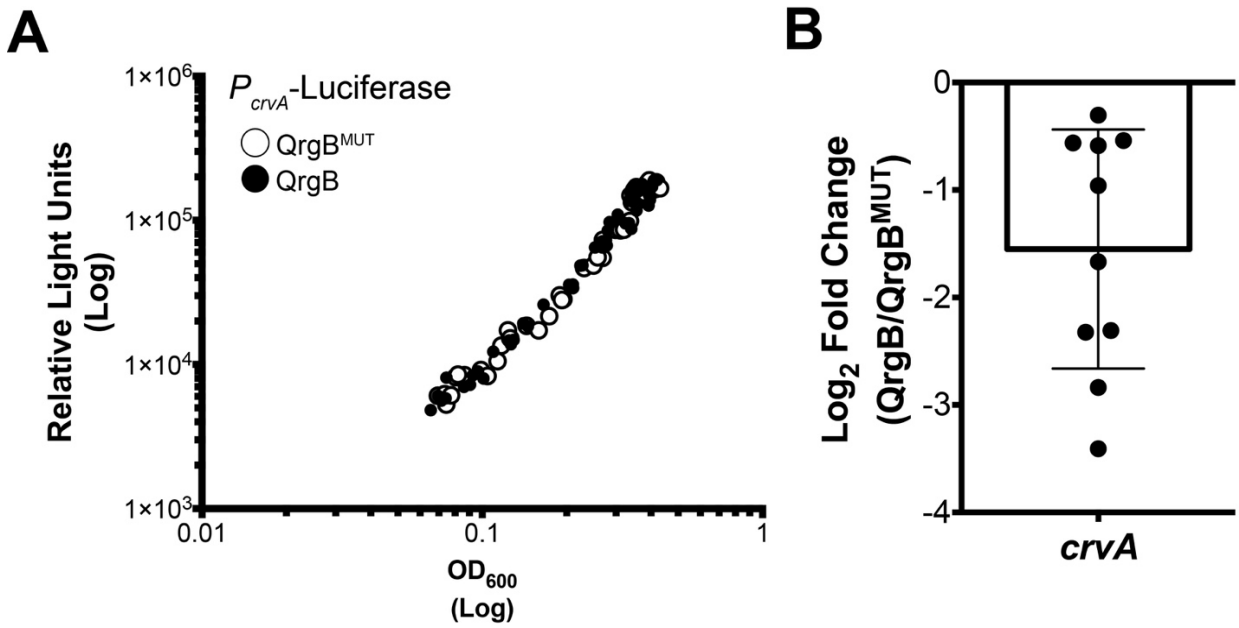

Figure 4.6: Regulation of *crvA* Expression Occurs at the Post-Transcriptional Level.
A) Luciferase reporter activity (relative light units, $\log_{10}$ transformed) of P_{crvA} – luciferase transcriptional fusion as a function of estimated cell concentration (CFU/mL, $\log_{10}$ transformed) under unaltered (QrgB^{MUT}, white) and high (QrgB, black) c-di-GMP conditions. Dots represent data for 4 biological replicates at different cell densities. **B)** qRT-PCR analysis of relative *crvA* transcript levels between high (QrgB) and unaltered (QrgB^{MUT}) c-di-GMP conditions. Each dot represents 1 biological replicate, the bar represents the mean fold change, and error bars indicate standard deviation.

Next, we tested if c-di-GMP impacted *crvA* mRNA abundance using qRT-PCR from RNA isolated from cultures with unaltered and high intracellular c-di-GMP. We found that strains with high intracellular c-di-GMP exhibited a significant 2.3-fold reduction in *crvA* transcripts compared to cells with unaltered c-di-GMP (Figure 4.5B). Together, these data suggest c-di-GMP negatively controls *crvA* expression at the post-

transcriptional level, resulting in decreased levels of CrvA and decreased cellular curvature.

4.4.4 – *V. cholerae* Adopts a Straight Morphology During Early Stages of Biofilm Formation

The ability of *V. cholerae* to colonize a surface and initiate biofilm formation is dependent on intracellular c-di-GMP as well as the transcription factors VpsR and VpsT. Strains with low c-di-GMP or lacking VpsR and/or VpsT are unable to form mature biofilms (49, 88, 144). Thus, that fact that decreased curvature under high c-di-GMP conditions is dependent on VpsT suggests this phenomenon occurs during biofilm

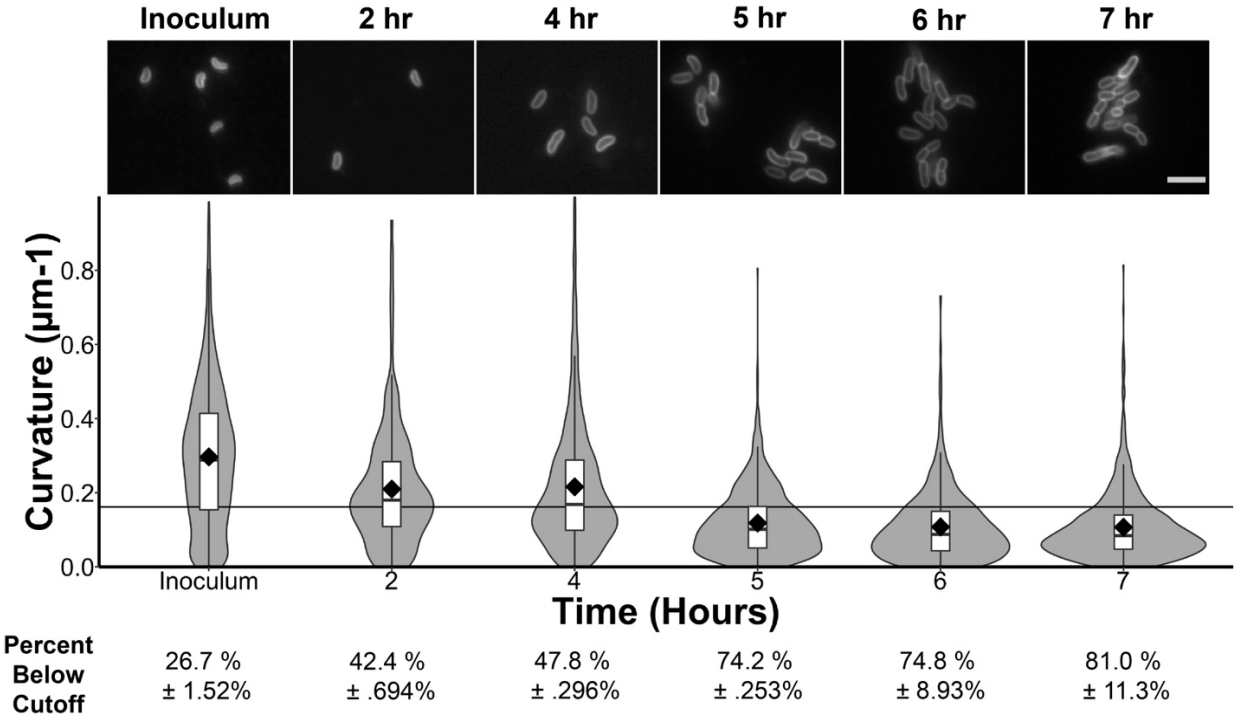

Figure 4.7: *V. cholerae* Has a Straight Cell Morphology in Microcolonies. **(Top)** Representative images of *V. cholerae* from the inoculum and 2, 4, 5, 6, and 7 hours post inoculation onto glass coverslips. Cells were stained with FM4-64 prior to imaging. Scale bar is 5 µm. **(Bottom)** Curvature of individual cells at different times during microcolony formation. Horizontal line indicates the curvature cutoff value (see Methods and Materials) and values below graph are the mean percent of cells below the curvature cutoff +/- the standard deviation. The experiment was repeated twice, and results are from n = 500-1000 cells.

formation, where c-di-GMP activated VpsT is concomitantly inducing expression of genes involved in production of Vibrio polysaccharide and associated biofilm matrix proteins (30, 31). To test the hypothesis that cells in biofilm inducing conditions adopt straight cell shapes, we grew biofilms under static conditions and measured single-cell morphology over time from initial attachment until early stages of microcolony formation. We chose these timepoints because during later stages of biofilm formation under similar conditions, *V. cholerae* grows in dense clusters with some cells in the biofilm becoming vertical relative to the surface, which complicates two-dimensional measurements of curvature (152, 153). Cells from the stationary phase cultures used to inoculate biofilms appeared mostly curved, with 26.7% having a curvature less than or equal to the mean curvature of the Δ*crvA* mutant indicated by the horizontal line Figure 4.6. Between two and four hours of static incubation, cells attached to the glass substratum retained a range of curvatures, however the average curvature decreased from 0.304 μm^{-1} in the inoculum to 0.221 μm^{-1} (Figure 4.6). At five hours, however, the average curvature of adhered cells had a curvature similar to the Δ*crvA* background with curvature decreasing at later time points (Figure 4.6). These data indicate cells undergoing biofilm formation lose two-dimensional curvature and adopt a straight cell morphology similar to that of the ΔcrvA deletion strain.

4.4.5 – Cell Shape Influences Biofilm Production at the Single-Cell and Population Level.

Since cells undergoing biofilm formation in submerged conditions adopt a straight cell shape, we wondered if locking cells in a curved morphology would impact biofilm formation. To accomplish this, we expressed CrvA from a multicopy plasmid using the

PBAD promoter and introduced it into the ΔcrvA background. We found basal expression of this construct (i.e. - no inducer added) was sufficient to complement the curvature phenotype (Figure 4.7). Thus, using the WT, Δ*crvA,* and Δ*crvA*-pCrvA strains, we generated cells that are able to transition between curved and straight analogous to the parent strain or are constitutively straight or constitutively curved (Figure 4.7). The average microcolony size for the WT strain harboring the control vector pHERD20C at 8 hours was 16 μm^2 (Figure 4.8A,B, left panel). This is approximately 5-times larger than the average area of an individual cell within a microcolony (2.7 μm^2, calculated from cells in Figure 4.6) indicating the WT strain is adhered in multicellular clumps (Figure 4.8A,B). Microcolonies formed by the Δ*crvA* background harboring the control vector

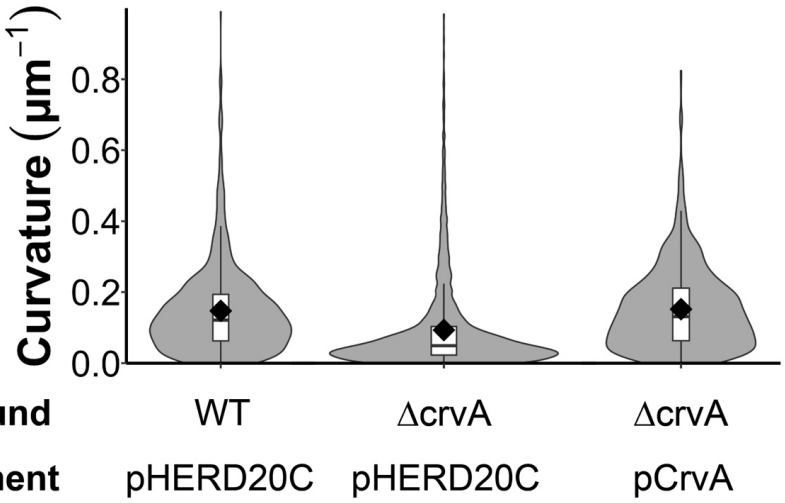

Figure 4.8: Complementation of the Δ*crvA* Background with pCrvA.
Analysis of curvature from complementation of Δ*crvA* background with either the empty vector (pHERD20C) or the CrvA expression plasmid pCrvA with varying concentrations of L-arabinose to induce protein expression. Complementation experiments were conducted in M9-glucose minimal media and LB with similar results. Data are pooled from two sets of experiments with two biological replicates each. N = 2000-3000 cells per violin plot.

looked similar to the WT background, with an average microcolony area of 18 μm^2 indicating lack of curvature does not alter microcolony formation (Figure 4.8B).

Additionally, WT and ΔcrvA-pHERD20C strains had similar levels of surface coverage (Figure 4.9). Next, we analyzed microcolony size with the Δ*crvA* background harboring the pCrvA expression plasmid. Development of *V. cholerae* biofilms is dependent on proper cell-cell and cell-surface contact, thus we hypothesized having curved cells

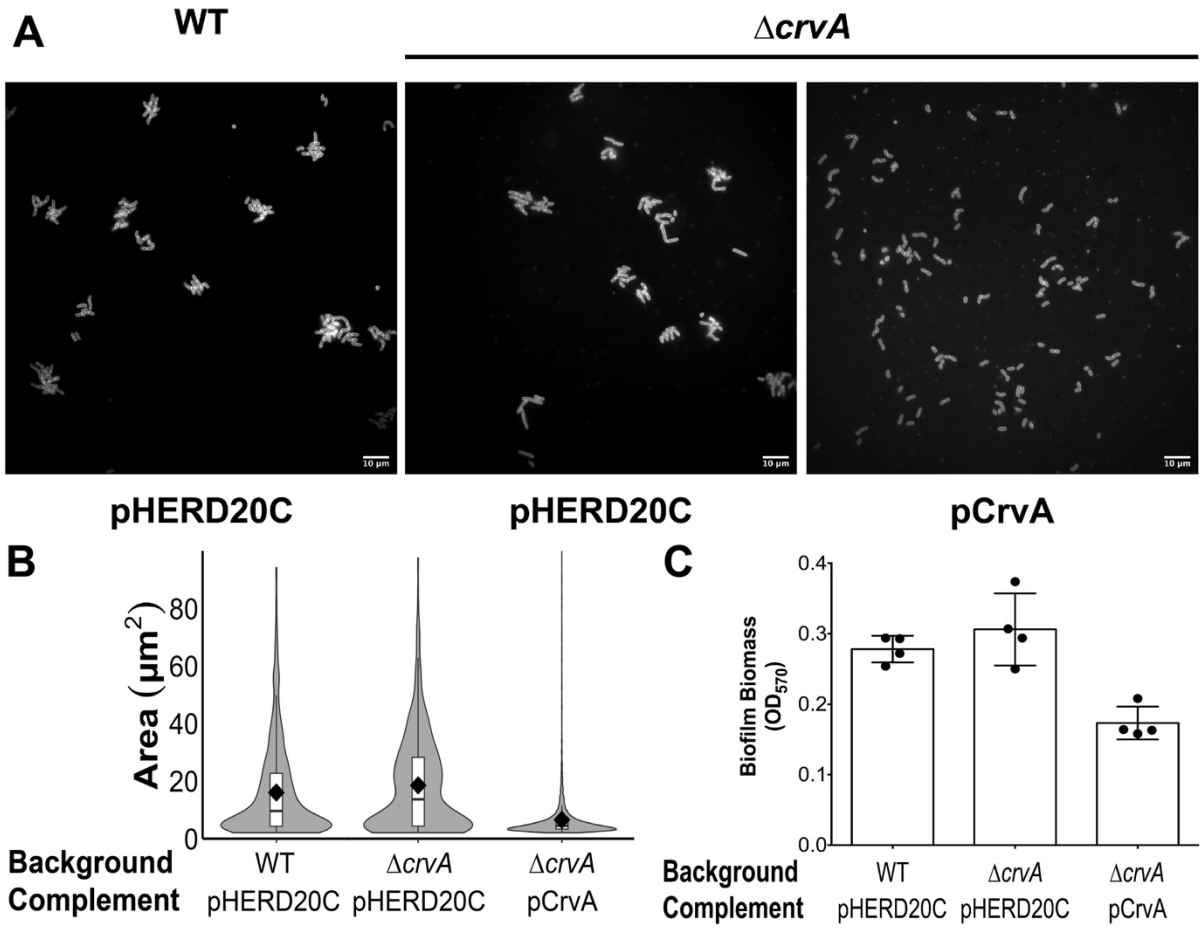

Figure 4.9: Curvature Influences Microcolony Development and Population Level Biofilm Formation.
A) Representative images of *V. cholerae* microcolonies of WT harboring the control vector pHERD20C (left panel), Δ*crvA* harboring the control vector pHERD20C (center panel), and Δ*crvA* harboring the CrvA expression vector pCrvA (right panel). Microcolonies were stained with FM4-64 prior to imaging. Scales in the bottom right of each image are 10 μm. **B)** Analysis of areas from objects detected in images from A. Results are pooled from two sets of experiments and are from n = 700-2000 objects. **C)** Biofilm formation at the population level measured by biofilm biomass accumulation. Each dot is the value of one biological replicate, the bars represent the mean value, and error bars are standard deviation.

during biofilm development would disrupt this process (153). Indeed, the average microcolony area for constitutively curved cells was 6.6 μm^2, which is 2.4-fold lower than the WT strain, indicating that cells were attached as individual cells or small microcolonies (Figure 4.8A,B). It is possible that constitutively curved cells were unable to adhere to the surface; however, an analysis of the total area covered indicated this is not the case as constitutively curved cells actually cover more of the substratum than the parent or constitutively straight cells (Figure 4.9). We then hypothesized that the decreased ability to form microcolonies in the Δ*crvA* – pCrvA background would lead to a decrease in biofilm formation. Using crystal violet to assess biofilm formation of static culture in glass tubes, we found that WT and Δ*crvA* harboring the control vector

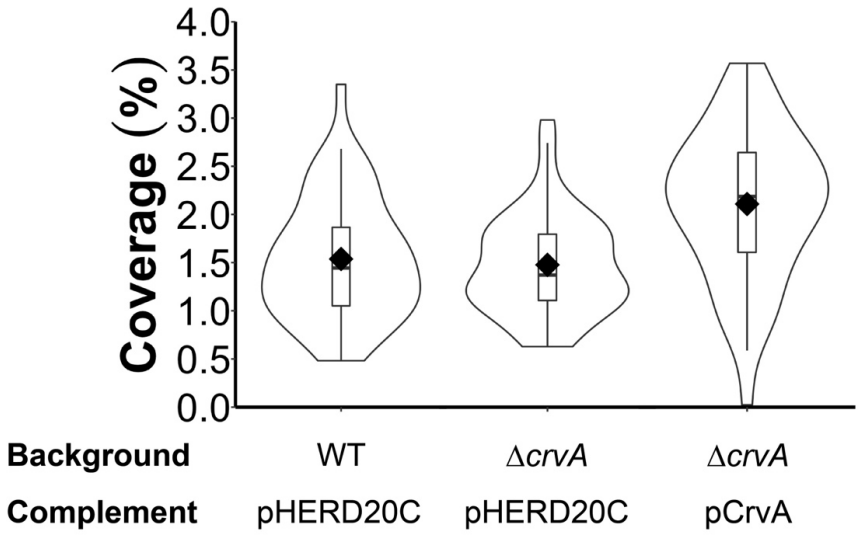

Figure 4.10: Curvature Does Not Alter Surface Coverage
Percent surface coverage of adhered objects was measured in WT (left), straight (Δ*crvA*-pHERD20C, middle), and curved (Δ*crvA*-pCrvA, right) backgrounds. Images from Figure 4.8A were used for analysis.

displayed similar accumulated biofilm biomass (Figure 4.8C). The Δ*crvA*-pCrvA background, however, had decreased biofilm biomass compared to the other strains, suggesting the lack of microcolony formation at the single-cell level reduces overall biofilm formation (Figure 4.8C). We examined the growth rate between the WT and

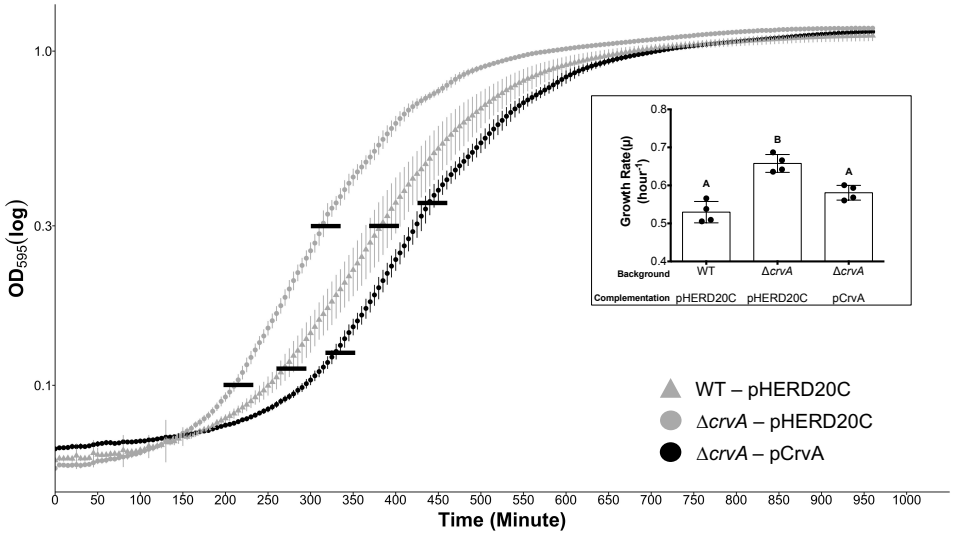

Figure 4.11: WT and Complemented Δ*crvA* Have Similar Growth Curves and Growth Rates.
A) Analysis of growth curves for WT – pHERD20C (triangles, gray), Δ*crvA* – pHERD20C (circles, gray), and Δ*crvA* – pCrvA (circles, black). Each symbol indicates the average OD_{595} of four biological replicates and error bars indicate standard deviation. Solid horizontal dashes for each curve indicate the region of the growth curve used to calculate growth rates. **Boxed Insert.** Growth rates of WT-pHERD20C, Δ*crvA*-pHERD20C, and Δ*crvA*-pCrvA calculated from growth curves in A. Bars indicate means, error bars indicate standard deviation, dots are the value for four biological replicates, and letters indicate statistically significant comparisons determined by One-Way ANOVA followed by Tukey's post-hoc multiple comparisons test ($p < 0.05$).

Δ*crvA* mutant harboring pHERD20C or pCrvA (Figure 4.10). We observed that the constitutively straight cells exhibited a decreased lag phage with increase growth rate whereas the constitutively curved cells exhibited an increased lag phage with a growth rate similar to the WT background. Given that both of these strains adhered to the surface equal to or greater than the WT control, these differences in growth rate are not sufficient to account for the differences in biofilm that we have observed.

Taken together, these results indicate change in cell shape is a regulated process during biofilm production and that decoupling of curvature from changes in c-di-GMP negatively affects biofilm formation in *V. cholerae* (Figure 4.11).

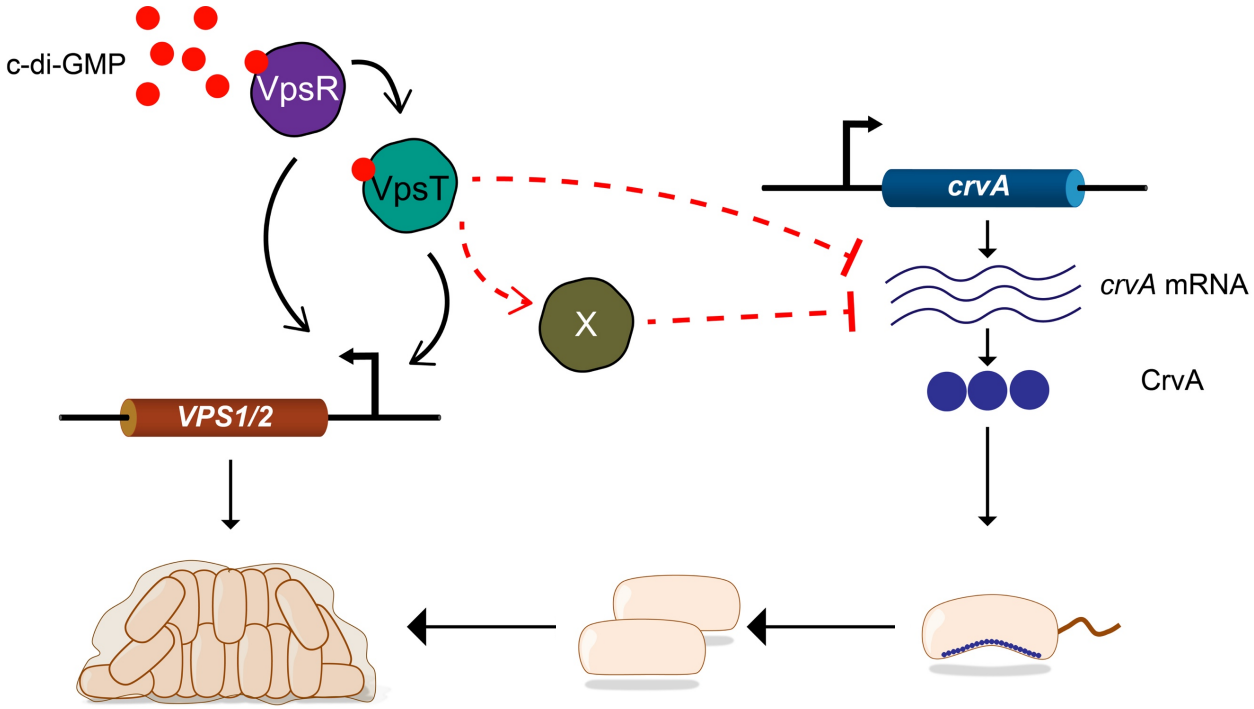

Figure 4.12: Model for c-di-GMP Regulated Transition from Curved to Straight Cells
High c-di-GMP conditions causes activation of the c-di-GMP dependent transcription factors VpsR and VpsT, which promote biofilm formation by inducing expression of *Vibrio* polysaccharide biosynthetic operons (VPS operon 1 and VPS operon 2). Through an uncharacterized mechanism (highlighted by the dashed, red lines), high c-di-GMP negatively regulates *crvA* at the post-transcriptional level by decreasing *crvA* mRNA abundance. As a result, CrvA is unable to decrease cell curvature as cells grow and divide. This transition from curved to straight cells is an important process in mature biofilm formation, as curvature retention decreases biofilm formation.

4.5 – Discussion

There is evidence that the rod-shape was one of the earliest established shapes in the bacterial world. As such, derivatives of the rod-shape, such as helical or vibrioid shapes, are novel adaptations produced by genes with specific functions in altering shape. These mechanisms are under selection to alter the physical properties of

bacterial cells and are likely to be differentially regulated by environmental conditions (137). However, mechanistic examples of coordinated shape change during bacterial lifestyle transitions are limited. In this study, we identified the bacterial second messenger c-di-GMP as a regulator of cell shape in the aquatic organism *V. cholerae*. Specifically, we found that c-di-GMP causes cells to decrease in curvature and appear as straight rods. This response was dependent on the IF-like gene *crvA* and transcription factors that control biofilm formation, prompting us to assess the implications of shape in biofilm formation. We found cells exist mostly as straight rods within microcolonies. Further, cells remaining curved had a defect in microcolony formation and mature biofilm production, highlighting the importance of cell shape in development of multicellular communities such as biofilms.

Our conclusion that c-di-GMP negatively regulates curvature and *crvA* mRNA abundance is supported by several studies. *V. cholerae* utilizes quorum sensing (QS) as one mechanism to change intracellular c-di-GMP, where cells in low-cell density cultures tend to have higher c-di-GMP than cells in high-cell density cultures (88, 154). Cell shape also correlates with culture density (142, 145). First demonstrated nearly 100 years ago, Alfred Henrici commented "The embryonic cells [those cells early in the growth curve] are therefore large, plump, and straight…Therefore, the mature cells are slender and curved, the typical *Vibrio* form" in his 1928 monograph on morphology and growth rates (142, 145). Thus, the finding that cells in low-cell density appear straight, as well as the finding that c-di-GMP can override QS signaling, support our conclusion that c-di-GMP controls cell shape (88, 142, 145). Additionally, RNA-seq studies measuring transcriptional changes between low cell density and high cell density

determined *crvA* is decreased at low cell density conditions (155).

We also found VpsT was sufficient for curvature inhibition under planktonic conditions (Figure 4.3D,G), suggesting VpsT negatively regulates *crvA* expression directly or indirectly at the post-transcriptional level. Indeed, earlier transcriptomic studies of VpsT identify *crvA* as a target of negative regulation (30, 49, 94). While we could not test it directly because Δ*vpsT* backgrounds are unable to form biofilms, our data strongly suggests VpsT is necessary for curvature inhibition during biofilm formation (30, 31, 49, 94). Since curvature inhibition is necessary for WT-like microcolony formation (Figure 4.8), our results outline a novel role for VpsR and VpsT in the development of biofilm structures in *V. cholerae*.

We found that cells adhered to a surface adopted a shape that was more similar to that of a Δ*crvA* background rather than the canonical vibrioid shape (Figure 4.6). Interestingly, in other studies of single-cell analysis of biofilm formation, cells appear straight rather than curved (152, 153, 156). The fact that curvature alters two-dimensional microcolony formation, which occurs prior to formation of densely packed vertical cells, was surprising given the influence of cell shape on cell packing in dense clusters (153, 157, 158). The mechanism driving this phenomenon is currently under investigation, however, the fact that curved cells (Δ*crvA*-pCrvA) were able to colonize the substratum equally well as WT and straight cells (Δ*crvA*-pHERD20C) (Figure 4.9) indicate the difference is not due to decreased adherence. Instead, the spatial distribution and area of cell clusters in the curved background suggests curved cells colonize and detach from the surface at greater rates than WT or straight cells.

Our results suggest a model where, under increasing c-di-GMP conditions, curved *V. cholerae* attaches to a surface and begins forming a biofilm. Increased c-di-GMP causes CrvA depletion in the founder cell and progeny, resulting in straight cells during microcolony formation. As the microcolony grows, the straight morphology allows for dense clustering and the formation of the "hedgehog"-like tertiary biofilm structure (152, 153). We speculate that as nutrients become unavailable and the biofilm lifestyle is no longer advantageous, decreases in c-di-GMP and increases of HapR expression cause cells to adopt the curved-shape which could facilitate dispersal from the biofilm matrix (142, 159).

Indeed, there are numerous examples of cell shape influencing the development of multicellular structures and activities. The inability to transition from rod-shaped cells to spores in *Myxococcus xanthus* causes detrimental effects to development of fruiting bodies (160). Additionally, mutations that alter the rod-shape in *Proteus mirabilis* and *Rhodobacter sphaeroides* negatively affects swarming motility and biofilm formation, respectively (161, 162). In the vibrioid shaped *C. crescentus,* curvature is important for biofilm formation under flow conditions but had no effect under static conditions (163). Our findings, in contrast, demonstrate retention of curvature during biofilm formation is detrimental toward mature biofilm production. These conflicting results are likely a function of the different processes during biofilm formation in the two organisms: *C. crescentus* attach and are positioned vertically through the use of a polar stalk while *V. cholerae* attach to surfaces horizontally via interactions with flagella and Type IV pili and transition to vertical positions as the biofilm grows (164, 152, 153). A recent study analyzing pandemic *V. cholerae* found that nutrient-starved isolates grew as filaments in

media mimicking natural conditions with fluid flow that allowed them to form dense multicellular structures on chitin particles (165). Images of the strains suggested these cells still retain curvature, with filamented cells appearing as corkscrew-like cells, supporting the authors' conclusion that biofilms by filamentous cells are independent of c-di-GMP signaling and VPS production (165). Together, our data and others indicate that maintenance or changing of shape can impact ecological adaptation through development of multicellular structures such as biofilms.

Chapter 5 – Concluding Remarks

5.1 – Conclusions and Significance

The wide-spread bacterial second messenger c-di-GMP is associated with adherence and motility in diverse microorganisms, including the human pathogen *V. cholerae.* However, multiple lines of evidence suggest c-di-GMP controls a wider range of bacterial phenotypes. Following a screen to identify c-di-GMP responsive genes, I found that high c-di-GMP promotes expression the DNA repair gene *tag* and provides tolerance to the DNA damaging agent MMS (Chapter 2). Additionally, I found that high c-di-GMP promotes catalase activity and tolerance to H_2O_2 by increasing expression of the catalase encoding gene *katB* (Chapter 3). Importantly, these two distinct, biofilm matrix independent phenotypes were linked by the c-di-GMP transcription factor VpsT.

Bacteria in biofilms tend to be more tolerant to stress and antimicrobials. In some cases, this can be attributed to the physical components of the biofilm, such as exopolymeric substances with chemical quenching abilities (166, 167). Additionally, cells within mature biofilms face environmental heterogeneity such as nutrient or oxygen deprivation, causing changes to global stress response systems leading to stress tolerance (168). My results, however, propose a different, more specific mechanism of biofilm tolerance: control of genes involved in stress responses by second messenger signal c-di-GMP. Further, the fact that VpsT is also necessary for c-di-GMP mediated regulation of stress responses (Chapter 2 and Chapter 3) suggests that cells upregulate *tag* and *katB* during biofilm formation or the biofilm lifestyle.

An interesting finding from this work is the potential for anticipatory or predictive signaling by bacteria. Under the growth conditions described in this work, there were no indications of DNA damage or oxidative stress. The only signal to change expression of

tag or *katB* was different levels of intracellular c-di-GMP, suggesting c-di-GMP modulation of *tag* and *katB* expression is in response to the stress they help mitigate, such as DNA damage or reactive oxygen species. Mathematical modeling and experiments in *E. coli* provide evidence for anticipatory regulation, where increases in temperature (akin to digestion by an animal host) lead to a transcriptional response promoting anaerobic metabolism, which could be beneficial during colonization of gastrointestinal tract (169). The results from Chapter 2 and 3 differ in that there are multiple signals that induce c-di-GMP production and biofilm formation in *V. cholerae* (57, 88, 170–172). Thus, by linking stress responses with c-di-GMP rather than a particular environmental signal assures cells are protected during the biofilm lifestyle.

Through evolution, bacteria encompass a diverse range of shapes that are likely important for survival in certain niches. In *V. cholerae,* the ability to transition between the well-known comma-shaped morphology to a straight rod has been acknowledged for nearly 100 years; however, how this occurs, or the ecological benefit of this shift, is not well understood (142, 145). In my thesis, I show that the transition between straight and curved cells is controlled by c-di-GMP and VpsT. I found that cells transition from curved planktonic cells to straight cells after they attach to a surface and form the early stages of mature biofilms, with curvatures similar to that of the straight rod-shaped bacterium *E. coli* or *V. cholerae* lacking the gene *crvA*. My finding that shape determination is a regulated process influenced by c-di-GMP allowed a different question to be asked: what is the role of shape transition in biofilm formation in *V. cholerae?* I found that retention of curvature during the biofilm formation process

results in decreased microcolony formation and biofilm production compared to constitutively straight cells or the wild-type strain.

Sustained c-di-GMP signaling negatively affects virulence in *V. cholerae*, which has been attributed to biofilm formation and down-regulation of expression of virulence factors (173). Interestingly, my results demonstrate that high c-di-GMP promotes generation of a straight cell phenotype. In separate studies of *V. cholerae* cell shape, straight cells (Δ*crvA*) have a virulence defect in animal models of infection compared to WT-cells (142). Thus, my findings open the possibility that c-di-GMP mediated changes in cell shape could also contribute to the virulence defect observed in high c-di-GMP strains (16, 173).

These findings also have implications for the process of biofilm formation. In mutants that disrupt cell shape in the Gram-negative rod-shaped *Rhodobacter sphaeroides* or *E. coli,* cause defects in biofilm formation, thus my result that shape is an important factor in *V. cholerae* biofilm formation aligns with data from other systems (162, 174). While biofilm formation is a well-studied topic in *V. cholerae,* the influence of cell shape on biofilm formation is largely uncharacterized (152, 153, 156, 157). A recent study identified natural isolates of *V. cholerae* filament upon nutrient depletion, which allowed cells to form multicellular communities on chitinous particles under flow conditions (165). The authors concluded that the biofilms formed under these conditions were independent of VPS, suggesting this phenotype is independent of c-di-GMP and may represent a more generalized response to nutrient deprivation (165). With the identification of *crvA* in *V. cholerae,* several research groups hypothesized about the potential role of curvature in motility in matrices, such as host mucin or the

biofilm matrix (139, 142). While I did not test it directly, these hypotheses make sense given that c-di-GMP decreases curvature and promotes biofilm formation; thus, cells dispersing from a biofilm likely have lower c-di-GMP and increased curvature.

I believe the mechanism connecting c-di-GMP, stress responses, and cell shape is a niche specific adaptation in *V. cholerae* rather than a general phenomenon in bacteria. While there are studies that link biofilm formation and an increase in stress tolerance, most described mechanisms are not dependent on c-di-GMP or c-di-GMP dependent transcription factors (166, 168). Further, there does not appear to be any correlation between cell shape transitions between planktonic and biofilm conditions and the presence or absence of c-di-GMP signaling systems (35). For example, the human pathogen *Helicobacter pylori* has a helical shape in planktonic conditions while approximately 80% of cells within in vitro biofilms appear as cocci or straight rods (175). However, *H. pylori* lacks genes necessary for c-di-GMP signaling (35). Thus, the use of c-di-GMP to modulate curvature and stress responses in *V. cholerae* may be a beneficial adaptation in the ever-changing aquatic environments where *V. cholerae* resides.

5.2 – Future Directions

5.2.1 – Single Cell Analysis Of *tag* And *katB* Expression During Different Stages of Biofilm Formation

To further the studies from Chapters 2 and 3, analysis of the spatial and temporal heterogeneity of *tag* and *katB* expressing cells would provide insight into how cells are positioned within biofilms. For instance, in statically grown *E. coli* biofilms, oxygen diffusion decreases toward the center of the biofilm (176). Similar dynamics are likely

present in *V. cholerae* biofilms, thus, even though cells within a biofilm have high c-di-GMP concentrations, the source for oxidative stress would be limited and there would be little ecological benefit to producing catalase. However, by spatially arranging catalase positive cells towards the periphery where damage by oxidative stress is greater, producing catalase could be advantageous. Utilizing fluorescent reporters of *katB* or *tag* and time-course confocal laser scanning microscopy (CLSM) on biofilms grown in static conditions, one can begin to explore the positioning and timing of gene expression within biofilms. Additionally, these gene expression patterns can be correlated with single cell measurements of c-di-GMP using fluorescent riboswitch c-di-GMP reporter constructs (177). By combining information on gene expression, c-di-GMP, and cell positioning, one can gain insights into how unicellular bacteria function together to divide labor during development of complex multicellular structures.

5.2.2 – Mechanism of Negative Regulation by VpsT

An interesting finding from Chapter 4 is negative regulation of expression by VpsT, which until now has only been characterized as a positive regulator of gene expression (30, 31, 49, 94), however there is evidence that VpsT causes down-regulation of genes at the mRNA level (30). Additionally, the fact that c-di-GMP causes a decrease in *crvA* transcript abundance provides another wrinkle in the mechanism of gene regulation by VpsT, which has only shown to act as DNA binding anti-repressor (31, 96).

My data suggest VpsT indirectly regulates *crvA* expression by altering expression of another factor that decreases mRNA stability. Thus, I propose a screen based on Tn5 mutagenesis and high-throughput screening utilizing flow cytometry to identify

genes necessary for curvature inhibition by VpsT. This screen requires an optimized flow cytometry protocol to enhance detection of small cells and changes to cell shape outlined by Sycuro *et al.* who implemented a similar experiment in *Helicobacter pylori* (178). After generation of the Tn5 mutant pool in a Δ*vpsT* background, an expression plasmid harboring VpsT would be moved into the pooled population by conjugation. Following growth to late exponential phase and induction of VpsT in the mutant pool, the cells would be introduced into the flow cytometer for shape analysis and sorting by forward and side scatter. Flow cytometry parameters will be optimized by using a straight cell population (Δ*vpsT*-pCMW132 (VpsT)) or a curved cell population (Δ*vpsT* – pBRP333 (Empty vector)). Mutants that maintain curvature after VpsT induction will be sorted and collected into LB medium and plated onto LB kanamycin plates. Isolated colonies from these plates are assumed to be independent mutants that harbor transposon mutations in genes necessary for curvature inhibition by VpsT. Clones will be rescreened by microscopy and single-cell analysis. Positive clones will be identified by either arbitrary PCR or plasmid rescue (179, 180).

5.2.2 – Mechanism of Curvature Mediated Decrease in Microcolony Formation

The finding that curvature inhibited microcolony formation is interesting but warrants further exploration into the mechanism of how this occurs. The scattered positions of the curved cells in Figure 4.8A suggests curvature influences the ability of the cells to remain adhered to a surface during growth of a microcolony. To test this hypothesis, the time of residence (length of time an individual cell remains on the surface prior to dispersal) of curved and straight cells could be measured by time-

course microscopy (as described here (181)). My hypothesis predicts that straight cells would have a longer time of residence compared to curved cells.

A decreased time of residence would suggest curved cells are defective in maintaining surface adherence as the microcolony increases in size. One potential explanation is that curvature negatively feeds back into c-di-GMP pools and biofilm matrix production, which is necessary to keep cells adhered to the surface (152, 156). This hypothesis predicts that curved cells have lower intracellular c-di-GMP and *vpsL* expression than straight cells, which can be measured in bulk populations or at the single cell level using fluorescent reporters.

If WT, straight, and curved cell populations display similar levels of c-di-GMP and biofilm matrix production, then the observed difference in microcolony formation could be attributed to the physical consequences of curvature. Mathematical modeling and analysis of verticalization of straight (Δ*crvA*) *V. cholerae* cells in biofilms found that horizontal cells become vertical only when the force of division of cells encased in a matrix cells is greater than the force of adhesion between the cell and the surface (157). Curved cells would have less points of contact with the surface, resulting in smaller adhesion forces necessary for verticalization (157). Thus, curved cells become vertical prior to straight cells under identical conditions. Since the timing of verticalization coincides with matrix production, early verticalization could produce three dimensional structures with less matrix, allowing cells to escape the matrix and colonize a new location.

APPENDICES

Appendix 1

Using Vibrio cholerae as a Heterologous Host to Study c-di-GMP Signaling in *Burkholderia cenocepacia*

Appendix 1.1 – Introduction

Burkholderia cenocepacia is a Gram-negative opportunistic pathogen known for its ability to chronically infect lungs of patients with cystic fibrosis (182). In its chronic infective state, *B. cenocepacia* is able to withstand the host immune system, most likely through its ability to form adhered microbial communities called biofilms (183). While biofilms play an important role in *B. cenocepacia* pathogenesis and other chronic infections, a more thorough understanding of how evolution shapes niche adaptation within biofilms is needed. Specifically, how the process of biofilm formation selects for adaptations that allow for better biofilm formation capability.

Experimental evolution is a powerful tool that utilizes selection for a trait as a powerful means to isolate mutants with adaptive traits (184). Until recently, evolution experiments in biofilms lacked appropriate generation times to uncover long-term effects of biofilm growth (185). Therefore, our collaborators established a high-throughput model of surface colonization, biofilm formation, and dispersal utilizing polystyrene beads and daily transfers while continuously sampling for biofilm phenotypes by colony morphology (185). Three distinct colony morphotypes arose (in descending frequency): studded (S), ruffled (R), and wrinkled (W). Whole genome sequencing (WGS) analysis uncovered the S and R morphologies have mutations in the putative quorum sensing regulator RpfR (186).

RpfR is a multidomain protein with 4 characterized domains: 1) FI (Rpf**F** interaction), 2) PAS, 3) diguanylate cyclase (DGC) with a GGDEF active sit motif, and 4) phosphodiesterase (PDE) with an EAL active site domain (Figure 5.1). The PAS domain of RpfR binds to the signaling factor *Burkholderia* Diffusible Signaling Factor

(BDSF), which is synthesized by RpfF, an enzyme with fatty acid biosynthesis activities (187). The FI-domain binds to RpfF, which causes a decrease in BDSF production (188). While the DGC domain has the appropriate residues for activity, there is no evidence of DGC activity. Rather, Deng *et al.* determined that RpfR predominately functions as a phosphodiesterase and that BDSF binding increases PDE activity (189). The S morphotype is caused by a mutation that results in the amino acid substitution Y355D (Figure 5.1, vertical purple bar in GGDEF domain) while the R morphotype is caused by the amino acid substitution A106P (Figure 5.1, vertical purple bar between the FI and PAS domains) (186). In planktonic and biofilm conditions, these mutations alone cause an increase in c-di-GMP concentrations in *B. cencocepacia* (Figure 5.2).

It is unclear how these evolved amino acid substitutions affect RpfR activity,

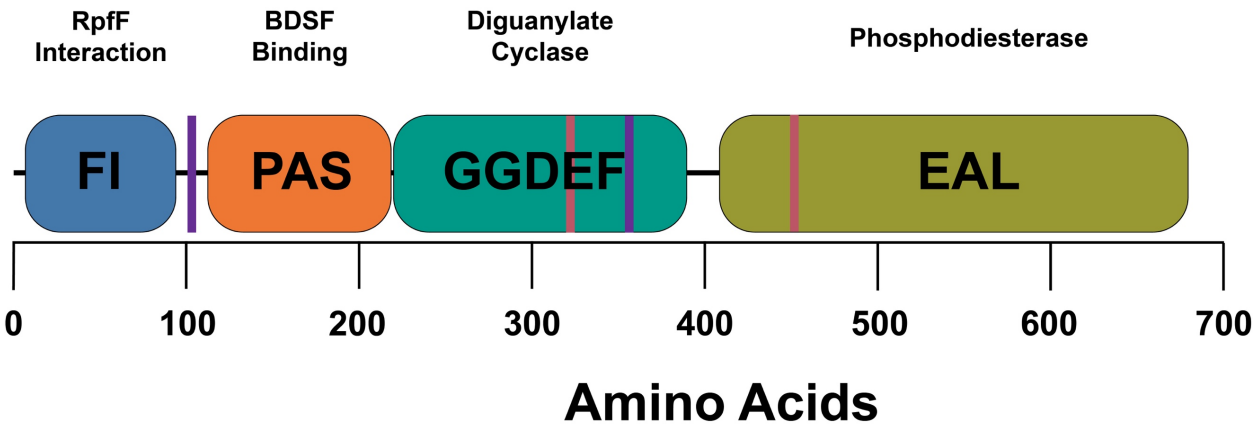

Figure 5.1: Diagram of RpfR
Domains are labeled by color with functions above. Active site motifs for GGDEF and EAL are vertical pink bars within the respective domain. Amino acid substitutions are marked by vertical purple lines (A106P – between FI and PAS domains, Y355D – downstream of GGDEF active site motif).

specifically its ability to synthesize and degrade cyclic dimeric guanosine monophosphate (c-di-GMP) to manifest the evolved colony morphology. However, the positions of these substitutions suggest the mechanism is more complex than

deactivation of PDE activity (Figure 5.1). Thus, we sought to explore the mechanism driving increased c-di-GMP and biofilm production by the evolved RpfR variants. During the course of our studies, we found that RpfR displays DGC activity when expressed in the heterologous host *Vibrio cholerae.* Using this system, we determined the evolved variants produce c-di-GMP and biofilms similarly to ancestor RpfR, suggesting the substitutions do not alter DGC activity. Lastly, since selection in biofilm environments in vivo are commonly associated with a decrease in acute virulence, we assessed the virulence capacity of the ancestor and the in vitro evolved *B. cenocepacia* and found, indeed, that selection during biofilm formation decreased acute virulence. Together, these studies begin to provide mechanistic insights into how amino acid substitutions arising through evolution can fine-tune signaling systems to allow adaptations to specific environmental niches.

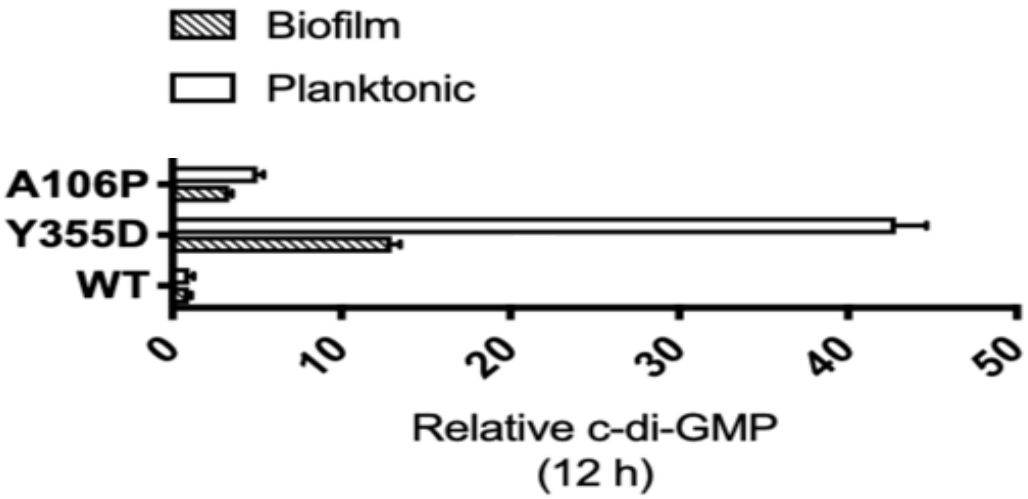

Figure 5.2: Evolved RpfR Alleles Have Higher Intracellular c-di-GMP Pools Compared to the Ancestor
Intracellular c-di-GMP was measured in B. cenocepacia grown in biofilm and planktonic conditions. Concentrations were normalized to the ancestor (WT) background. Bars represent averages and error bars are 95% confidence interval. Data generated by Eisha Marte, Dan Snyder, and Vaugh Cooper (Unpublished).

Appendix 1.2 – Methods and Materials

A1.2.1 – DNA Manipulations and Growth Conditions

Plasmid were constructed using restriction enzyme cloning. Plasmid pEVS143 was digested with AvrII and BamHI (NEB) and gel purified (Wizard Gel and PCR Cleanup, Promega). Ancestor, Y355D, and A106P RpfR were amplified from genomic DNA isolated from the respective *B. cenocepacia* mutants, digested with AvrII and BamHI, and PCR purified. Inserts and vectors were mixed at a 3:1 insert:vector ratio in a 20 µL DNA ligase reaction with 800 U DNA ligase (NEB). Reactions were incubated at 16^{o}C overnight and were transformed into S17 *E. coli.* Correct clones were identified by colony PCR and sequenced by sanger sequencing (Genewiz, Inc). *V. cholerae* strain C6706 Str2 and *B. cenocepacia* HI2424 and evolved mutants were used in this study and grown in 2 mL LB overnight prior to experiments. Antibiotics and reagents were used at the following concentrations unless stated otherwise: Kanamycin (100 µg/mL), 100 µM isopropyl β-D-1-thiogalactopyranoside (IPTG), and 10 µM *Burkholderia* Diffusible Signaling Factor (BDSF, cis-2-dodecenoic acid). Lyophilized BDSF was resuspended in DMSO at a final concentration of 50 mM.

A1.2.2 – Crystal Violet Biofilm Assay

Overnight cultures of WT *V. cholerae* harboring ancestor, Y355D, A106P, or an empty vector were diluted 1:100 in LB supplemented with Kanamycin, IPTG, and either BDSF or equally diluted DMSO. 150 µL of diluted cell cultures were added to wells in a clear 96-well plate (Costar®) and cultures were grown at 35^{o}C while shaking at 220 RPM until late log-phase. Cultures were removed from the wells and analyzed for intracellular c-di-GMP (see below). The wells were washed twice with 1X phosphate buffered saline

(PBS) by adding 150 µL and aspirating the wash solution using a vacuum aspirator. 150 µL of crystal violet (CV) solution (0.41% crystal violet, 12% ethanol w/v) was added and biomass was stained for 10 minutes. After staining, CV was aspirated away, and the wells were washed twice with 1X PBS. CV was eluted by adding 150 µL 95% ethanol to each well and gently pipetting to mix the solution. The absorbance at 570 nm was measured using a Perkin Elmer Envision plate reader. For solutions that saturated the absorbance range of the plate reader (OD_{570} > 2.0), 1:10 dilutions of eluted CV were made in 150 µL final volumes using 95% ethanol and absorbance was measured. Final OD_{570} values were adjusted by multiplying the value by the dilution factor. For experiments where BDSF was added, data presented are the percent reduction from BDSF addition ($\frac{X_i - X_o}{X_i} * 100\%$), where X_i is the biofilm biomass from untreated cultures and X_o is the biofilm biomass from untreated samples.

A1.2.3 – Quantification of Intracellular c-di-GMP

Cultures for each strain and condition from 4 wells (approximately 600 µL) were pooled and analyzed for intracellular c-di-GMP and total protein concentration. For protein concentration quantification, 100 µL of culture was removed from each sample, pelleted by centrifugation at full speed (15,000 x g) for 1 minute, resuspended in 50 µL 1X PBS with 10% sodium dodecyl sulfate (SDS), and boiled at 95°C for 10 minutes. Lysed cell solutions were centrifuged at 15,000 x g for 1 minute and the supernatant containing protein was removed and placed in new tubes. Total protein was quantified using the DC Protein Assay (Bio-Rad) following the instructions in the manual. Protein standards consisting of bovine serum albumin (provided in DC Protein Assay kit) were used to generate a standard curve to interpolate sample concentrations. 550 µL of the

remaining culture were pelleted at 15,000 x g for 1 minute in a benchtop microcentrifuge. The supernatants were removed, and the remaining pellets were resuspended in 100 µL nucleotide extraction buffer (40:40:20 methanol/acetonitrile/water with 0.1 N formic acid). The extraction solution was incubated at 20°C for 20 minutes and pelleted for 10 minutes at 15,000 x g. The supernatants were placed into new microcentrifuge tubes, and the solutions were dried overnight using a heated, vacuum centrifuge (SpeedVac Concentrator, Savant). The resulting dried pellets were resuspended in 100 µL HPLC-grade water and subjected to mass spectrometry analysis for quantification of c-di-GMP (128). Final c-di-GMP concentrations are in pmol c-di-GMP * mg^{-1} total protein. For BDSF treated samples, data presented are the percent reduction from BDSF addition ($\frac{X_i - X_o}{X_i} * 100\%$), where X_i is the c-di-GMP concentration in untreated cultures and X_o is the c-di-GMP concentration in untreated samples.

A1.2.4 – C-di-GMP Production in V. cholerae Cell Lysates

A1.2.4.1 – Lysate Generation.

Overnight cultures of *V. cholerae* harboring ancestral and evolved RpfR alleles or an empty vector were diluted in 1:100 in 5 mL LB Kan in 25 mL baffled flasks and grown until an OD_{600} of 1.25. 100 µM IPTG was added to all cultures to induce RpfR and cultures were grown for an additional hour. After induction, cultures were pelleted by centrifugation (7800 RPM for 2 minutes) in 15 mL conical tubes. The cell pellets were resuspended in cold 1 mL TELCA buffer (25 mM TRIS-HCl, 5 mM $MgCl_2$, 5 mM NaCl, pH – 7.5) (190)and moved to a 1.5 mL microcentrifuge tube. Cells were lysed by freeze-thaw cycles where cells were frozen in a dry ice/ethanol bath and thawed in a

water bath set to 37°C. 6 freeze-thaw cycles were sufficient to lyse approximately 95% of the population. Insoluble material was pelleted by centrifugation (15,000 x g for 1 minute) and supernatants were moved to new tubes. Protein concentrations in lysates were determined by the DC Protein Assay (Bio-Rad). Lysates were stored at -20C for up to 1 week.

A1.2.4.2 – In vitro DGC Activity in Lysates.

Analysis of in vitro DGC activity in lysates was derived from the TELCA assay with changes (190). Lysates (1 mg/mL) were incubated with TELCA buffer and 1 mM ^{13}C-GTP in 100 µL final volume. Reactions were incubated at 37°C and 30 µL aliquots were removed at 30, 60, and 120 minutes and heat inactivated at 95°C for 10 minutes. 30 µL phenol:chloroform:isoamyl alcohol 25:24:1 were mixed with the reactions and centrifuged for 30 seconds at 15,000 x g. 25 µL of the aqueous (top) layer were removed, placed in mass spectrometry vials, mixed with 25 µL HPLC-grade water, and both ^{12}C-c-di-GMP and ^{13}C-cyclic-di-GMP were detected by monitoring the *m/z* of the precursor ion and fragment ion.

A1.2.4.3 – *Galleria mellonela* infection assay

Overnight cultures of ancestor, Y355D, or A106P *B. cenocepacia* were pelleted, washed in sterile 1X PBS, and diluted to 1 x 10^6 CFU/mL in sterile 1X PBS. Larva of the wax worm *Galleria mellonela* were purchased from Speedy Worm (Alexandria, Minnesota). Prior to experiments, worms with a dry mass between .1 and .2 mg were collected to normalize for worm size. 10 worms were injected with 10 µL of 1X PBS (negative control) or ancestral, Y355D, A106P *B. cenocepacia* to deliver 10^4 CFU per worm using insulin syringes (BD Veo™, 6 mm, 15/64" – 31G, ½ mL). Inoculated worms

(10) were kept in 100 x 15 mm sterile petri dishes at 30°C. Each experiment included three biological replicates of bacteria and 3 sets of 10 worms along with 1 set of 10 worms injected with 1X PBS. Survival, measured by lack of response to physical stimuli, was scored after 2.5 days. Three experiments were carried out on separate days and the 1X PBS (negative death control) had 100% survival in each experiment. Data presented are the pooled data from each experiment, with each dot representing the survival experiment from 1 biological bacterial replicate.

A1.2.4.4 – Statistical Analysis.

Data are represented as the mean ± SD. Statistical analyses (details in figure legends) were calculated with GraphPad Prism Ver. 6 (GraphPad, San Diego, CA). A p-value of < 0.05 was considered statistically significant.

Appendix 1.3 – Results

A1.3.1 – RpfR Has Net DGC Activity in A Heterologous Host.

While in vitro measurements of enzymatic activity would be ideal for these analysis, expression and purification of RpfR and the evolved alleles have been challenging using conventional protein expression hosts and technology. After troubleshooting conditions, we found the A106P and Y355D alleles had issues expressing and producing working amounts of soluble protein in *E. coli* BL21 (DE3) – pLysS. We then began exploring enzyme activity in vivo using the heterologous host *Vibrio cholerae*. This host was chosen for the following reasons: i) c-di-GMP can be measured directly through mass spectrometry (88), ii) changes in intracellular concentrations can be inferred indirectly and qualitatively through measuring changes in biofilm formation (2), and iii) *V. cholerae* has the capacity to withstand wide ranges of

intracellular c-di-GMP without displaying growth defects, which is not the case for other heterologous hosts such as *E. coli* (55, 191). Additionally, *V. cholerae* has been used as a heterologous host for analyzing DGC enzymes from *Clostridium difficile,* an anaerobic microorganism that does not display easily measured c-di-GMP regulated phenotypes (192).

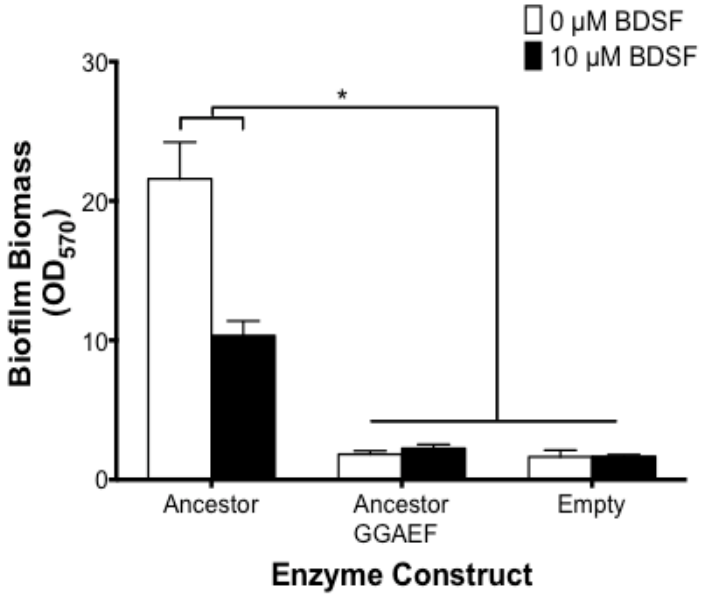

Figure 5.3: Ancestor RpfR Influences Biofilm Formation in *Vibrio cholerae*
Biofilm formation was measured in V. cholerae expressing the ancestor RpfR or RpfR with the inactive DGC motif GGAEF. An empty vector was included as a control. When indicated, BDSF was added at a final concentration of 10 μM. Brackets indicate comparisons with a. p-value < 0.05 determined by Two-Way ANOVA followed by Tukey's multiple comparisons testing. Bars indicate average and error bars indicate standard deviation. N = 6.

Using the *V. cholerae* heterologous host system, we found that over-production of ancestral RpfR increased biofilm formation in *V. cholerae* compared to the vector control (Figure 5.3). To rule out the possibility that RpfR was altering biofilm formation through some other, *V. cholerae* specific mechanism, we substituted aspartate for alanine in the active site motif (GGDEF → GGAEF) and did not observe biofilm formation relative to the vector control. Further, addition of exogenous *Burkholderia* diffusible signaling factor (BDSF) which has shown to increase PDE activity of RpfR

(189), causes a decrease in biofilm formation which was not observed in the empty vector (Figure 5.3). Together, this data suggests RpfR has DGC activity in a heterologous host model and that addition of BDSF changes activity from net DGC activity to net PDE activity. In support of this hypothesis, we found that WT RpfR increases intracellular c-di-GMP in *V. cholerae* compared to an empty vector control (Figure 5.4A).

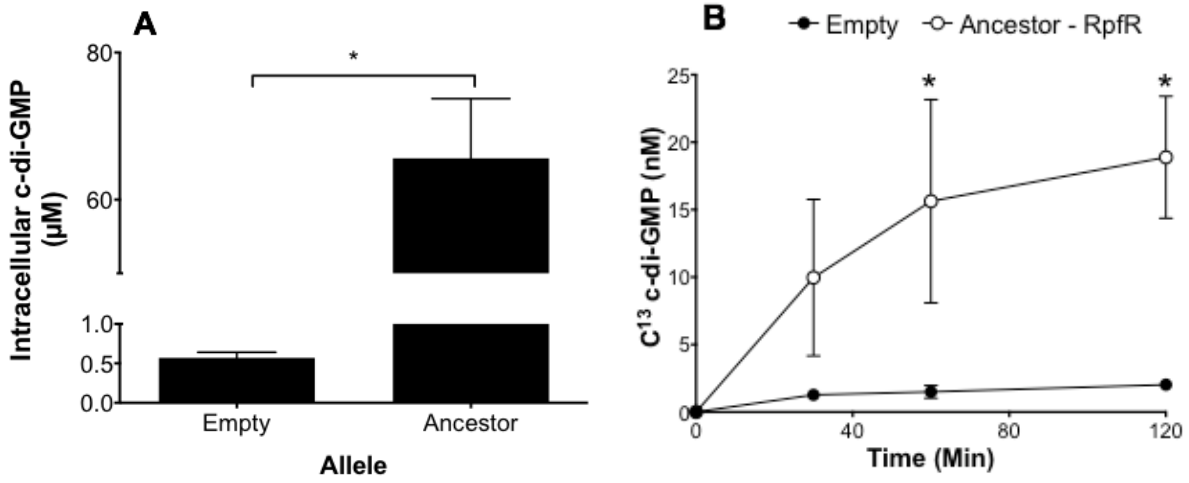

Figure 5.4: RpfR Produces c-di-GMP in *Vibrio cholerae*
A) RpfR increases intracellular c-di-GMP in *V. cholerae*. RpfR was over-produced in V. *cholerae* and intracellular c-di-GMP was measured using mass spectrometry. Bars indicate average and error bars indicate standard deviation. * indicates a p-value < 0.05 determine by a Student's T-test. N = 3. **B)** c-di-GMP synthesis was measured from cell lysates generated from cultures over-producing ancestor RpfR. As a control, lysates from cultures with the empty vector was included. At time 0, stable-labeled C^{13} GTP was added to the reaction mixture and timepoints were removed at regular intervals. C^{13}-c-di-GMP production was measured by mass spectrometry. Circles indicate averages and error bars indicate standard deviation. * indicate a p-value < 0.05 when comparing Ancestor RpfR to the empty vector at a given timepoint. N = 3.

We next wanted to directly measure c-di-GMP synthesis by RpfR. To do this, we utilized a technique called TELCA where lysates from *V. cholerae* expressing RpfR were mixed with stable-labeled C^{13}-GTP and C^{13}-c-di-GMP synthesis was measured by mass spectrometry (190). We observed greater C^{13} c-di-GMP synthesis when over-

producing RpfR compared to the empty vector, indicating RpfR can synthesize c-di-GMP (Figure 5.4B). The role of DGC activity of RpfR has not fully been addressed in the literature, nor have there been any reported experiments to test DGC activity in vitro or a heterologous host. Thus, this is the first example demonstrating the DGC activity of RpfR.

A1.3.2 – Ancestral and Evolved RpfR Alleles Have Similar Biofilm and C-di-GMP Phenotypes in V. cholerae

Since the evolved RpfR alleles A106P and Y355D resulted in hyper-biofilm phenotypes in *B. cenocepacia,* we hypothesized expressing these variants in *V. cholerae* would also cause hyper biofilm formation due to increased intracellular c-di-GMP. We tested this hypothesis by expressing the ancestor and evolved alleles in *V. cholerae* and measured biofilm formation and intracellular c-di-GMP. Similar to our initial findings we found that ancestral RpfR had higher biofilm production compared to the empty vector (Figure 5.5A). A106P, interestingly, had decreased biofilm biomass compared to the ancestor and was similar to the empty vector control (Figure 5.5A). Biofilm biomass was 20% lower in the Y355D background; however, it was still higher than A106P and the empty vector (Figure 5.5A). To determine if the changes observed in biofilm biomass by the evolved alleles correlated with intracellular c-di-GMP, we measured c-di-GMP using mass spectrometry. We found that, indeed, intracellular c-di-GMP mirrored biofilm biomass (Figure 5.5C). Intracellular c-di-GMP was approximately 2-fold higher in A106P compared to the empty vector, but this difference was not enough to alter the biofilm biomass phenotype (Figure 5.5AC). Y355D had similar levels of intracellular c-di-GMP compared to the ancestor background and 3-fold higher levels than A106P and

the empty vector (Figure 5.5C). Together, these results suggest that despite the hyper-biofilm and high intracellular c-di-GMP phenotypes in *B. cenocepacia*, the evolved alleles are unable to recapitulate similar phenotypes when expressed in the heterologous host *V. cholerae.*

One potential explanation for the above results is that the amino acid substitutions do not alter enzymatic activity per se, but rather they disrupt the ability of BDSF to increase PDE activity (189). Thus, to determine if the evolved alleles still responded to BDSF in *V. cholerae*, we repeated the biofilm biomass assay while adding 10 μM to the cultures prior to incubation. In *V. cholerae* expressing the ancestor allele, we found that BDSF addition decreased biofilm biomass by nearly 50% (Figure 5.5B). BDSF addition to strains expressing A106P caused a slight increase (12%) in biofilm biomass, however, this was not statistically significantly different from the empty vector control (Figure 5.5B). Similar to the ancestor, BDSF caused approximately a 40% reduction in biofilm biomass in strains expressing Y355D. Since BDSF decreased biofilm biomass in the ancestor and Y355D expressing strains, we hypothesized intracellular c-di-GMP also decreased under these conditions. Additionally, since BDSF had no effect on reducing biofilm biomass in strains expressing A106P, we hypothesized intracellular c-di-GMP would be unchanged in this background. The ancestor and evolved alleles had a similar 50% decrease in intracellular c-di-GMP in the presence of BDSF (Figure 5.5D). As a control, we included BDSF in strains harboring the empty vector and observed an 18% in intracellular c-di-GMP. Upon further examination, however, we found that these data were not significantly different from a percent reduction of 0, while the ancestor and evolved alleles were (One-sample T-test,

alpha = 0.05, Ancestor – p = 0.011, A106P – p = 0.0068, Y355D – p = 0.0259, EV – p = 0.7186). Thus, these data demonstrate that the evolved alleles of RpfR respond

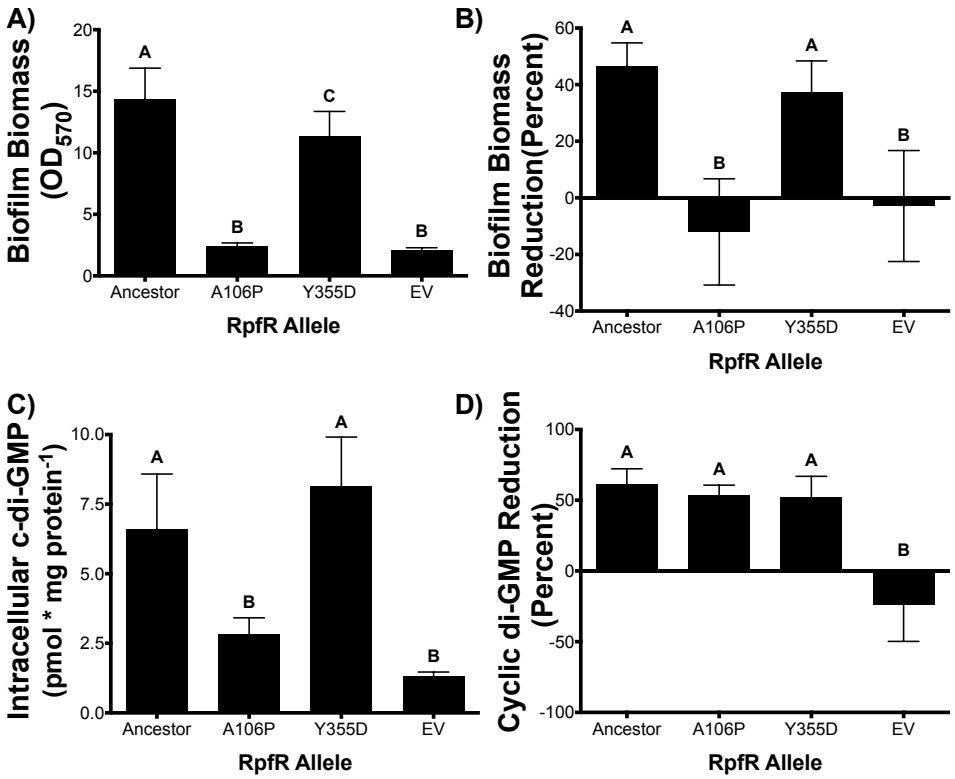

Figure 5.5: Biofilm and Intracellular c-di-GMP for Evolved Alleles in the Presence and Absence of BDSF

A) *V. cholerae* biofilm biomass measured in strains expressing either the ancestral RpfR or the evolved alleles (A106P, Y355D). Bars are means with error bars as standard deviation. **B)** Biofilm biomass reduction caused by the addition of 10 μM BDSF during biofilm formation (percent reduction equation in Methods section for Appendix 1). **C)** Intracellular c-di-GMP measurements from *V. cholerae* strains expressing ancestral or evolved (A106P or Y355D) RpfR. **D)** C-di-GMP reduction caused by the addition of 10 μM BDSF during incubation. For all graphs, different letters indicate statistically significant differences ($p < 0.05$) determined by one-way ANOVA followed by Tukey's multiple comparison post-test. For experiments in panels **A** and **B,** N = 12. For experiments in panels **C** and **D,** N = 3. Experiments were repeated at least twice.

similarly to BDSF compared to the ancestor allele in *V. cholerae*. Additionally, these data do not support the hypothesis of differential DGC and/or PDE activity as an explanation for the evolved hyper-biofilm phenotypes in *B. cenocepacia.*

A1.3.3 – *B. cenocepacia* Harboring the Evolved Y355D RpfR Allele Is Attenuated in a Wax Worm Model of Acute Infection.

In bacterial pathogens that form in vivo biofilms in chronic infections, there is a common trade-off between chronic infection and acute virulence: isolates form in vivo biofilms tend to be less virulent in acute infection models (193). Thus, we were interested in whether in vitro evolved biofilms also displayed a decrease in acute virulence. To test whether the hyper biofilm mutants in *B. cenocepacia,* which have

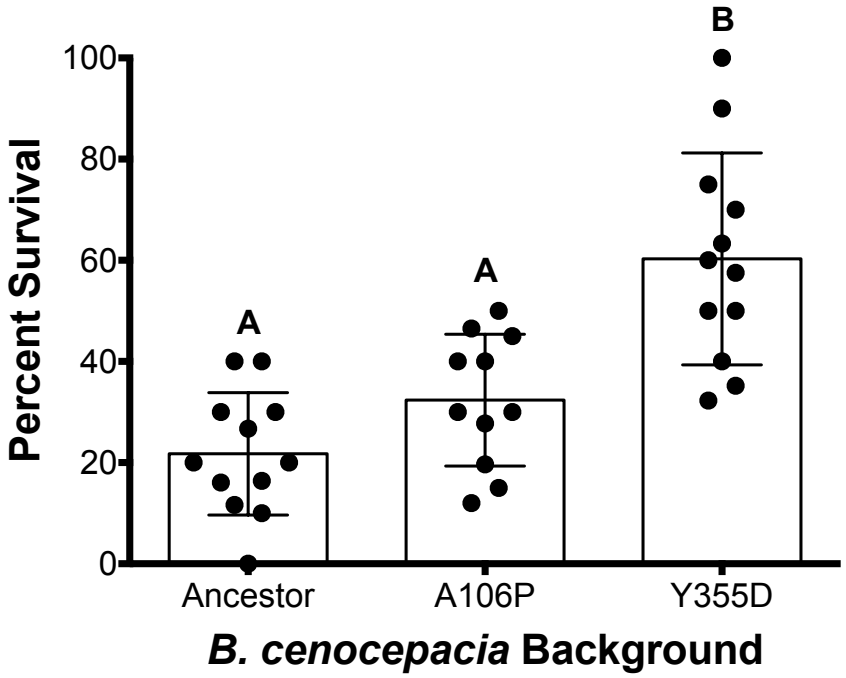

Figure 5.6: Hyperbiofilm Mutants of *Burkholderia cenocepacia* are Attenuated for Acute Virulence in *Galleria mellonella* Model of Infection
G. mellonela survival was scored after 72 hours post inoculation with 10^4 CFU of ancestor or evolved variants (A106P RpfR or Y355D RpfR) of *B. cenocepacia*. Each dot represents an experiment where 10 wax worms were injected with *B. cenocepacia*. Bars represent the average percent survival and error bars are standard deviation. Different letters indicate statistically significant differences ($p < 0.05$) determined by one-way ANOVA followed by Tukey's multiple comparison post-test. N = 12 for ancestor and Y355D and N=11 for A106P.

elevated levels of c-di-GMP compared to the ancestor (Figure 5.2), also demonstrated a loss of acute virulence, we developed a *Galleria mellonela* larva *in vivo* infection model.

This model has been used to assess acute virulence in other species of *Burkholderia* and in other bacteria (194–196). After 72 hours post injection with 10^4 CFU of ancestor *B. cenocepacia*, approximately 20% of the *G. mellonela* population remained alive (Figure 5.6). Repeating the experiment with the evolved alleles of RpfR, we found that both were attenuated in *G. mellonela* killing, with 30% and 60% remaining alive when injected with A106P and Y355D, respectively (Figure 5.6). However, only Y355D was significantly different from the ancestor strain ($p < 0.05$). These data support the hypothesis that in vitro biofilm evolution undergoes similar processes as in vivo biofilm evolution, demonstrating the utility of in vitro models of biofilm evolution.

Appendix 1.4 – Discussion

Whether in soil or during infection of a human host, biofilm formation is an important part of the *B. cenocepacia* lifestyle. Importantly, the ability to form biofilms and disperse when appropriate is integral to the colonization of new habitats. Repeated rounds of biofilm formation, dispersal, and colonization of new surfaces allowed for the evolution of hyperbiofilm variants of *B. cenocepacia* (185). WGS identified multiple targets of selection, however one gene, *rpfR*, was targeted in multiple parallel experiments and was strongly associated with increased intracellular c-di-GMP and biofilm formation (186). In my work, I begin to uncover the molecular mechanism driving increased c-di-GMP and biofilm formation by the evolved RpfR alleles.

A1.4.1 – Model for RpfR DGC Activity in WT and Evolved Alleles

The most prominent study of RpfR identified as an enzyme with primarily PDE activity, despite having an intact active site in the DGC domain (189). Moreover, a direct test of the potential DGC activity is missing in the literature. Thus, studies on the

activity and biological role of the DGC domain were warranted in light of the evolved, hyperbiofilm RpfR variants.

We found that expression of RpfR in the heterologous host *V. cholerae* caused increased biofilm formation and c-di-GMP production and was dependent on the GGDEF active site motif (Figure 5.3 & Figure 5.4). Additionally, the evolved variants displayed similar abilities to produce c-di-GMP in *V. cholerae* (Figure 5.5). These data suggest the hyperbiofilm phenotypes of the evolved RpfR alleles in *B. cenocepacia* may not be caused by differences in DGC activity *per se*, but rather from activation of the DGC domain through an unknown mechanism.

A1.4.2 – Evolutionary Trade Off Between Biofilm Formation and Acute Virulence

We found that our experimentally evolved alleles of RpfR, which form more robust biofilms in vitro compared to the ancestor allele, were attenuated in a wax worm model of acute infection (Figure 5.6). Y355D, which has higher intracellular c-di-GMP and capacity to form biofilms than A106P and the ancestor, had the greatest attenuation, followed by A106P and the ancestor. These data suggest RpfR could be a potential target of selection during *B. cenocepacia* infection and colonization of human hosts. Indeed, whole genome sequencing of a related *Burkholderia* species isolated from a patient with cystic fibrosis identified non-synonymous mutations in RpfR (197). Using the model of experimental evolution, we can further probe the mechanism driving selection of RpfR variants in biofilm formation and potentially uncover novel mechanisms and approaches to disrupt *B. cenocepacia* biofilm formation in complex environments.

Appendix 1.5 – Future Directions

A1.5.1 – Purification of HIS-tagged RpfR and Identification of RpfR Interacting Proteins from *B. cenocepacia*

A possible explanation for the apparent lack of DGC activity when RpfR is studied in *B. cenocepacia* is that RpfR functions within a complex of proteins that regulate enzyme activity. An *E. coli* homologue of RpfR, PdeR, has a PAS-DGC-EAL domain structure but there is no evidence that it can produce c-di-GMP in vitro or in vivo (198, 199). Rather, PdeR acts to modulate expression of genes involved in curli biogenesis by sensing and degrading c-di-GMP. During this process, intermolecular interactions between PdeR and the transcription factor MlrA, allowing MlrA to activate transcription (198).

RpfR differs from PdeR in that RpfR can produce c-di-GMP and, currently, is only known to interact with the BDSF synthase RpfF (188) and a transcription factor GtrR (200). Co-expression of RpfR with RpfF in *V. cholerae* does not alter biofilm formation, motility, or intracellular c-di-GMP (data not shown), however in vitro and in vivo, RpfR interaction with RpfF decreases BDSF production (188). Thus, future work on this project will focus on identifying protein partners that modulate RpfR DGC activity.

To this end, we are currently cloning N-terminal and C-terminal 6 HIS-tagged versions of ancestor and evolved alleles of RpfR. We plan to purify the proteins from *V. cholerae,* rather than the conventional *E. coli* BL21 backgrounds, and assay enzyme activity in vitro to compare activities across ancestor and evolved alleles. Future experiments include co-expressing GtrR and RpfR together in *V. cholerae* and measuring changes in biofilm formation and intracellular c-di-GMP. We hypothesize

that GtrR will decrease biofilm formation and intracellular c-di-GMP when co-expressed with RpfR compared to RpfR alone. Another approach could be an untargeted method utilizing HIS-tagged RpfR in a pull-down assay with *B. cenocepacia* lysates. We hypothesize that potential targets that inhibit DGC activity of RpfR would be abundant under planktonic conditions where intracellular c-di-GMP concentrations are low and scarce under biofilm conditions where intracellular c-di-GMP concentrations are high. Protein partners would be isolated and identified using mass spectrometry, then tested for interactions in vitro and in vivo.

Appendix 2

Strains, Plasmids, and Oligonucleotides

Table 1: Plasmid Names and Descriptions

Plasmid	Description	Chapter	Reference
pBBRlux	*luxABCDE* containing promoter-less plasmid, Cam^R	2,3,4	Lab collection
pEVS143	*pTac* overexpression vector, Kan^R	2,3	(201)
pKAS32	Sucide vector for mutant construction, Amp^R	2,3,4	(89)
pBRP333	Control expression vector, Kan^R	2,3	(55)
6:C9	*tag1* promoter in pBBlux, Cam^R	2	(81)
pALN17	*tag2* promoter in pBBRlux, Cam^R	2	Chapter 2
pDS129	*tag3* promoter in pBBRlux, Cam^R	2	Chapter 2
pNF022	*tag4* promoter in pBBRlux, Cam^R	2	Chapter 2
pBRP1	*qrgB** (inactive DGC) cloned into expression vector pMMB67Eh, Amp^R	2,3,4	(55)
pBRP2	*qrgB* (active DGC) cloned into expression vector, pMMB67Eh, Amp^R	2,3,4	(55)
pCMW131	*vpsR* in pEVS143, Kan^R	2,4	Chapter 2
pCMW132	*vpsT* in pEVS143, Kan^R	2,4	Chapter 2
pNF011	*vpsT* in pET28b (C-terminal HIS-tag), Kan^R	2,3	Chapter 2
pDS138	pKAS32 *tag* deletion construct, Amp^R	2	Chapter 2
pDS139	*tag* in pEVS143, Kan^R	2	Chapter 2
pNF031	*katB1* promoter in pBBlux, Cam^R	3	Chapter 3
pNF032	*katB2* promoter in pBBRlux, Cam^R	3	Chapter 3
pNF033	*katB3* promoter in pBBRlux, Cam^R	3	Chapter 3
pNF036	*katB4* promoter in pBBRlux, Cam^R	3	Chapter 3
pNF038	*katB5* promoter in pBBRlux, Cam^R	3	Chapter 3
pNF030	*katG* promoter in pBBRlux, Cam^R	3	Chapter 3
pHERD20T	P_{BAD} Expression vector	3,4	(125)
pNF057	pHERD20T $_p$BAD expression vector with Cam^R replacing Amp^R	3,4	Chapter 3
pNF067	*katB* in pNF057, Cam^R	3	Chapter 3
pNF068	*katG* in pNF057, Cam^R	3	Chapter 3
pNF045	Deletion construct for *katB* in pKAS32, Amp^R	3	Chapter 3
pNF048	Deletion construct for *katG* in pKAS32, Amp^R	3	Chapter 3
pNF069	358 bp upstream of ATG of *crvA* (P_{crvA}) in pBBRlux	4	Chapter 4
pNF070	Deletion construct for *crvA* in pKAS32, Amp^R	4	Chapter 4
pNF071	VC1807 knock-in construct, Amp^R	4	Chapter 4
pNF072	VC1807 knock-In construct with CrvA driven by native promoter P_{crvA}, Amp^R	4	Chapter 4
pNF073 (pCrvA)	CrvA from C6706 gDNA into pNF057	4	Chapter 4

Table 2: Strains Names and Descriptions

Strain	Description	Chapter	Reference
	Escherichia coli		
DH10b	F⁻*mcr*A Δ(*mrr-hsd*RMS-*mcr*BC) Φ80*lac*ZΔM15 Δ*lac*X74 *rec*A1 *end*A1 *ara*D139Δ(*ara*, *leu*)7697 *gal*U *gal*K λ⁻*rps*L *nup*G	2,3	Thermo Fisher Scientific
S17-λpir	Tpr Smr *recA thi pro hsdR17*($r_K^-m_K^+$) *RP4::2-Tc*::Mu Km Tn7 λpir	2,3,4, Appendix 1	Lab stock
BL21(DE 3)	F⁻ *ompT hsdSB*($r_B^-m_B^+$) *gal dcm* (DE3)	2,3	Invitrogen
	Vibrio cholerae		
C6706	Wild Type	2-4, Appendix 1	Lab Stock
NF02	C6706Δ*tag*	2	Chapter 2
CW2034	C6706Δ*vpsL*	2-4	(88)
JC1195	CW2034Δ*vpsT*	2-4	(81)
WN310	CW2034Δ*vpsR*	2-4	(81)
DS12	CW2034Δ*flrA*	2	(50)
DS14	CW2034Δ*tag*	2	Chapter 2
NF03	CW2034Δ*katB*	3	Chapter 3
NF04	CW2034Δ*katG*	3	Chapter 3
NF05	CW2034Δ*katB*Δ*katG*	3	Chapter 3
JC1220	CW2034Δ*vpsT*Δ*vpsR*	4	Lab Stock
NF6	CW2034Δ*crvA*	4	Chapter 4
NF7	Δ*crvA*	4	Chapter 4
NF8	CW2034Δ*crvA* VC1807::P_{crvA}-*crvA*	4	Chapter 4
HI2424	Clinical isolate of *Burkholderia cenocepacia*	Appendix 1	(202)
BcA106P	HI2424 RpfR A106P	Appendix 1	(186)
BcY355D	HI2424 RpfR Y355D	Appendix 1	(186)

Table 3: Oligonucleotides for Vector and Strain Construction

Construct	Chp.	F/R	5' Overhang	3' Gene Specific
pALN17	2	Forward	gcggccgctctagaa	CGGTGCCTA CAACATCCG
pALN17	2	Reverse	cggccgcaactagag	GGATCATACCGAGTA
pDS129	2	Forward	gcggccgctctagaa	CTTTGTTTAAAACCATGC
pDS129	2	Reverse	cggccgcaactagag	GCTTATCCTTCTTCATTC
pDS138 (Upstream)	2	Forward	cgggccctatatatggatcc	TCGGTGAAGGAGTCGC
pDS138 (Upstream)	2	Reverse		AGCTCTTGGTGAATCAGC TTATCCTTCTTCAT
pDS138 (Downstream)	2	Forward		ATGAAGAAGGATAAGCTGA TTCACCAAGAGCT
pDS138 (Downstream)	2	Reverse	gctgatatcgatcgcgcgca	GCCAGCATGAACAAAA
pDS139	2	Forward	tttagcttccttagctcctg	AGGAGCTAAGGAAGCTAAAA TGATGAATGCGGAACA
pDS139	2	Reverse	gcttgctcaatcaatcaccg	TCAGAGCTTGTCTGC
pNF022	2	Forward	gcggccgctctagaa	CGAGCAAGGCCATAAACC
pNF022	2	Reverse	cggccgcaactagag	GCTTCTTGAGTCTTTCGG
pNF011	2	Forward	ctttaagaaggagatatac	ATGAAAGATGAAAACAAACT
pNF011	2	Reverse	gcttgctcaatcaatcaccg	TCAGAGCTTGTCTGC
pNF031	3	Forward	cggtggcggccgctctagaa	TTCACATTTGCTGGTTCAAAGG
pNF032	3	Forward	cggtggcggccgctctagaa	AAACGCCCGAGAATAGAGA
pNF033	3	Forward	cggtggcggccgctctagaa	TTGGCTTAAAATAATGACGGTTG
pNF036	3	Forward	cggtggcggccgctctagaa	AAGTCATCTAAAACTTTCGTTT AAATCGATTTTC
pNF038	3	Forward	cggtggcggccgctctagaa	TTTCTCTATTAAATTCATCGTTA TTTCCCATTTAG
pNF031-33,036,038	3	Reverse	ccattttgcggccgcaactagag	GGTTGCTCTCCAATGCGAC
pNF030	3	Forward	cggtggcggccgctctagaa	CAAACAGCGCGATATCTTCTT
pNF030	3	Reverse	ccattttgcggccgcaactagag	TTTAGCGCTTTAGGCCACC
pNF057	3	*Forward_1	-	CACATTTCCCCGAAAAGTG
pNF057	3	*Reverse_1	-	CTGTCAGACCAAGTTTACTC

Table 3 (cont'd)

Construct	Chp.	F/R	5' Overhang	3' Gene Specific
pNF057	3	#Forward_2	gcacttttcggggaaatgtg	TTAATGAATCGGCCAACG
pNF057	3	#Reverse_2	gagtaaacttggtctgacag	TGATCGGCACGTAAGAGG
pNF067	3	Forward	atctgataagaattcgagct	ATGCATATGTCAAAAAGCTTT
pNF067	3	Reverse	tgcatgcctgcaggtcgact	TTACATCGCGGCCAGTTTTG
pNF068	3	Forward	atctgataagaattcgagct	ATGGAGCACAATAAAGC
pNF068	3	Reverse	tgcatgcctgcaggtcgact	TTACACCAGATCAAATCG
pNF045 (Upstream)	3	Forward	agctatagttctagaggtac	GGTGGTGGTGAAGACAATTC
pNF045 (Upstream)	3	Reverse	gtggaattcccgggagagct	ATTTTTACTTATCAACCGTCA TTATTTTAAG
pNF045 (Downstream)	3	Forward	agctatagttctagaggtac	CCGATAAAAATTTGCCCC
pNF045 (Downstream)	3	Reverse	gtggaattcccgggagagct	GATCACCCAAGTGATTGTC
pNF048 (Upstream)	3	Forward	agctatagttctagaggtac	ACCTGAGTTGCAATAACCAAAG
pNF048 (Upstream)	3	Reverse	gtggaattcccgggagagct	TGATTACTCCTTGCTTCGCAT
pNF048 (Downstream)	3	Forward	agctatagttctagaggtac	TCCATCTCACCATCCCTTTCA
pNF048 (Downstream)	3	Reverse	gtggaattcccgggagagct	GATGAGATGGTCGCCCCC
pNF069	4	Forward	cggtggcggccgctctagaa	GGTATCTCAAATTGCTTCAAAA C
pNF069	4	Reverse	ccattttgcggccgcaactagag	AAAGTGGGAAAGACAAAC
pNF070 (Upstream)	4	Forward	tgcgcatgctagctatagtt	CAGTAGTAGCGGATCATC
pNF070 (Upstream)	4	Reverse	ttttgtgcgg	AAAGTGGGAAAGACAAAC
pNF070 (Downstream)	4	Forward	ttcccacttt	CCGCACAAAAATCCAACG
pNF070 (Downstream)	4	Reverse	gtggaattcccgggagagct	TGGTGAAGCTGACTTTTTG
pNF071 (Upstream)	4	Forward	tgcgcatgctagctatagtt	ATTTTTCAGTTGGCCTAC
pNF071 (Upstream)	4	Reverse	ttttgtgcgg	TAGTCACCTCTATTGTTAACTTG

Table 3 (cont'd)

Construct	Chp.	F/R	5' Overhang	3' Gene Specific
pNF071 (Downstream)	4	Forward	ttcccacttt	TAGTCGAAAATAAAAAAAAGAGG
pNF071 (Downstream	4	Reverse	gtggaattcccgggagagct	CGATGAGGATAAAAAACAC
pNF072	4	Forward	acaatagaggtgactaggta	GGTATCTCAAATTGCTTCAAAAC
pNF072	4	Reverse	cgactagagctcaccggtac	CTAGCTGTCTTTGTTTGG
pNF073	4	Forward	atctgataagaattcgagct	ATGTGGCTAAACATAAATATGTTG
pNF073	4	Reverse	tctagaggatccccgggtac	CTAGCTGTCTTTGTTTGG

* - Forward_1 and Reverse_1: Primers used for inverse PCR to amplify pHERD20T backbone without the ampicillin resistance gene
# - Forward_2 and Reverse_2: Primers used to amplify the chloramphenicol acetyltransferase from pBBRlux

Table 4: Oligonucleotides for Experiments

Experiment	Description	Sequence (5' to 3')	Chapter
qRT-PCR	*gyrA*-For	AAATTCATCTTCATGGCAAC	2,3,4
qRT-PCR	*gyrA*-Rev	GCGATGTTTTCTTCACAG	2,3,4
qRT-PCR	*katB*-For	CGTATGCCGATACACAGCTTTA	3
qRT-PCR	*katB*-Rev	ACGACTGGGTTGGTAGTTAATG	3
qRT-PCR	*tag*-For	CGTTACAACAGGAGTTCGGC	2
qRT-PCR	*tag*-Rev	CGGGTACATCGCTCATGC	2
qRT-PCR	*crvA*-For	GTACTCCCGTTGAACTCGTATT	4
qRT-PCR	*crvA*-Rev	CCGTAATCACACGATTGTAGGT	4
EMSA	pBBRLux-FAM-For	**FAM -** ATTTTGCGGCCGCAACTAGA	2,3
EMSA	pBBRLux-FAM-Rev	**FAM -** CCGCGGTGGCGGCCGCTCTA	2,3
EMSA (31)	WT-VpsT Binding Site-For	AAAGTAAACTAAAGTTTATTTT	2,3
EMSA	WT-VpsT Binding Site-Rev	AAAATAAACTTTAGTTTACTTT	2,3
EMSA	MT-VpsT Binding Site-For	AAAAGGTCTAAAACTAGGTT	2,3
EMSA	MT-VpsT Binding Site-Rev	AACCTAGTTTTAGACCTTTT	2,3

BIBLOGRAPHY

BIBLIOGRAPHY

1. Laub MT, Goulian M. 2007. Specificity in Two-Component Signal Transduction Pathways. Annu Rev Genet 41:121–145.

2. Conner JG, Zamorano-Sánchez D, Park JH, Sondermann H, Yildiz FH. 2017. The ins and outs of cyclic di-GMP signaling in *Vibrio cholerae*. Curr Opin Microbiol 36:20–29.

3. Pérez-Mendoza D, Coulthurst SJ, Humphris S, Campbell E, Welch M, Toth IK, Salmond GPC. 2011. A multi-repeat adhesin of the phytopathogen, *Pectobacterium atrosepticum*, is secreted by a Type I pathway and is subject to complex regulation involving a non-canonical diguanylate cyclase: Complex regulation of a *Pectobacterium* type I-secreted adhesin. Mol Microbiol 82:719–733.

4. Hunter JL, Severin GB, Koestler BJ, Waters CM. 2014. The *Vibrio cholerae* diguanylate cyclase VCA0965 has an AGDEF active site and synthesizes cyclic di-GMP. BMC Microbiol 14:22–22.

5. Romling U, Galperin MY, Gomelsky M. 2013. Cyclic di-GMP: The First 25 Years of a Universal Bacterial Second Messenger. Microbiol Mol Biol Rev 77:1–52.

6. Orr MW, Donaldson GP, Severin GB, Wang J, Sintim HO, Waters CM, Lee VT. 2015. Oligoribonuclease is the primary degradative enzyme for pGpG in *Pseudomonas aeruginosa* that is required for cyclic-di-GMP turnover. Proc Natl Acad Sci 112:E5048–E5057.

7. Cohen D, Mechold U, Nevenzal H, Yarmiyhu Y, Randall TE, Bay DC, Rich JD, Parsek MR, Kaever V, Harrison JJ, Banin E. 2015. Oligoribonuclease is a central feature of cyclic diguanylate signaling in *Pseudomonas aeruginosa*. Proc Natl Acad Sci 112:11359–11364.

8. Qi Y, Rao F, Luo Z, Liang Z-X. 2009. A Flavin Cofactor-Binding PAS Domain Regulates c-di-GMP Synthesis in *Ax* DGC2 from *Acetobacter xylinum*. Biochemistry 48:10275–10285.

9. Hickman JW, Tifrea DF, Harwood CS. 2005. A chemosensory system that regulates biofilm formation through modulation of cyclic diguanylate levels. Proc Natl Acad Sci 102:14422–14427.

10. Sudarsan N, Lee ER, Weinberg Z, Moy RH, Kim JN, Link KH, Breaker RR. 2008. Riboswitches in Eubacteria Sense the Second Messenger Cyclic Di-GMP. Science 321:411–413.

11. McKee RW, Harvest CK, Tamayo R. 2018. Cyclic Diguanylate Regulates Virulence Factor Genes via Multiple Riboswitches in *Clostridium difficile*. mSphere 3:1–15.

12. Kariisa AT, Grube A, Tamayo R. 2015. Two nucleotide second messengers regulate the production of the *Vibrio cholerae* colonization factor GbpA. BMC Microbiol 15.

13. Ross P, Aloni Y, Weinhouse C, Michaeli D, Weinberger-Ohana P, Meyer R, Benziman M. 1985. An unusual guanyl oligonucleotide regulates cellulose synthesis in *Acetobacter xylinum*. FEBS Lett 186:191–196.

14. Ross P, Weinhouse H, Aloni Y, Michaeli D, Weinberger-Ohana P, Mayer R, Braun S, de Vroom E, van der Marel GA, van Boom JH, Benziman M. 1987. Regulation of cellulose synthesis in *Acetobacter xylinum* by cyclic diguanylic acid. Nature 325:279–281.

15. Paul R, Weiser S, Amiot NC, Chan C, Schirmer T, Giese B, Jenal U. 2004. Cell cycle-dependent dynamic localization of a bacterial response regulator with a novel di-guanylate cyclase output domain. Genes Dev 18:715–727.

16. Tamayo R, Pratt JT, Camilli A. 2007. Roles of Cyclic Diguanylate in the Regulation of Bacterial Pathogenesis. Annu Rev Microbiol 61:131–148.

17. Lori C, Ozaki S, Steiner S, Böhm R, Abel S, Dubey BN, Schirmer T, Hiller S, Jenal U. 2015. Cyclic di-GMP acts as a cell cycle oscillator to drive chromosome replication. Nature 523:236–239.

18. Bush MJ, Tschowri N, Schlimpert S, Flärdh K, Buttner MJ. 2015. c-di-GMP signalling and the regulation of developmental transitions in streptomycetes. Nat Rev Microbiol 13:749–760.

19. Hobley L, Fung RKY, Lambert C, Harris MATS, Dabhi JM, King SS, Basford SM, Uchida K, Till R, Ahmad R, Aizawa S-I, Gomelsky M, Sockett RE. 2012. Discrete Cyclic di-GMP-Dependent Control of Bacterial Predation versus Axenic Growth in *Bdellovibrio bacteriovorus*. PLoS Pathog 8:e1002493.

20. Kearns DB. 2010. A field guide to bacterial swarming motility. Nat Rev Microbiol 8:634–644.

21. Baraquet C, Harwood CS. 2016. FleQ DNA Binding Consensus Sequence Revealed by Studies of FleQ- Dependent Regulation of Biofilm Gene Expression in Pseudomonas aeruginosa 198:178–186.

22. Paul K, Nieto V, Carlquist WC, Blair DF, Harshey RM. 2010. The c-di-GMP Binding Protein YcgR Controls Flagellar Motor Direction and Speed to Affect Chemotaxis by a “Backstop Brake” Mechanism. Mol Cell 38:128–139.

23. Craig L, Forest KT, Maier B. 2019. Type IV pili: dynamics, biophysics and functional consequences. Nat Rev Microbiol 17:429–440.

24. Skotnicka D, Petters T, Heering J, Hoppert M, Kaever V, Søgaard-Andersen L. 2016. Cyclic Di-GMP Regulates Type IV Pilus-Dependent Motility in *Myxococcus xanthus*. J Bacteriol 198:77–90.

25. Jain R, Behrens A-J, Kaever V, Kazmierczak BI. 2012. Type IV Pilus Assembly in *Pseudomonas aeruginosa* over a Broad Range of Cyclic di-GMP Concentrations. J Bacteriol 194:4285–4294.

26. Jain R, Sliusarenko O, Kazmierczak BI. 2017. Interaction of the cyclic-di-GMP binding protein FimX and the Type 4 pilus assembly ATPase promotes pilus assembly. PLOS Pathog 13:e1006594.

27. Mann EE, Wozniak DJ. 2012. *Pseudomonas* biofilm matrix composition and niche biology. FEMS Microbiol Rev 36:893–916.

28. Yildiz F, Fong J, Sadovskaya I, Grard T, Vinogradov E. 2014. Structural Characterization of the Extracellular Polysaccharide from *Vibrio cholerae* O1 El-Tor. PLoS ONE 9:e86751.

29. Baraquet C, Murakami K, Parsek MR, Harwood CS. 2012. The FleQ protein from Pseudomonas aeruginosa functions as both a repressor and an activator to control gene expression from the Pel operon promoter in response to c-di-GMP. Nucleic Acids Res 40:7207–7218.

30. Krasteva PV, Fong JCN, Shikuma NJ, Beyhan S, Navarro MVAS, Yildiz FH, Sondermann H. 2010. *Vibrio cholerae* VpsT Regulates Matrix Production and Motility by Directly Sensing Cyclic di-GMP. Science 327:866–868.

31. Zamorano-Sánchez D, Fong JCN, Kilic S, Erill I, Yildiz FH. 2015. Identification and Characterization of VpsR and VpsT Binding Sites in *Vibrio cholerae*. J Bacteriol 197:1221–1235.

32. Fang N, Qu S, Yang H, Fang H, Liu L, Zhang Y, Wang L, Han Y, Zhou D, Yang R. 2014. HmsB enhances biofilm formation in *Yersinia pestis*. Front Microbiol 5.

33. Weinhouse H, Sapir S, Amikam D, Shilo Y, Volman G, Ohana P, Benziman M. 1997. c-di-GMP-binding protein, a new factor regulating cellulose synthesis in *Acetobacter xylinum*. FEBS Lett 416:207–211.

34. Steiner S, Lori C, Boehm A, Jenal U. 2012. Allosteric activation of exopolysaccharide synthesis through cyclic di-GMP-stimulated protein–protein interaction. EMBO J 32:354–368.

35. Galperin MY, Higdon R, Kolker E. 2010. Interplay of heritage and habitat in the distribution of bacterial signal transduction systems. Mol Biosyst 6:721.

36. Hallez R, Delaby M, Sanselicio S, Viollier PH. 2017. Hit the right spots: cell cycle control by phosphorylated guanosines in alphaproteobacteria. Nat Rev Microbiol 15:137–148.

37. Wang SP, Sharma PL, Schoenlein PV, Ely B. 1993. A histidine protein kinase is involved in polar organelle development in Caulobacter crescentus. Proc Natl Acad Sci 90:630–634.

38. Abel S, Chien P, Wassmann P, Schirmer T, Kaever V, Laub MT, Baker TA, Jenal U. 2011. Regulatory Cohesion of Cell Cycle and Cell Differentiation through Interlinked Phosphorylation and Second Messenger Networks. Mol Cell 43:550–560.

39. Negus D, Moore C, Baker M, Raghunathan D, Tyson J, Sockett RE. 2017. Predator Versus Pathogen: How Does Predatory *Bdellovibrio bacteriovorus* Interface with the Challenges of Killing Gram-Negative Pathogens in a Host Setting? Annu Rev Microbiol 71:441–457.

40. Rotem O, Nesper J, Borovok I, Gorovits R, Kolot M, Pasternak Z, Shin I, Glatter T, Pietrokovski S, Jenal U, Jurkevitch E. 2016. An extended cyclic di-GMP network in the predatory bacterium Bdellovibrio bacteriovorus. J Bacteriol 198:127–137.

41. Den Hengst CD, Tran NT, Bibb MJ, Chandra G, Leskiw BK, Buttner MJ. 2010. Genes essential for morphological development and antibiotic production in Streptomyces coelicolor are targets of BldD during vegetative growth: The Streptomyces BldD regulon. Mol Microbiol 78:361–379.

42. Tschowri N, Schumacher MA, Schlimpert S, Chinnam NB, Findlay KC, Brennan RG, Buttner MJ. 2014. Tetrameric c-di-GMP mediates effective transcription factor dimerization to control streptomyces development. Cell 158:1136–1147.

43. Tamayo R, Tischler AD, Camilli A. 2005. The EAL domain protein VieA is a cyclic diguanylate phosphodiesterase. J Biol Chem 280:33324–33330.

44. WHO. Weekly Epidemiological Record. WHO 92:521–536.

45. Silva AJ, Benitez JA. 2016. Vibrio cholerae Biofilms and Cholera Pathogenesis. PLoS Negl Trop Dis 10:e0004330.

46. Lim B, Beyhan S, Yildiz FH. 2007. Regulation of Vibrio polysaccharide synthesis and virulence factor production by CdgC, a GGDEF-EAL domain protein, in Vibrio cholerae. J Bacteriol 189:717–729.

47. Shikuma NJ, Fong JCN, Yildiz FH. 2012. Cellular Levels and Binding of c-di-GMP Control Subcellular Localization and Activity of the *Vibrio cholerae* Transcriptional Regulator VpsT. PLoS Pathog 8:e1002719.

48. Yildiz FH, Dolganov NA, Schoolnik GK. 2001. VpsR, a Member of the Response Regulators of the Two-Component Regulatory Systems, Is Required for Expression of vps Biosynthesis Genes and EPSETr-Associated Phenotypes in *Vibrio cholerae* O1 El Tor. J Bacteriol 183:1716–1726.

49. Casper-Lindley C, Yildiz FH. 2004. VpsT Is a Transcriptional Regulator Required for Expression of vps Biosynthesis Genes and the Development of Rugose Colonial Morphology in Vibrio cholerae. J Bacteriol 186:1574–1578.

50. Srivastava D, Hsieh M-L, Khataokar A, Neiditch MB, Waters CM. 2013. Cyclic di-GMP inhibits *Vibrio cholerae* motility by repressing induction of transcription and inducing extracellular polysaccharide production. Mol Microbiol 90:1262–1276.

51. Weinberg Z, Barrick JE, Yao Z, Roth A, Kim JN, Gore J, Wang JX, Lee ER, Block KF, Sudarsan N, Neph S, Tompa M, Ruzzo WL, Breaker RR. 2007. Identification of 22 candidate structured RNAs in bacteria using the CMfinder comparative genomics pipeline. Nucleic Acids Res 35:4809–4819.

52. Syed K a., Beyhan S, Correa N, Queen J, Liu J, Peng F, Satchell KJF, Yildiz F, Klose KE. 2009. The Vibrio cholerae Flagellar Regulatory Hierarchy Controls Expression of Virulence Factors. J Bacteriol 191:6555–6570.

53. Jude BA, Martinez RM, Skorupski K, Taylor RK. 2009. Levels of the secreted Vibrio cholerae attachment factor GbpA are modulated by quorum-sensing-induced proteolysis. J Bacteriol 191:6911–6917.

54. Kariisa AT, Weeks K, Tamayo R. 2016. The RNA Domain Vc1 Regulates Downstream Gene Expression in Response to Cyclic Diguanylate in *Vibrio cholerae*. PLOS ONE 11:e0148478.

55. Pursley BR, Maiden MM, Hsieh ML, Fernandez NL, Severin GB, Waters CM. 2018. Cyclic di-GMP Regulates TfoY in *Vibrio cholerae* To Control Motility by both Transcriptional and Posttranscriptional Mechanisms. J Bacteriol 200.

56. Beyhan S, Tischler AD, Camilli A, Yildiz FH. 2006. Transcriptome and Phenotypic Responses of *Vibrio cholerae* to Increased Cyclic di-GMP Level. J Bacteriol 188:3600–3613.

57. Karatan E, Duncan TR, Watnick PI. 2005. NspS, a Predicted Polyamine Sensor, Mediates Activation of Vibrio cholerae Biofilm Formation by Norspermidine. J Bacteriol 187:7434–7443.

58. Ross P, Weinhouse H, Aloni Y, Michaeli D, Weinberger-Ohana P, Mayer R, Braun S, Vroom E de, G. A. van der M, Boom JH van, Benziam M. Regulation of cellulose synthesis in *Acetobacter xylinum* by cyclic diguanylic acid.

59. Galperin MY, Nikolskaya a N, Koonin E V. 2001. Novel domains of the prokaryotic two-component signal transduction systems.[erratum appears in FEMS Microbiol Lett 2001 Oct 16;204(1):213-4]. FEMS Microbiol Lett 203:11–21.

60. Orr MW, Donaldson GP, Severin GB, Wang J, Sintim HO, Waters CM, Lee VT. 2015. Oligoribonuclease is the primary degradative enzyme for pGpG in *Pseudomonas aeruginosa* that is required for cyclic-di-GMP turnover. Proc Natl Acad Sci 112:E5048–E5057.

61. Ramírez-Guadiana FH, del Carmen Barajas-Ornelas R, Ayala-García VM, Yasbin RE, Robleto E, Pedraza-Reyes M. 2013. Transcriptional coupling of DNA repair in sporulating *Bacillus subtilis* cells. Mol Microbiol 90:1088–1099.

62. Tschowri N, Schumacher MA, Schlimpert S, Chinnam NB, Findlay KC, Brennan RG, Buttner MJ. 2014. Tetrameric c-di-GMP mediates effective transcription factor dimerization to control streptomyces development. Cell 158:1136–1147.

63. Paul R, Weiser S, Amiot NC, Chan C, Schirmer T, Giese B, Jenal U. 2004. Cell cycle-dependent dynamic localization of a bacterial response regulator with a novel di-guanylate cyclase output domain. Genes Dev 18:715–727.

64. Abel S, Chien P, Wassmann P, Schirmer T, Kaever V, Laub MT, Baker TA, Jenal U. 2011. Regulatory Cohesion of Cell Cycle and Cell Differentiation through Interlinked Phosphorylation and Second Messenger Networks. Mol Cell 43:550–560.

65. Tamayo R, Tischler AD, Camilli A. 2005. The EAL domain protein VieA is a cyclic diguanylate phosphodiesterase. J Biol Chem 280:33324–33330.

66. Sloup RE, Konal AE, Severin GB, Korir ML, Bagdasarian MM, Bagdasarian M, Waters CM. 2017. Cyclic Di-GMP and VpsR Induce the Expression of Type II Secretion in *Vibrio cholerae*. J Bacteriol 199:10–12.

67. Alam MT, Ray SS, Chun CN, Chowdhury ZG, Rashid MH, Madsen Beau De Rochars VE, Ali A. 2016. Major Shift of Toxigenic *V. cholerae* O1 from Ogawa to Inaba Serotype Isolated from Clinical and Environmental Samples in Haiti. PLoS Negl Trop Dis 10:1–9.

68. Susan A. Bartels etal. 2010. Investigation of a Cholera Outbreak. Am Med Assoc 1:1–6.

69. Kuna A, Gajewski M. 2017. Cholera — the new strike of an old foe. Int Marit Health 68:163–167.

70. Tischler AD, Camilli A. 2004. Cyclic diguanylate (c-di-GMP) regulates *Vibrio cholerae* biofilm formation. Mol Microbiol 53:857–869.

71. Beyhan S, Tischler AD, Camilli A, Yildiz FH. 2006. Transcriptome and Phenotypic Responses of *Vibrio cholerae* to Increased Cyclic di-GMP Level. J Bacteriol 188:3600–3613.

72. Lutz C, Erken M, Noorian P, Sun S, McDougald D. 2013. Environmental reservoirs and mechanisms of persistence of *Vibrio cholerae*. Front Microbiol 4:1–15.

73. Tamayo R, Patimalla B, Camilli A. 2010. Growth in a biofilm induces a hyperinfectious phenotype in *Vibrio cholerae*. Infect Immun 78:3560–3569.

74. Millet Y a., Alvarez D, Ringgaard S, von Andrian UH, Davis BM, Waldor MK. 2014. Insights into *Vibrio cholerae* Intestinal Colonization from Monitoring Fluorescently Labeled Bacteria. PLoS Pathog 10:e1004405.

75. Butler SM, Camilli A. 2004. Both chemotaxis and net motility greatly influence the infectivity of *Vibrio cholerae*. Proc Natl Acad Sci 101:5018–5023.

76. Koestler BJ, Waters CM. 2014. Bile Acids and Bicarbonate Inversely Regulate Intracellular Cyclic di-GMP in *Vibrio cholerae*. Infect Immun 82:3002–3014.

77. Casper-lindley C, Yildiz FH. 2004. VpsT Is a Transcriptional Regulator Required for Expression of vps Biosynthesis Genes and the Development of Rugose Colonial Morphology in Vibrio VpsT Is a Transcriptional Regulator Required for Expression of vps Biosynthesis Genes and the Development of 186:1574–1578.

78. Fong JCN, Syed K a., Klose KE, Yildiz FH. 2010. Role of Vibrio polysaccharide (vps) genes in VPS production, biofilm formation and *Vibrio cholerae* pathogenesis. Microbiology 156:2757–2769.

79. Fong JCN, Yildiz FH. 2007. The rbmBCDEF gene cluster modulates development of rugose colony morphology and biofilm formation in *Vibrio cholerae*. J Bacteriol 189:2319–2330.

80. Kovacikova G, Lin W, Skorupski K. 2005. Dual regulation of genes involved in acetoin biosynthesis and motility/biofilm formation by the virulence activator AphA and the acetate-responsive LysR-type regulator AlsR in *Vibrio cholerae*. Mol Microbiol 57:420–433.

81. Srivastava D, Harris RC, Waters CM. 2011. Integration of Cyclic di-GMP and Quorum Sensing in the Control of *vpsT* and *aphA* in *Vibrio cholerae*. J Bacteriol 193:6331–6341.

82. Metzger LC, Stutzmann S, Scrignari T, Van der Henst C, Matthey N, Blokesch M. 2016. Independent Regulation of Type VI Secretion in *Vibrio cholerae* by TfoX and TfoY. Cell Rep 15:951–958.

83. Pursley BR, Maiden MM, Hseih M-L, Fernandez NL, Severin GB, Waters CM. 2017. Cyclic di-GMP regulates TfoY in *Vibrio cholerae* to control motility by both transcriptional and posttranscriptional mechanisms. J Bacteriol In Press.

84. Davies BW, Bogard RW, Dupes NM, Gerstenfeld T a I, Simmons L a., Mekalanos JJ. 2011. DNA damage and reactive nitrogen species are barriers to *Vibrio cholerae* colonization of the infant mouse intestine. PLoS Pathog 7.

85. Krokan HE, Bjoras M. 2013. Base excision repair. Cold Spring Harb Perspect Biol 5:a012583.

86. Gómez-Marroquín M, Vidales LE, Debora BN, Santos-Escobar F, Obregón-Herrera A, Robleto E a., Pedraza-Reyes M. 2015. Role of *Bacillus subtilis* DNA Glycosylase MutM in Counteracting Oxidatively Induced DNA Damage and in Stationary-Phase-Associated Mutagenesis. J Bacteriol 197:1963–1971.

87. Ogasawara H, Teramoto J, Hirao K, Yamamoto K, Ishihama A, Utsumi R. 2004. Negative Regulation of DNA Repair Gene (ung) Expression by the CpxR / CpxA Two-Component System in *Escherichia coli* K-12 and Induction of Mutations by Increased Expression of CpxR. Society 186:8317–8325.

88. Waters CM, Lu W, Rabinowitz JD, Bassler BL. 2008. Quorum Sensing Controls Biofilm Formation in *Vibrio cholerae* through Modulation of Cyclic Di-GMP Levels and Repression of *vpsT*. J Bacteriol 190:2527–2536.

89. Skorupski K, Taylor RK. 1996. Positive selection vectors for allelic exchange. Gene 169:47–52.

90. Green MR, Sambrook J. 2014. Molecular Cloning: A Laboratory Manual.

91. Heidelberg JF, Eisen JA, Nelson WC, Clayton RA, Gwinn ML, Dodson RJ, Haft DH, Tettelin Â, Hickey EK, Peterson JD, Umayam L, Gill SR, Nelson KE, Read TD, Richardson D, Ermolaeva MD, Vamathevan J, Bass S, Qin H, Dragoi I, Sellers P, Mcdonald L, Utterback T, Fleishmann RD, Nierman WC, White O, Salzberg SL, Smith HO, Colwell RR, Mekalanos JJ, Venter JC, Fraser CM. 2000. DNA sequence of both chromosomes of the cholera pathogen *Vibrio cholerae* 406:477–484.

92. Radman M. 1975. SOS repair hypothesis: phenomenology of an inducible DNA repair which is accompanied by mutagenesis., p. 355–367. *In* Basic Life Sciences. Springer US, Boston, MA.

93. Beyhan S, Bilecen K, Salama SR, Casper-Lindley C, Yildiz FH. 2007. Regulation of rugosity and biofilm formation in Vibrio cholerae: Comparison of VpsT and VpsR regulons and epistasis analysis of vpsT, vpsR, and hapR. J Bacteriol 189:388–402.

94. Beyhan S, Bilecen K, Salama SR, Casper-Lindley C, Yildiz FH. 2007. Regulation of rugosity and biofilm formation in Vibrio cholerae: Comparison of VpsT and VpsR regulons and epistasis analysis of vpsT, vpsR, and hapR. J Bacteriol 189:388–402.

95. Conner JG, Zamorano-Sánchez D, Park JH, Sondermann H, Yildiz FH. 2017. The ins and outs of cyclic di-GMP signaling in *Vibrio cholerae*. Curr Opin Microbiol 36:20–29.

96. Ayala JC, Wang H, Silva AJ, Benitez JA. 2015. Repression by H-NS of genes required for the biosynthesis of the *Vibrio cholerae* biofilm matrix is modulated by the second messenger cyclic diguanylic acid: Regulation of biofilm formation by H-NS. Mol Microbiol 97:630–645.

97. Sikora A, Mielecki D, Chojnacka A, Nieminuszczy J, Wrzesiński M, Grzesiuk E. 2010. Lethal and mutagenic properties of MMS-generated DNA lesions in *Escherichia coli* cells deficient in BER and AlkB-directed DNA repair. Mutagenesis 25:139–147.

98. Römling U, Galperin MY, Gomelsky M. 2013. Cyclic di-GMP: the first 25 years of a universal bacterial second messenger. Microbiol Mol Biol Rev MMBR 77:1–52.

99. Hickman JW, Harwood CS. 2008. Identification of FleQ from Pseudomonas aeruginosa as a c-di-GMP-responsive transcription factor. Mol Microbiol 69:376–389.

100. Lim B, Beyhan S, Meir J, Yildiz FH. 2006. Cyclic-diGMP signal transduction systems in *Vibrio cholerae*: Modulation of rugosity and biofilm formation. Mol Microbiol 60:331–348.

101. Bina XR, Provenzano D, Nguyen N, Bina JE. 2008. *Vibrio cholerae* RND family efflux systems are required for antimicrobial resistance, optimal virulence factor production, and colonization of the infant mouse small intestine. Infect Immun 76:3595–3605.

102. Lombardo M-J, Michalski J, Martinez-Wilson H, Morin C, Hilton T, Osorio CG, Nataro JP, Tacket CO, Camilli A, Kaper JB. 2007. An in vivo expression technology screen for *Vibrio cholerae* genes expressed in human volunteers. Proc Natl Acad Sci U S A 104:18229–34.

103. Kim D, Hong JS-J, Qiu Y, Nagarajan H, Seo J-H, Cho B-K, Tsai S-F, Palsson BØ. 2012. Comparative Analysis of Regulatory Elements between *Escherichia coli* and *Klebsiella pneumoniae* by Genome-Wide Transcription Start Site Profiling. PLoS Genet 8:e1002867.

104. Bradley ES, Bodi K, Ismail AM, Camilli A. 2011. A genome-wide approach to discovery of small RNAs involved in regulation of virulence in vibrio cholerae. PLoS Pathog 7.

105. Srivastava D, Harris RC, Waters CM. 2011. Integration of cyclic di-GMP and quorum sensing in the control of vpsT and aphA in *Vibrio cholerae*. J Bacteriol 193:6331–6341.

106. Wang H, Ayala JC, Benitez JA, Silva AJ. 2014. The LuxR-Type Regulator VpsT Negatively Controls the Transcription of *rpoS*, Encoding the General Stress Response Regulator, in *Vibrio cholerae* Biofilms. J Bacteriol 196:1020–1030.

107. Zhang XS, Garcia-Contreras R, Wood TK. 2007. YcfR (BhsA) influences *Escherichia coli* biofilm formation through stress response and surface hydrophobicity. J Bacteriol 189:3051–3062.

108. Gotoh H, Zhang Y, Dallo SF, Hong S, Kasaraneni N, Weitao T. 2008. *Pseudomonas aeruginosa*, under DNA replication inhibition, tends to form biofilms via Arr. Res Microbiol 159:294–302.

109. Gotoh H, Kasaraneni N, Devineni N, Dallo SF, Weitao T. 2010. SOS involvement in stress-inducible biofilm formation. Biofouling 26.

110. Boles BR, Singh PK. 2008. Endogenous oxidative stress produces diversity and adaptability in biofilm communities. Proc Natl Acad Sci U S A 105:12503–12508.

111. Lutz C, Erken M, Noorian P, Sun S, McDougald D. 2013. Environmental reservoirs and mechanisms of persistence of *Vibrio cholerae*. Front Microbiol 4.

112. Cooper WJ, Zika RG, Petasne RG, Plane JMC. 1988. Photochemical formation of hydrogen peroxide in natural waters exposed to sunlight. Environ Sci Technol 22:1156–1160.

113. Glippa O, Engström-Öst J, Kanerva M, Rein A, Vuori K. 2018. Oxidative stress and antioxidant defense responses in *Acartia* copepods in relation to environmental factors. PLOS ONE 13:e0195981.

114. Diaz JM, Plummer S. 2018. Production of extracellular reactive oxygen species by phytoplankton: past and future directions. J Plankton Res 40:655–666.

115. Wang H, Naseer N, Chen Y, Zhu AY, Kuai X, Galagedera N, Liu Z, Zhu J. 2017. OxyR2 Modulates OxyR1 Activity and *Vibrio cholerae* Oxidative Stress Response. Infect Immun 85.

116. Xia X, Larios-Valencia J, Liu Z, Xiang F, Kan B, Wang H, Zhu J. 2017. OxyR-activated expression of Dps is important for *Vibrio cholerae* oxidative stress resistance and pathogenesis. PLOS ONE 12:e0171201.

117. Heidelberg JF, Eisen JA, Nelson WC, Clayton RA, Gwinn ML, Dodson RJ, Haft DH, Hickey EK, Peterson JD, Umayam L, Gill SR, Nelson KE, Read TD, Tettelin H, Richardson D, Ermolaeva MD, Vamathevan J, Bass S, Qin H, Dragoi I, Sellers P, McDonald L, Utterback T, Fleishmann RD, Nierman WC, White O, Salzberg SL, Smith HO, Colwell RR, Mekalanos JJ, Venter JC, Fraser CM. 2000. DNA sequence of both chromosomes of the cholera pathogen *Vibrio cholerae*. Nature 406:477–483.

118. Wai SN, Mizunoe Y, Takade A, Kawabata S-I, Yoshida S-I. 1998. *Vibrio cholerae* O1 Strain TSI-4 Produces the Exopolysaccharide Materials That Determine Colony Morphology, Stress Resistance, and Biofilm Formation. APPL Env MICROBIOL 64:8.

119. Chen L-H, Köseoğlu VK, Güvener ZT, Myers-Morales T, Reed JM, D'Orazio SEF, Miller KW, Gomelsky M. 2014. Cyclic di-GMP-dependent Signaling Pathways in the Pathogenic Firmicute *Listeria monocytogenes*. PLoS Pathog 10:e1004301.

120. Wang H, Xing X, Wang J, Pang B, Liu M, Larios-Valencia J, Liu T, Liu G, Xie S, Hao G, Liu Z, Kan B, Zhu J. 2018. Hypermutation-induced in vivo oxidative stress resistance enhances *Vibrio cholerae* host adaptation. PLOS Pathog 14:e1007413.

121. Hsieh M-L, Hinton DM, Waters CM. 2018. VpsR and cyclic di-GMP together drive transcription initiation to activate biofilm formation in *Vibrio cholerae*. Nucleic Acids Res 46:8876–8887.

122. Metzger LC, Stutzmann S, Scrignari T, Van der Henst C, Matthey N, Blokesch M. 2016. Independent Regulation of Type VI Secretion in *Vibrio cholerae* by TfoX and TfoY. Cell Rep 15:951–958.

123. Fernandez NL, Srivastava D, Ngouajio AL, Waters CM. 2018. Cyclic di-GMP Positively Regulates DNA Repair in *Vibrio cholerae*. J Bacteriol 200:13.

124. Thelin KH, Taylor RK. 1996. Toxin-Coregulated Pilus, but Not Mannose-Sensitive Hemagglutinin, Is Required for Colonization by *Vibrio cholerae* O1 El Tor Biotype and O139 Strains. Infect Immun 64:4.

125. Qiu D, Damron FH, Mima T, Schweizer HP, Yu HD. 2008. P_{BAD}-Based Shuttle Vectors for Functional Analysis of Toxic and Highly Regulated Genes in *Pseudomonas* and *Burkholderia* spp. and Other Bacteria. Appl Environ Microbiol 74:7422–7426.

126. Iwase T, Tajima A, Sugimoto S, Okuda K, Hironaka I, Kamata Y, Takada K, Mizunoe Y. 2013. A Simple Assay for Measuring Catalase Activity: A Visual Approach. Sci Rep 3:3081.

127. Fernandez N, Waters CM. 2018. Analyzing Diguanylate Cyclase Activity In Vivo using a Heterologous *Escherichia coli* Host. Curr Protoc Microbiol e74.

128. Massie JP, Reynolds EL, Koestler BJ, Cong J-P, Agostoni M, Waters CM. 2012. Quantification of high-specificity cyclic diguanylate signaling. Proc Natl Acad Sci 109:12746–12751.

129. Mishra S, Imlay J. 2012. Why do bacteria use so many enzymes to scavenge hydrogen peroxide? Arch Biochem Biophys 525:145–160.

130. Wang H, Chen S, Zhang J, Rothenbacher FP, Jiang T, Kan B, Zhong Z, Zhu J. 2012. Catalases Promote Resistance of Oxidative Stress in *Vibrio cholerae*. PLoS ONE 7:e53383.

131. Li W, Li M, Hu L, Zhu J, Xie Z, Chen J, He Z-G. 2018. HpoR, a novel c-di-GMP effective transcription factor, links the second messenger's regulatory function to the mycobacterial antioxidant defense. Nucleic Acids Res 46:3595–3611.

132. Elkins JG, Hassett DJ, Stewart PS, Schweizer HP, Mcdermott TR. 1999. Protective Role of Catalase in *Pseudomonas aeruginosa* Biofilm Resistance to Hydrogen Peroxide. APPL Env MICROBIOL 65:7.

133. Shin D-H, Choi Y-S, Cho Y-H. 2008. Unusual Properties of Catalase A (KatA) of *Pseudomonas aeruginosa* PA14 Are Associated with Its Biofilm Peroxide Resistance. J Bacteriol 190:2663–2670.

134. Karatan E, Duncan TR, Watnick PI. 2005. NspS, a Predicted Polyamine Sensor, Mediates Activation of *Vibrio cholerae* Biofilm Formation by Norspermidine. J Bacteriol 187:7434–7443.

135. Yildiz FH, Schoolnik GK. 1999. *Vibrio cholerae* O1 El Tor: Identification of a gene cluster required for the rugose colony type, exopolysaccharide production, chlorine resistance, and biofilm formation. Proc Natl Acad Sci 96:4028–4033.

136. Yildiz FH, Liu XS, Heydorn A, Schoolnik GK. 2004. Molecular analysis of rugosity in a *Vibrio cholerae* O1 El Tor phase variant: Regulation of rugosity. Mol Microbiol 53:497–515.

137. Young KD. 2007. Bacterial morphology: why have different shapes? Curr Opin Microbiol 10:596–600.

138. van Teeseling MCF, de Pedro MA, Cava F. 2017. Determinants of Bacterial Morphology: From Fundamentals to Possibilities for Antimicrobial Targeting. Front Microbiol 8.

139. Taylor JA, Sichel SR, Salama NR. 2019. Bent Bacteria: A Comparison of Cell Shape Mechanisms in Proteobacteria. Annu Rev Microbiol 73:1–24.

140. Ausmees N, Kuhn JR, Jacobs-Wagner C. 2003. The Bacterial Cytoskeleton: An Intermediate Filament-Like Function in Cell Shape. Cell 114:705–713.

141. Cabeen MT, Charbon G, Vollmer W, Born P, Ausmees N, Weibel DB, Jacobs-Wagner C. 2009. Bacterial cell curvature through mechanical control of cell growth. EMBO J 28:1208–1219.

142. Bartlett TM, Bratton BP, Duvshani A, Miguel A, Sheng Y, Martin NR, Nguyen JP, Persat A, Desmarais SM, VanNieuwenhze MS, Huang KC, Zhu J, Shaevitz JW,

Gitai Z. 2017. A Periplasmic Polymer Curves Vibrio cholerae and Promotes Pathogenesis. Cell 168:172-185.e15.

143. Huq A, Small EB, West PA, Huq MI, Rahman R, Colwell RR. 1983. Ecological relationships between Vibrio cholerae and planktonic crustacean copepods. Appl Environ Microbiol 45:275–283.

144. Rashid MH, Rajanna C, Zhang D, Pasquale V, Magder LS, Ali A, Dumontet S, Karaolis DKR. 2004. Role of exopolysaccharide, the rugose phenotype and VpsR in the pathogenesis of epidemic Vibrio cholerae. FEMS Microbiol Lett 230:105–113.

145. Henrici AT. 1928. Morphologic Variations of the Cholera Vibrio, p. 117–124. *In* Morphological Variation and The Rate of Growth of Bacteria. Charles C. Thomas.

146. Fernandez NL, Srivastava D, Ngouajio AL, Waters CM. 2018. Cyclic di-GMP Positively Regulates DNA Repair in Vibrio cholerae. J Bacteriol 200:1–13.

147. Fernandez NL, Waters CM. 2019. Cyclic di-GMP Increases Catalase Production and Hydrogen Peroxide Tolerance in *Vibrio cholerae*. Appl Environ Microbiol 85:e01043-19.

148. Skorupski K, Taylor RK. 1996. Positive selection vectors for allelic exchange. Gene 169:47–52.

149. Dalia AB, McDonough E, Camilli A. 2014. Multiplex genome editing by natural transformation. Proc Natl Acad Sci 111:8937–8942.

150. Ducret A, Quardokus EM, Brun YV. 2016. MicrobeJ, a tool for high throughput bacterial cell detection and quantitative analysis. Nat Microbiol 1:1–7.

151. Schindelin J, Arganda-Carreras I, Frise E, Kaynig V, Longair M, Pietzsch T, Preibisch S, Rueden C, Saalfeld S, Schmid B, Tinevez J-Y, White DJ, Hartenstein V, Eliceiri K, Tomancak P, Cardona A. 2012. Fiji: an open-source platform for biological-image analysis. Nat Methods 9:676–682.

152. Drescher K, Dunkel J, Nadell CD, Van Teeffelen S, Grnja I, Wingreen NS, Stone HA, Bassler BL. 2016. Architectural transitions in Vibrio cholerae biofilms at single-cell resolution. Proc Natl Acad Sci U S A 113:E2066–E2072.

153. Yan J, Sharo AG, Stone HA, Wingreen NS, Bassler BL. 2016. Vibrio cholerae biofilm growth program and architecture revealed by single-cell live imaging. Proc Natl Acad Sci 113:E5337–E5343.

154. Mukherjee S, Bassler BL. 2019. Bacterial quorum sensing in complex and dynamically changing environments. Nat Rev Microbiol 17:371–382.

155. Papenfort K, Förstner KU, Cong J-P, Sharma CM, Bassler BL. 2015. Differential RNA-seq of Vibrio cholerae identifies the VqmR small RNA as a regulator of biofilm formation. Proc Natl Acad Sci 112:E766–E775.

156. Berk V, Fong JCN, Dempsey GT, Develioglu ON, Zhuang X, Liphardt J, Yildiz FH, Chu S. 2012. Molecular architecture and assembly principles of Vibrio cholerae biofilms. Science 337:236–9.

157. Beroz F, Yan J, Meir Y, Sabass B, Stone HA, Bassler BL, Wingreen NS. 2018. Verticalization of bacterial biofilms. Nat Phys 14:954–960.

158. Volfson D, Cookson S, Hasty J, Tsimring LS. 2008. Biomechanical ordering of dense cell populations. Proc Natl Acad Sci 105:15346–15351.

159. Singh PK, Bartalomej S, Hartmann R, Jeckel H, Vidakovic L, Nadell CD, Drescher K. 2017. *Vibrio cholerae* Combines Individual and Collective Sensing to Trigger Biofilm Dispersal. Curr Biol 27:3359-3366.e7.

160. Dahl JL, Tengra FK, Dutton D, Yan J, Andacht TM, Coyne L, Windell V, Garza AG. 2007. Identification of Major Sporulation Proteins of *Myxococcus xanthus* Using a Proteomic Approach. J Bacteriol 189:3187–3197.

161. Hay NA, Tipper DJ, Gygi D, Hughes C. 1999. A Novel Membrane Protein Influencing Cell Shape and Multicellular Swarming of *Proteus mirabilis*. J BACTERIOL 181:9.

162. Lin T-Y, Santos TMA, Kontur WS, Donohue TJ, Weibel DB. 2015. A Cardiolipin-Deficient Mutant of *Rhodobacter sphaeroides* Has an Altered Cell Shape and Is Impaired in Biofilm Formation. J Bacteriol 197:3446–3455.

163. Persat A, Stone HA, Gitai Z. 2014. The curved shape of *Caulobacter crescentus* enhances surface colonization in flow. Nat Commun 5:1–9.

164. Utada AS, Bennett RR, Fong JCN, Gibiansky ML, Yildiz FH, Golestanian R, Wong GCL. 2014. Vibrio cholerae use pili and flagella synergistically to effect motility switching and conditional surface attachment. Nat Commun 5:1–8.

165. Wucher BR, Bartlett TM, Hoyos M, Papenfort K, Persat A, Nadell CD. 2019. *Vibrio cholerae* filamentation promotes chitin surface attachment at the expense of competition in biofilms. Proc Natl Acad Sci 116:14216–14221.

166. Stewart PS, Franklin MJ, Williamson KS, Folsom JP, Boegli L, James GA. 2015. Contribution of Stress Responses to Antibiotic Tolerance in *Pseudomonas aeruginosa* Biofilms. Antimicrob Agents Chemother 59:3838–3847.

167. Jolivet-Gougeon A, Bonnaure-Mallet M. 2014. Biofilms as a mechanism of bacterial resistance. Drug Discov Today Technol 11:49–56.

168. Landini P. 2009. Cross-talk mechanisms in biofilm formation and responses to environmental and physiological stress in *Escherichia coli*. Res Microbiol 160:259–266.

169. Tagkopoulos I, Liu YC, Tavazoie S. 2008. Predictive behavior within microbial genetic networks. Science 320:1313–1317.

170. Hung DT, Zhu J, Sturtevant D, Mekalanos JJ. 2006. Bile acids stimulate biofilm formation in Vibrio cholerae. Mol Microbiol 59:193–201.

171. Koestler BJ, Waters CM. 2014. Bile Acids and Bicarbonate Inversely Regulate Intracellular Cyclic di-GMP in Vibrio cholerae. Infect Immun 82:3002–3014.

172. Townsley L, Yildiz FH. 2015. Temperature affects c-di-GMP signalling and biofilm formation in Vibrio cholerae. Environ Microbiol 17:4290–4305.

173. Tischler AD, Lee SH, Camilli A. 2002. The Vibrio cholerae vieSAB Locus Encodes a Pathway Contributing to Cholera Toxin Production. J Bacteriol 184:4104–4113.

174. Gallant CV, Daniels C, Leung JM, Ghosh AS, Young KD, Kotra LP, Burrows LL. 2005. Common β-lactamases inhibit bacterial biofilm formation. Mol Microbiol 58:1012–1024.

175. Hathroubi S, Zerebinski J, Ottemann KM. 2018. *Helicobacter pylori* Biofilm Involves a Multigene Stress-Biased Response, Including a Structural Role for Flagella. mBio 9.

176. DePas WH, Hufnagel DA, Lee JS, Blanco LP, Bernstein HC, Fisher ST, James GA, Stewart PS, Chapman MR. 2013. Iron induces bimodal population development by <>Escherichia coli</i>. Proc Natl Acad Sci 110:2629–2634.

177. Weiss CA, Hoberg JA, Liu K, Tu BP, Winkler WC. 2019. Single-Cell Microscopy Reveals That Levels of Cyclic di-GMP Vary among *Bacillus subtilis* Subpopulations. J Bacteriol 201.

178. Sycuro LK, Rule CS, Petersen TW, Wyckoff TJ, Sessler T, Nagarkar DB, Khalid F, Pincus Z, Biboy J, Vollmer W, Salama NR. 2013. Flow cytometry-based enrichment for cell shape mutants identifies multiple genes that influence *Helicobacter pylori* morphology: FACS-based identification of cell shape mutants. Mol Microbiol 90:869–883.

179. Das S, Noe JC, Paik S, Kitten T. 2005. An improved arbitrary primed PCR method for rapid characterization of transposon insertion sites. J Microbiol Methods 63:89–94.

180. Larsen R, Wilson M, Guss A, Metcalf W. 2002. Genetic analysis of pigment biosynthesis in *Xanthobacter autotrophicus* Py2 using a new, highly efficient

transposon mutagenesis system that is functional in a wide variety of bacteria. Arch Microbiol 178:193–201.

181. Laventie BJ, Sangermani M, Estermann F, Manfredi P, Planes R, Hug I, Jaeger T, Meunier E, Broz P, Jenal U. 2019. A Surface-Induced Asymmetric Program Promotes Tissue Colonization by Pseudomonas aeruginosa. Cell Host Microbe 25:140-152.e6.

182. Drevinek P, Mahenthiralingam E. 2010. Burkholderia cenocepacia in cystic fibrosis: epidemiology and molecular mechanisms of virulence. Clin Microbiol Infect Off Publ Eur Soc Clin Microbiol Infect Dis 16:8218–8230.

183. Sousa SA, Feliciano JR, Pita T, Guerreiro SI, Leitão JH. 2017. Burkholderia cepacia complex regulation of virulence gene expression: A review. Genes 8.

184. Cooper VS. 2018. Experimental Evolution as a High-Throughput Screen for Genetic Adaptations. mSphere 3:1–7.

185. Poltak SR, Cooper VS. 2011. Ecological succession in long-term experimentally evolved biofilms produces synergistic communities. ISME J 5:369–378.

186. Traverse CC, Mayo-Smith LM, Poltak SR, Cooper VS. 2013. Tangled bank of experimentally evolved Burkholderia biofilms reflects selection during chronic infections. Proc Natl Acad Sci U S A 110:E250–E259.

187. Bi H, Christensen QH, Feng Y, Wang H, Cronan JE. 2012. The *Burkholderia cenocepacia* BDSF quorum sensing fatty acid is synthesized by a bifunctional crotonase homologue having both dehydratase and thioesterase activities: BDSF synthetic pathway. Mol Microbiol 83:840–855.

188. Waldron EJ, Snyder D, Fernandez NL, Sileo E, Inoyama D, Freundlich JS, Waters CM, Cooper VS, Neiditch MB. 2019. Structural basis of DSF recognition by its receptor rpfr and its regulatory interaction with the DSF synthase RpfF.

189. Deng Y, Schmid N, Wang C, Wang J, Pessi G, Wu D, Lee J, Aguilar C, Ahrens CH, Chang C, Song H, Eberl L, Zhang L-H. 2012. Cis-2-dodecenoic acid receptor RpfR links quorum-sensing signal perception with regulation of virulence through cyclic dimeric guanosine monophosphate turnover. Proc Natl Acad Sci 109:15479–15484.

190. Koestler BJ, Waters CM. 2013. Exploring Environmental Control of Cyclic di-GMP Signaling in *Vibrio cholerae* by Using the *Ex Vivo* Lysate Cyclic di-GMP Assay (TELCA). Appl Environ Microbiol 79:5233–5241.

191. Ryjenkov DA, Tarutina M, Moskvin OV, Gomelsky M. 2005. Cyclic Diguanylate Is a Ubiquitous Signaling Molecule in Bacteria: Insights into Biochemistry of the GGDEF Protein Domain. J Bacteriol 187:1792–1798.

192. Bordeleau E, Fortier L-C, Malouin F, Burrus V. 2011. c-di-GMP Turn-Over in *Clostridium difficile* Is Controlled by a Plethora of Diguanylate Cyclases and Phosphodiesterases. PLoS Genet 7:e1002039.

193. Dennis JJ. 2017. Burkholderia cenocepacia virulence microevolution in the CF lung: Variations on a theme. Virulence 8:618–620.

194. Scalfaro C, Iacobino A, Nardis C, Franciosa G. 2017. *Galleria mellonella* as an in vivo model for assessing the protective activity of probiotics against gastrointestinal bacterial pathogens. FEMS Microbiol Lett 364.

195. Seed KD, Dennis JJ. 2008. Development of *Galleria mellonella* as an Alternative Infection Model for the Burkholderia cepacia Complex. Infect Immun 76:1267–1275.

196. Jander G, Rahme LG, Ausubel FM. 2000. Positive Correlation between Virulence of Pseudomonas aeruginosa Mutants in Mice and Insects. J Bacteriol 182:3843–3845.

197. Silva IN, Santos PM, Santos MR, Zlosnik JEA, Speert DP, Buskirk SW, Bruger EL, Waters CM, Cooper VS, Moreira LM. 2016. Long-Term Evolution of *Burkholderia multivorans* during a Chronic Cystic Fibrosis Infection Reveals Shifting Forces of Selection. mSystems 1.

198. Lindenberg S, Klauck G, Pesavento C, Klauck E, Hengge R. 2013. The EAL domain protein YciR acts as a trigger enzyme in a c-di-GMP signalling cascade in E. coli biofilm control. EMBO J 32:2001–2014.

199. Hengge R, Gründling A, Jenal U, Ryan R, Yildiz F. 2016. Bacterial Signal Transduction by Cyclic Di-GMP and Other. J Bacteriol 198:15–26.

200. Yang C, Cui C, Ye Q, Kan J, Fu S, Song S, Huang Y, He F, Zhang LH, Jia Y, Gao YG, Harwood CS, Deng Y. 2017. Burkholderia cenocepacia integrates cis-2-dodecenoic acid and cyclic dimeric guanosine monophosphate signals to control virulence. Proc Natl Acad Sci U S A 114:13006–13011.

201. Dunn AK, Millikan DS, Adin DM, Bose JL, Stabb E V. 2006. New *rfp*- and pES213-derived tools for analyzing symbiotic *Vibrio fischeri* reveal patterns of infection and *lux* expression in situ. Appl Environ Microbiol 72:802–10.

202. LiPuma JJ, Spilker T, Coenye T, Gonzalez CF. 2002. An epidemic *Burkholderia cepacia* complex strain identified in soil. The Lancet 359:2002–2003.